PL-TR-96-2224

SUPPORT OF ENVIRONMENTAL REQUIREMENTS FOR CLOUD ANALYSIS AND ARCHIVE (SERCAA): FINAL REPORT

Gary B. Gustafson
Robert P. d'Entremont
Ronald G. Isaacs

Atmospheric and Environmental Research, Inc.
840 Memorial Drive
Cambridge, MA 02139-3794

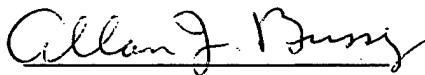14 August 1996

Final Report
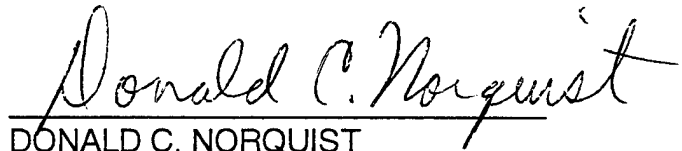14 August 1992 - 13 August 1996

DTIC QUALITY INSPECTED 4

PHILLIPS LABORATORY
Directorate of Geophysics
AIR FORCE MATERIEL COMMAND
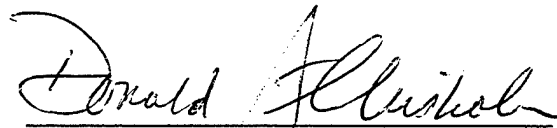**HANSCOM AIR FORCE BASE, MA 01731-3010**

"This technical report has been reviewed and is approved for publication."

ALLAN J. BUSSEY
Contract Manager

DONALD C. NORQUIST
Acting Chief, Satellite Analysis and Weather
Prediction Branch
Atmospheric Sciences Division

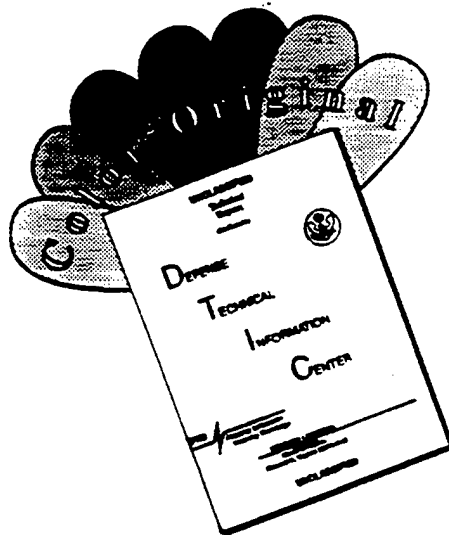DONALD A. CHISHOLM, Acting Director
Atmospheric Sciences Division

DISCLAIMER NOTICE

THIS DOCUMENT IS BEST QUALITY AVAILABLE. THE COPY FURNISHED TO DTIC CONTAINED A SIGNIFICANT NUMBER OF COLOR PAGES WHICH DO NOT REPRODUCE LEGIBLY ON BLACK AND WHITE MICROFICHE.

REPORT DOCUMENTATION PAGE

Form Approved
OMB No. 0704-0188

1. AGENCY USE ONLY *(Leave blank)*	2. REPORT DATE 14 August 1996	3. REPORT TYPE AND DATES COVERED Final 14 August 1992–13 Aug.1996

4. TITLE AND SUBTITLE
Support of Environmental Requirements for Cloud Analysis and Archives (SERCAA): Final Report

5. FUNDING NUMBERS
PE 35160F
PRDSPO TA GR
WU AA
F19628-92-C-0149

6. AUTHOR(S)
G.B. Gustafson, R.P. d'Entremont and
R.G. Isaacs

7. PERFORMING ORGANIZATION NAME(S) AND ADDRESS(ES)
Atmospheric and Environmental Research, Inc.
840 Memorial Drive
Cambridge, MA 02139-3794

8. PERFORMING ORGANIZATION REPORT NUMBER

9. SPONSORING/MONITORING AGENCY NAME(S) AND ADDRESS(ES)
Phillips Laboratory
29 Randolph Road
Hanscom AFB, MA 01731-3010
Contract Manager: Allan Bussey/GPAB

10. SPONSORING/MONITORING AGENCY REPORT NUMBER
PL-TR-96-2224

11. SUPPLEMENTARY NOTES
Sponsored by joint Department of Defense, Department of Energy, and Environmental Protection Agency Strategic Environmental Research and Development Program (SERDP)

12a. DISTRIBUTION/AVAILABILITY STATEMENT
Approved for public release; distribution unlimited

12b. DISTRIBUTION CODE

13. ABSTRACT *(Maximum 200 words)*

Support of Environmental Requirements for Cloud Analysis and Archives (SERCAA) was a four-year, two-phase research and development program. Program goals were to produce a global multispectral, multisensor cloud analysis capability for retrieval of spatial, radiative, microphysical, and environmental cloud properties through analysis of sensor data from multiple operational environmental satellites. Program accomplishments during Phase 1 included development of three customized cloud-detection algorithms for analysis of NOAA/AVHRR, DMSP/OLS, and geostationary sensor data; a new algorithm for discrimination of vertical cloud layers within a 25 km grid cell; and an innovative analysis-integration algorithm for optimally combining the results of the source-specific cloud analysis modules. During Phase 2, retrieval capabilities were expanded to include cloud particle size, emissivity/transmissivity, optical depth, and altitude. Additional work toward characterization of cloud-free bidirectional reflectance provides a basis for enhanced analysis of visible-channel data in the cloud detection process. SERCAA algorithms have been selected for operational implementation at the Air Force Global Weather Central.

14. SUBJECT TERMS
cloud, nepnanalysis, satellite meteorology, cirrus

15. NUMBER OF PAGES
80

16. PRICE CODE

17. SECURITY CLASSIFICATION OF REPORT Unclassified	18. SECURITY CLASSIFICATION OF THIS PAGE Unclassified	19. SECURITY CLASSIFICATION OF ABSTRACT Unclassified	20. LIMITATION OF ABSTRACT Unlimited

TABLE OF CONTENTS

TABLE OF CONTENTS
(continued)

LIST OF FIGURES

LIST OF FIGURES
(continued)

LIST OF TABLES

EXECUTIVE SUMMARY

This final report describes a two-part research and development program to produce a global multispectral, multisensor cloud analysis capability for retrieval of spatial, radiative, microphysical and environmental cloud properties through analysis of sensor data from multiple environmental satellites. Jointly sponsored by the Department of Defense, Department of Energy, and Environmental Protection Agency through the Strategic Environmental Research and Development Program (SERDP) and the Air Force Phillips Laboratory (PL), the Support of Environmental Requirements for Cloud Analysis and Archive (SERCAA) program achieved the project goals through development and testing of a series of cloud analysis algorithms. A key attribute of the SERCAA algorithms is their ability to analyze and integrate data from multiple environmental satellite systems consisting of the U.S. military (DMSP) and civilian (NOAA/POES) polar orbiting sensor platforms and international geostationary systems from the U.S. (GOES), Japan (GMS), and Europe (METEOSAT). The program was broken into two development phases. Phase I focused on analysis of imaging-sensor data for cloud detection and retrieval of cloud spatial properties including location, extent, fractional amount, cloud-top altitude, and cloud type. Important elements are multiple cloud detection algorithms designed to best exploit the information content from each class of satellite, a new layering and typing algorithm based on generalized image processing classification techniques, and a unique analysis integration algorithm that optimally combines analyzed cloud products from each data source into a single consistent analysis. Phase II used the cloud spatial information as the first step in retrieval of cloud emissivity, phase, and particle size. Emissivity algorithms use multispectral infrared data to simultaneously solve multiple radiative transfer equations for the emission term. From emission, a first-order estimate of optical depth inferred. For accurate estimation of cloud emission, it is first necessary to know cloud phase. A deterministic phase algorithm was developed that exploits unique cloud signatures at mid-wave and long-wave infrared wavelengths from liquid water and ice cloud. While imaging sensors provide insufficient information to retrieve a cloud drop distribution, a useful bulk-property parameterization (e.g., mode radius) can be retrieved. A mode-radius retrieval algorithm was developed for water droplets based on theoretically-derived look-up tables of expected monochromatic infrared radiance values as a function of atmospheric profile, view angle, and cloud altitude. Monochromatic radiances were convolved with sensor response functions for IR channel configurations on available environmental satellites. Where available, collocated sounding instruments were used in addition to the imager data to retrieve temperature and moisture profile information in the vicinity of cloud. A unified retrieval algorithm was used wherein all available sensor information is used to produce an optimal retrieval.

1.0 Introduction

A global cloud detection and analysis technology, operating continuously and in real-time, which more completely exploits the information in present satellite sensors, has been a recognized and stated requirement to support the operations of the United States Department of Defense (DoD) for a number of years. Also, the environmental monitoring and global change research communities have identified clouds as having a preponderant impact on climate and climate change. They have given top priority to improved global cloud specification although real-time cloud product generation is not a requirement for these groups. Progress from the global change community has occurred, specifically the International Satellite Cloud Climatology Project (ISCCP). However, fiscal and technological constraints have prevented the development and implementation of a multi-satellite multispectral cloud analysis technology capable of utilizing in an operational mode the abundant sensor information presently on orbit. The need has been identified, the measurement capabilities have been in place, the missing component has been an advanced satellite-based operational cloud retrieval technology.

This report describes the Support of Environmental Requirements for Cloud Analysis and Archive (SERCAA) research and development program which has produced such a technology and provides a technical description of the component algorithms. The program was accepted by the DoD portion of the Strategic Environmental Research and Development Program (SERDP) and supported under the Remote Sensing Thrust as a project of the "Definition and Demonstration of Remote Sensing Capability to Contribute to Environmental Understanding and Support for Environmental Issues", administered by the Defense Support Projects Office (DSPO) through a contract with the Air Force Phillips Laboratory.

The overall SERCAA program objective was to provide a satellite-based global cloud analysis capability for determining the spatial, radiative and microphysical properties of clouds. The two-phases of the program have resulted in development and demonstration of cloud algorithms for retrieval of: (1) continuously updated cloud spatial properties, and (2) augmented cloud optical, microphysical, and environmental properties. The combined algorithms form a cloud analysis model that is intended to serve a large number of environmental users, both within and outside of DoD. The SERCAA model can be used to help in determining and validating the distribution of clouds and their associated hydrological and radiative effects on climate and on global climate change. It will also constitute a substantial upgrade to the presently operating Real-Time Nephanalysis (RTNEPH) cloud analysis model at the Air Force Global Weather Center (AFGWC). In this role SERCAA is a fundamental component in the Cloud Depiction and Forecast System (CDFS) being carried out by the Air Weather Service of the U. S. Air Force.

Under Phase I, the objective of improved satellite cloud detection capabilities for global applications was addressed through development of an integrated ensemble of global cloud analysis algorithms applicable to sensor data from both civilian and military satellites. The SERCAA multiplatform, multisensor, multispectral cloud product analysis algorithms (Isaacs et al., 1993; Gustafson et al., 1994) incorporate high-resolution sensor data into a real-time cloud analysis. Multispectral cloud analysis techniques are used for the detection and specification of clouds, especially cirrus and low clouds. Geostationary sensor data augment polar-orbiting data to improve the timeliness of analyses, particularly in tropical regions. The steps required to process the raw sensor data, collected from each of the satellite platforms, into each of the individual cloud analysis products include total cloud algorithms for the Defense Meteorological Satellite Program (DMSP) Operational Linescan System (OLS), the National Oceanic and Atmospheric Administration (NOAA) Advanced Very High Resolution Radiometer (AVHRR), and geostationary platforms; cloud layer and

1

type algorithms; and a new analysis integration algorithm. SERCAA data products include: total cloud cover fraction, number of cloud layers (up to four floating layers), cloud layer coverage fraction, cloud type, cloud height, and analysis confidence level. These products will be provided on a 16th mesh (24 km grid true at 60 degrees latitude) polar stereographic grid.

In Phase II, the goal was to extend the multiple-source optimal satellite retrieval strategy that was successfully applied for cloud spatial characteristics (cloud amount, height, layers, and type), to the augmented cloud properties (optical, microphysical, environmental) specification. This was accomplished by emphasizing infrared and microwave sounder data in conjunction with cloud detection from visible and infrared satellite imagers. Optical properties are emissivity, reflectivity, and optical depth; microphysical attributes are particle size distribution and phase; environmental parameters are water vapor profiles, temperature profiles and cloud liquid water.

2.0 Program Requirements

In the U.S. Global Change Research Program, the role of clouds has been identified as the number one science priority and also the most important environmental factor (Correll, 1990) affecting global climate change processes. The reliable determination of cloud parameters on a global scale is fundamental to understanding that role (Schiffer and Rossow, 1983). The U.S. Interagency Committee on Earth and Environmental Sciences (CEES) has also specified clouds and the hydrologic cycle as elements sharing the highest scientific priority for global change research. The two-decade-long Global Energy and Water Cycle Experiment (GEWEX), part of the World Climate Research Programme (WCRP), has singled out the cloud-radiation feedback process as primary among its most critical problems (WMO, 1989). GEWEX emphasizes that satellite detection of cloud physical and radiative properties on a global basis will require significant enhancement if the goal is to be achieved of specifying the complex role clouds have in climate and climate change (Chahine, 1992). Also, the American Meteorological Society Council (AMS, 1992) has stated, "Clouds are the most critical factor causing uncertainties in model estimates of global warming."

The requirements for detailed representative global cloud analyses have increased over the last decade. Advancement of cloud forecasting models and the accurate simulation of cloud effects on the radiative feedback processes in global/medium-range numerical weather prediction (NWP) and climate models is impeded by the lack of accurate cloud analyses (Isaacs et al., 1983). Applied meteorology's goal of improved short and medium range cloud forecasting is limited in significant part to the accuracy of cloud parameterizations employed by forecast modelers. In the summer of 1983, the ISCCP started as a part of the WCRP. One of the primary objectives of the ISCCP is to derive and validate a global cloud climatology that will allow for improved parameterizations of clouds and therefore their associated radiation feedback processes in climate models (Schiffer and Rossow et al., 1985).

The impact of clouds on Department of Defense (DoD) activities is also of first order. Improved cloud forecasting and improved cloud data handling and analysis are among the highest prioritized Air Force requirements. The DoD policy of quantifying the environment's impact on new systems before they enter the acquisition process has placed increased emphasis on having accurate and multi-parameter cloud archives against which system performance can be evaluated. The need for superior global cloud analysis and archive products is critical. Presently the best, and for certain cloud characteristics, the only operational real-time global cloud analysis is the RTNEPH (Hamill et al., 1992),

residing at the Air Force Global Weather Central (AFGWC). It became operational in 1983, replacing the earlier 3-Dimensional Nephanalysis, or 3DNEPH. Unfortunately, the cloud analysis techniques and database management contained in the RTNEPH make minimal use of existing advanced technologies. Currently, only Operational Linescan System (OLS) visible and infrared channel radiances, or single-channel Advanced Very High Resolution Radiometer (AVHRR) infrared data, are accepted for processing. Even this limited data set is then degraded in both spatial and spectral resolution and geometrically transformed to fit a standardized fixed grid structure. Restrictions on the satellite data sources made available for processing and the amount of ad hoc tuning and manual interaction required by the current RTNEPH introduce serious limitations for climate research purposes. Additionally, RTNEPH products are immediately available only to government, and in particular DoD weather forecast facilities. RTNEPH information is archived at the National Climatic Data Center (NCDC), Asheville, NC by the United States Air Force Combat Climatology Center (USAFCCC). From a climate standpoint, the quality and therefore the usefulness of these archive products is limited by the lack of data source information and the lack of continuity in analysis algorithms in the RTNEPH over the past two decades.

Recent advances in satellite cloud detection using multispectral analysis techniques have demonstrated a superior quantification of cloud characteristics utilizing near-infrared (NIR) and medium-wavelength infrared (MWIR) data from the AVHRR sensor. For example, the location, height, amount, and optical properties of cirrus clouds can be better quantified; low cloud and fog can also be more confidently detected at night and during the daytime over melting snow (d'Entremont, 1986; d'Entremont and Thomason, 1987; d'Entremont et al., 1990; Stowe et al., 1991; d'Entremont et al., 1992). Application of these retrieval techniques was successfully achieved within DoD under the TACNEPH development project conducted by researchers at the Phillips Laboratory, Geophysics Directorate (PL/GPA) and AER (Gustafson and d'Entremont, 1992). The objective of TACNEPH was to produce a stand-alone, deployable satellite cloud analysis capability on a regional scale to support tactical operations (Gustafson et al., 1993b). The TACNEPH heritage lies in the global Real Time Nephanalysis or RTNEPH model (Hamill et al., 1992) run operationally at the Air Force Global Weather Central (AFGWC).

Incorporation of improved satellite cloud detection capabilities for global applications was a primary goal of SERCAA. The three principal accomplishments of SERCAA were: 1) to incorporate high-resolution sensor data from multiple military and civilian satellites, polar and geostationary, into a real-time cloud analysis model, 2) to demonstrate multispectral cloud analysis techniques that improve the detection and specification of clouds, especially cirrus and low clouds, and 3) to provide augmented parameter, algorithm, and data base specifications for an improved cloud retrieval model including cloud environmental, radiative, and microphysical properties.

3.0 SERCAA Phase I Overview

The focus of the Phase I effort (Gustafson et al., 1994) was development of an integrated nephanalysis model to retrieve cloud spatial properties using imaging sensor measurements from three categories of environmental satellites as the primary data source. NOAA Polar Orbiting Environmental Satellites (POES) carry the five-channel AVHRR imaging sensor. DMSP satellites use the two-channel OLS. The constellation of international geostationary satellites include two United States Geostationary Operational Environmental Satellites (GOES) which carry five-channel imagers, the Japanese Geostationary Meteorological Satellite (GMS) which uses a four-channel instrument, and the European Space Agency's Meteorological Satellite (METEOSAT) with a three-channel

3

sensor. Data from each category of satellite are analyzed using separate cloud detection algorithms specifically designed to exploit the specific information content of each system. Satellite sensor data are processed as they are received from the Satellite Data Handling System by the CDFS II. For polar-orbiting satellites, the basic processing unit is one orbit of data, for geostationary satellites the amount of data received from any one satellite varies according to a data acquisition schedule defined by the operating nation(s).

The SERCAA nephanalysis model consists of four processing levels. Level 1 is ingest processing that includes unpacking of the telemetry stream, sensor data calibration, and Earth location. Level 2 is cloud detection performed on a pixel-by-pixel basis using sensor-specific algorithms to analyzed data transmitted from each satellite. Level 3 is cloud layering and typing to provide a vertical stratification of the cloudy pixels detected in Level 2. Level 3 output is remapped to the standard AFGWC polar-stereographic grid projection at a resolution of 16th mesh. Level 1, 2, and 3 are event driven processes triggered by the receipt of new data from any of the satellite sources. Level 4 is merge processing wherein the most recent analyzed products from each satellite are combined to produce a single optimal integrated analysis. When implemented in CDFS II, a fifth level of processing will be added that uses hourly integrated cloud analyses to initialize a short-term and a long-term cloud forecast model. Levels 4 and 5 will be clock driven processes run hourly under a user-defined schedule.

Three cloud detection algorithms are used to analyze data from the different imaging sensor systems utilized in CDFS II. Each cloud algorithm is designed to exploit the unique strengths of the respective sensor system. DMSP/OLS data have the highest spatial resolution and a constant instantaneous field of view (IFOV) across a scan line but are limited to two broad band channels, one visible and one infrared. NOAA/AVHRR data have a relatively coarse spatial resolution that degrades toward the edge of scan balanced by five narrow band channels with high spectral resolution. Geostationary sensors vary by satellite but have at least one visible and one infrared channel in common. GOES carries a five-channel imager, GMS a four channel, METEOSAT three, and INSAT two.

3.1 DMSP/OLS

The OLS two-channel radiometer has broad-band channels in the visible to near infrared (0.40-1.10 μm) and the long wave infrared (10.5-12.6 μm). Analysis of OLS data is accomplished through a dual threshold technique that operates on two dimensional visible-infrared data during daytime and on single-channel IR data at night. Separate cutoff thresholds are established to discriminate completely cloud free and cloud filled pixels. Threshold determination, and hence algorithm accuracy, is critically dependent on an ability to accurately predict the background visible and infrared radiance that the sensor would measure in the absence of cloud. An independent analysis of surface skin temperature produced by an analysis model such as SFCTMP (Kopp et al., 1994a) is used as a first guess to this clear-column infrared brightness temperature prediction. The first guess is adjusted by using a nearby cotemporal satellite measurement to establish a reference temperature correction to account for differences between the modeled and satellite observed temperatures. Once established, the reference temperature correction is used to adjust the skin temperature field to predict the clear-column brightness temperature for all pixels within a local analysis region.

The reference temperature correction factor calculation requires collocated IR sensor data and modeled skin temperature fields. Satellite data are segmented into a series of small, local analysis regions. The size of each region is determined by the relative spatial scales of the AFGWC skin temperature database and the satellite sensor data. For each

4

cloud analysis grid box a separate surface skin temperature correction is computed by obtaining the difference between the observed satellite brightness temperature for a reference pixel and the corresponding collocated and time interpolated skin temperature. If the reference pixel can be established to be cloud free then the reference temperature difference is used to predict the clear scene brightness temperature for all remaining pixels in the analysis region. To maximize the likelihood that the reference pixel is cloud free it is selected as the pixel with the largest IR brightness temperature within the analysis region.

The critical step in estimation of the clear scene brightness temperature is insuring that the reference pixel is free from cloud contamination. This is done by comparing the magnitude of reference temperature difference against the range of expected temperature differences for a given time, location and satellite. Statistics on clear scene temperature differences are produced as byproducts of the nephanalysis algorithm and are maintained in a database stratified by location, surface type (land, water, desert), satellite, and time of day. Cloudy pixels are eliminated by running the nephanalysis algorithm using conservative cloud detection thresholds. Assumed natural variability of this quantity for a given satellite pass is calculated from a time weighted average of difference statistics accumulated over the previous ten days. If the reference temperature difference lies within the averaged limits, it is assumed to fall within the naturally occurring variability for cloud free conditions and the reference value is assumed to be cloud free.

If the reference pixel can be established to be cloud free, then the predicted clear scene brightness temperature for any pixel within the analysis box is computed by adding the reference temperature difference to the time interpolated AFGWC surface skin temperature at the desired pixel location. If the reference pixel is determined to be cloud contaminated then a default correction based on the time weighted mean of the historical temperature differences is used as the reference temperature.

Visible channel clear-scene statistics are maintained globally on an 8th mesh grid using a technique developed for the RTNEPH (Kiess and Cox, 1988). Similar to the IR procedure described above, visible-channel clear scene statistics are computed as a byproduct of the nephanalysis. For each 8th mesh grid cell, all clear scene visible-channel pixel values are accumulated and the mean calculated. The visible background database is updated continuously as new data are received. To avoid anomalous values from corrupting the database, information is added only if the new value does not vary from the magnitude of the stored value by more than a preset threshold. If the newly computed mean reflectance value passes this criteria then the database is updated using a weighted average of the previous and new values. Thus the clear column visible background database contains a continuously updated record of the satellite observed clear column visible count at each grid cell location.

The OLS cloud algorithm is based on a statistical threshold approach designed to operate using either a single infrared thermal window channel alone or in combination with a visible channel. Each requires the predicted clear scene bandpass weighted brightness temperature and, during daytime, the visible background values described above. An empirically derived dynamic correction factor is used to collectively account for all sources of error in the predicted clear-scene values without the need to understand and quantify the individual contributions. Error sources include sensor calibration errors, incomplete modeling of atmospheric transmission, and poor or unrepresentative estimates of the clear-scene skin temperature.

Separate cloud detection criteria are used for processing combined visible-infrared data and infrared data alone. Use of visible data is restricted to conditions where the solar zenith angle is less than a preset threshold that is defined to discontinue visible-data proces-

5

sing well before the daylight terminator. Objective processing of daytime OLS visible data beyond this cutoff is problematic because of rapid changes made to visible sensor gain control performed on-board the satellite. Visible sensor gain is controlled by the value of the scene solar elevation (i.e., the solar elevation at the viewed point on the Earth). Gain changes are relatively smooth at high solar elevations, however, as the scan approaches the terminator the granularity of incremental changes in the solar elevation increases resulting in rapid changes in sensor gain adjustment (Bunting and d'Entremont, 1982). Under daytime conditions, when usable visible and infrared data are available, a bispectral algorithm is executed. During nighttime conditions a single channel IR test is used.

The OLS single channel IR algorithm is a three step procedure: 1) predict the clear scene bandpass weighted brightness temperature; 2) compare satellite observed IR brightness temperatures to the predicted temperature; and 3) based on the magnitude of the difference between the two temperatures, classify each pixel as either cloud-filled or cloud-free. The dynamic threshold approach described above is used to predict the brightness temperature that the satellite would measure for a clear scene. Two separate thresholds are applied to the corrected temperature to account for any remaining uncertainties in the clear scene estimate. One threshold is used to establish a cutoff value for completely cloud filled pixels and the second for completely cloud free. Data points that lie between the two cutoff values are treated as cloud filled but the analysis is assumed to be less reliable.

The two channel OLS algorithm is an extension of the single channel approach into two spectral dimensions. When usable visible data are available, data from both OLS sensor channels are analyzed simultaneously using two pairs of cutoff values, one pair for each channel. Pixels with lower brightness temperatures than the IR cutoff and/or higher brightness values than the visible cutoff are classified as cloud. Warm bright regions require an additional a priori background type classification to remove ambiguity caused by similarities in the radiative signatures of desert, snow or ice backgrounds with low cloud. Data points that fall between all four cutoff values are classified as cloud filled but are considered less reliable.

3.2 NOAA/AVHRR

The AVHRR sensor is a five-channel radiometer with two channels sensitive to reflected solar, channels 1 centered at 0.6 μm and 2 at 0.9 μm; two channels that measure only emitted IR energy, channels 4 at 10.5 μm and 5 at 12.0 μm; and one channel that is sensitive to both reflected solar and emitted IR, channel 3 at 3.7 μm. The multispectral information content from these channels was used to develop a cloud algorithm that is less dependent on accurate characterization of the cloud-free background than the OLS algorithm. The AVHRR multispectral algorithms are based on the approach of Saunders and Kriebel (1988) wherein a hierarchy of cloud detection and background discrimination tests, each exploiting a different cloud radiative signature, are run in series on each pixel within the scene. The algorithms are capable of operating on all five AVHRR channels simultaneously or on any combination of channels. A cloud analysis is produced through interpretation of results from all available cloud and background tests.

Separate snow and sun glint tests are used to identify problematic background conditions. Generally, tests that rely on reflected solar radiation (i.e., AVHRR channels 1, 2, or 3) can misclassify sun glint, snow, or ice as cloud. The main exception are tests that use channel 3 data over frozen water backgrounds since ice and snow are relatively non-reflective at these wavelengths, however, sun glint affects all three channels. Some information on snow cover and sea ice is available from the SNODEP model and from the Navy, however, experience has demonstrated that these databases have insufficient

6

accuracy to support the nephanalysis. To supplement the available databases snow, ice and sun glint algorithms were developed using the multispectral sensor data alone. Snow and ice are detected by comparing the solar component of daytime channel 3 data to channel 1 visible data. Cloud surface tend to be reflective at both wavelengths, however snow and ice surfaces have a significantly lower reflectivity at the channel-3 mid wave IR (MWIR) wavelengths than in the visible. Thus for cloud, both channels will exhibit a strong reflected solar signature while for snow or ice surfaces the signature is much greater in the visible channel. Similar to snow and ice, sun glint from water surfaces can produce a cloud-like signature in the visible to MWIR channels. Specular reflection from water surfaces occurs when the sensor is scanning toward the sun and the satellite zenith angle matches the solar zenith angle. Although these angles can be calculated with sufficient precision to identify the specular point, accurate identification of sun glint from water surfaces remains a problem. This is due to the well-known occurrence of sun glint well away from the specular point under conditions when the water surface is agitated. Since information on sea state and wind direction is not directly available, a multispectral sun glint algorithm was developed to test for conditions that resemble cloud in the reflected solar tests but do not in tests that rely on emitted IR radiation only. However, this condition alone is not sufficient to detect glint since some liquid water clouds can exhibit the same characteristics. An additional criteria requires that the magnitude of the channel 3 data approach sensor saturation, a condition that normally occurs only in glint conditions since the derived channel 3 brightness temperature is very sensitive to even small amounts of reflected solar.

AVHRR cloud tests generally rely on channel differences or ratios to discriminate cloud signatures from those of terrestrial backgrounds. Due to the unique radiative characteristics of low clouds and fog at 3.7 μm relative to long wave IR channels, comparison of channel 3 and 4 brightness temperatures is a powerful low cloud discrimination technique during both day and nighttime. At 3.7 μm liquid water clouds radiate as gray bodies (i.e., both emit and reflect energy) whereas at 10.5 μm they are nearly black (d'Entremont et al., 1987). As a result, liquid water cloud emissivity can be significantly less than 1 resulting in a lower nighttime equivalent blackbody brightness temperature computed from channel 3 relative to channel 4. However, during the daytime the combined emitted and reflected solar components cause the computed brightness temperature to be relatively large compared to channel 4 where there is only emitted radiation. Additionally, for a partially filled IFOV (e.g., cold cloud and warm background in the same IFOV) the relative contribution to the derived brightness temperature from warm and cold surfaces differs between the channels 3 and 4 due to the highly non-linear shape of the Planck function between the two channel wavelengths. At 3.7 μm the emitted energy from the warm background is the dominant contribution to the computed brightness temperature whereas at 11 μm the relative contributions from the background and cloud are roughly equal. This signature is useful for detecting broken and transmissive high (cold) cloud at night, particularly optically thin cirrus.

Other cloud tests use relative differences between the split visible (1 and 2) and split long wave IR channels (4 and 5). Relative visible and near IR clear scene albedo measurements will differ depending on background. Over water both channel reflectances tend to be low, but enhanced atmospheric aerosol scattering at the shorter channel 1 wavelengths generally results in a slightly higher scene reflectance. Over land the signature reverses except in cases of extreme aerosol loading since vegetated surfaces reflect preferentially in the longer channel 2 wavelengths. Clouds reflect approximately equally in both channels and as such tend to obliterate the background signatures. Thus a split visible cloud test checks for roughly equal channel 1 and 2 reflectance values. However, the absolute magnitude of the measured channel 1 and 2 radiances can vary significantly over a scene depending on the relative reflectivity of the observed surface, solar geometry, and

anisotropic effects making selection of a channel-difference threshold problematic. To cancel these effects out of the cloud detection algorithm the ratio of the two channels is used as opposed to a channel difference to discriminate the background signatures from the cloud. A cloud signature is assumed to be a channel ratio of approximately 1.0. Split IR data (channels 4 and 5) are used to detect ice cloud and small particles along cloud edges, independent of time of day. Even in cloud-free conditions, inter-channel brightness temperature differences are expected to exist due primarily to preferential water vapor absorption at channel 5 wavelengths. However, in the presence of cloud the differences increase beyond the level predicted theoretically. Inoue (1987) recognized that this departure was caused by unequal extinction from thin ice clouds at 11 and 12 μm, with the greater extinction occurring at 12 μm. Prabhakara et al. (1988) extended this signature to include both liquid water and ice clouds when the droplet or particle size was smaller than the channel wavelength. Saunders and Kriebel (1988) developed a test to exploit these signatures through a theoretically derived look-up table of expected clear scene channel differences. When the channel differences exceed the theoretically predicted amount cloud is assumed to be present in the volume.

3.3 Geostationary

The cloud detection algorithm for geostationary satellite platforms employs a hybrid approach to identify cloudy pixels within an analysis scene. The approach consists of three algorithms that are applied in series: temporal differencing, dynamic thresholding, and spectral discriminant tests. The procedure is applicable to any geostationary satellite with at least one visible and one long wave IR channel.

The first level of processing utilizes a temporal differencing technique to identify new cloud development or cloud motion over either previously clear background or lower level cloud. The algorithm exploits the high temporal resolution of geostationary data by testing for rapid changes in infrared brightness temperature and/or visible reflectance in collocated pixels taken from sequential satellite images. Cloud detection is accomplished by identifying pixels that change by an amount greater than the clear-scene conditions are expected to change. Expected changes in clear-scene background characteristics are computed from time series of surface skin temperature and visible background brightness databases. During daytime conditions a bispectral technique is employed that simultaneously evaluates the change in infrared brightness temperature and visible reflectance. At night only the change in IR brightness temperature is evaluated. A pixel is flagged as cloud filled if the change in collocated pixel values over a one hour time period exceeds the expected change by greater than a predetermined threshold amount. Otherwise, the pixel is flagged as cloud free.

The temporal difference test is only expected to identify some fraction of the cloud in a scene, however the confidence level for these clouds is very high. The dynamic thresholding algorithm uses information on the radiative characteristics of cloud identified through temporal differencing to detect nearby cloud with similar characteristics. The image is segmented into a regular grid and the minimum and maximum brightness temperatures (visible reflectance) of the pixels classified as cloudy by the temporal differencing test within each grid cell are identified. The maximum temperature is used to define an infrared brightness temperature cloud threshold for the remaining pixels within a cell. The threshold is set at the maximum temperature minus an offset to eliminate anomalous values. Separate cloud thresholds are calculated for each grid cell and all pixels within the cell with a lower brightness temperature or higher visible count are classified as cloudy.

8

Following the temporal differencing and dynamic threshold processing, it is still possible that clouds with spatial and spectral attributes that have not changed over the analysis time interval remain undetected. The final step in the geostationary processing applies a series of spectral discriminant tests to the remaining unclassified pixels. Spectral discriminant tests use sensor channel information in the same manner as the OLS and AVHRR algorithms to detect spectral signatures of cloud. Since geostationary sensors have different configurations depending on platform, the suite of tests employed depends on the set of data channels available. Since all geostationary imaging sensors have at least one visible and one long wave IR channel, single-channel visible and IR threshold tests can be applied universally.

The recently launched GOES-8 and 9 satellites, along with GMS-5 are the first in a series of next-generation geostationary systems that have introduced multispectral imaging sensors that have potential for significantly improving geostationary cloud detection. New channels include two split-window LWIR channels at $10.2 - 11.2\mu m$ and $11.5 - 12.5\mu m$, and on GOES, a mid-wavelength infrared (MWIR) channel at $3.8 - 4.0\mu m$. The new satellites provide all channels simultaneously on a full-time basis. The geostationary algorithm exploits these new channels, when available, through the addition of multispectral cloud tests similar to the AVHRR tests described above. The algorithm automatically determines which tests are applicable based on the individual sensor configurations.

3.4 Cloud Layering and Typing

Vertical stratification of the cloud data into layers is accomplished using a single cloud layering algorithm for all geostationary and polar orbiter satellite data. The layering algorithm only operates on LWIR channel data from pixels previously classified as cloudy by the appropriate Level 2 processing algorithm. A three-step procedure is used: first a maximum likelihood classification algorithm is applied to separate the LWIR brightness temperature data into thermally homogeneous layers. Next each pixel is assigned a cloud type using local spatial information. The final step consists of accumulating the pixel data into 16th mesh grid cells, clustering of the pixels into local cloud layers, and assigning a predominant cloud type to each layer.

Cloud layering begins by stratifying the cloudy LWIR brightness temperature data over a large region (on the order of a few thousand scan lines) using a generic unsupervised clustering algorithm. The clustering process defines homogeneous groupings within the spectral domain of the input data. User input controls the minimum spectral distance between pixel temperatures and the cluster centroid but the maximum number of layers is left a free parameter. Once clusters are defined a Bayesian maximum likelihood classifier is used to assign each pixel to a cluster. Clusters are now treated as vertical slices through the atmosphere based on an inverse relationship between cluster-mean brightness temperature and height.

Cloud typing occurs by analyzing data one layer at a time starting from the top-most (coldest) layer. Each pixel and its contiguous neighbors are grouped using a region growing routine. The number of contiguous pixels in each group is used to assign a cloud type classification of either stratiform or cumuliform. A number threshold is used to make the assignments such that groups with pixel counts below the threshold are classified cumuliform and those above as stratiform. The region growing and type assignment process continues for each group in the layer until all pixels assigned to that layer by the maximum likelihood classifier have been processed. Subsequent processing moving from high to lower (cold to warmer) layers is accomplished by combining all the pixels from higher layers with the pixels of the current layer before the region growing process occurs.

9

Cloud type assignment occurs as before but only for pixels in the current layer, pixels in higher layers that were previously assigned a cloud type retain that classification even if the new grouping places them in a different category. The inherent assumption is that cumuliform clouds have a greater vertical extent than stratiform while stratiform have the larger horizontal range. By processing one layer at a time from the top down, features such as cumulus towers embedded in a lower stratiform deck will be correctly classified.

The final processing step occurs after all cloudy pixels have been assigned a cloud type. In this step cloudy pixel LWIR data are first accumulated into 16th mesh grid cells by simply identifying, based on latitude and longitude, which grid cell each pixel belongs to. Unsupervised clustering of the LWIR data is then repeated but this time on a floating window of 3X3 grid cell arrays and with the maximum number of clusters set to four. Individual pixels are then assigned to each cluster using a maximum likelihood classifier, but only for the pixels in the center grid cell of the 3X3 array. The moving 3X3 window of 16th mesh grid cells is used to establish local cloud cluster attributes for the center grid cell that minimize artificial discontinuities across grid cell boundaries. The populated clusters are interpreted as cloud layers and cluster statistics are used to compute fractional cloud amount, mean cloud top temperature, and predominant cloud type for each layer. Note that in this process each grid cell will have a maximum of four cloud layers. In this way each 16th mesh grid cell is populated, cloud layers defined, and layer statistics computed. Level 3 output parameters for each grid cell include the valid time of the satellite data, total cloud amount and, for each layer, fractional cloud amount, mean cloud top temperature, and a stratiform/cumuliform designation.

3.5 Cloud Analysis Integration

As discussed above, separate cloud analysis algorithms are used to analyze cloud spatial properties from each sensor system. At the end of Level 3 processing, three independent gridded cloud analyses have been produced: one derived from DMSP/OLS data, one from NOAA/AVHRR data, and the third from the constellation of geostationary sensors. The analyses at each cell in the three 16th mesh hemispheric grids may have a different valid time based on the time of the input satellite measurements. To create the integrated analysis, analyzed cloud data from each of the three analysis grids are input into an analysis integration algorithm to produce a single, optimal analysis based on the relative timeliness and accuracy of the input data.

The general conceptual approach to the integration problem is one that utilizes both rule-based concepts as well as principles from statistical objective analysis (Lorenc, 1981; Hamill and Hoffman, 1993). The unique nature of the satellite-derived cloud parameters drive the way in which the cloud analysis data are combined. For example, some cloud parameters such as cloud type and number of layers are discrete quantities and cannot be "averaged" in any physically meaningful way. Computational concerns also argue for applying rule-based ideas which allow the preferential selection of one satellite analysis over all others thereby avoiding weighted averaging of the data as much as possible. Additionally, the tradeoff between the relative timeliness and accuracy of the input analyses is a major consideration in the development of the integration algorithms. For instance, analyses derived from DMSP or AVHRR visible and infrared imagery are potentially more accurate than those obtained from lower spatial resolution geostationary data. However, there may be large time gaps between consecutive analyses derived from polar orbiting data while new geostationary analyses are generally available at least once per hour.

Integration of total cloud amount precedes integration of layer quantities since the estimates of total cloud fraction are believed to be more reliable than any individual layer

10

fraction (due to small sample sizes and the potential for height assignment errors). Processing occurs independently for each grid cell. First a series of rules are applied to determine if any one of the input analyses is superior to the other two. If none of the input grids have been updated since the time of the previous Worldwide Merged Analysis then the previous analysis is persisted. If new analyses are available, a check is made to determine if more than one are timely. If only one timely analysis is available, the merged total cloud fraction is set to the value of this analysis. If more than one analysis satisfies timeliness requirements, these analyses are examined to determine if they are all either completely cloudy or completely cloud free. If so, total cloud fraction is set to either 100 or 0 percent, respectively. If multiple timely analyses exist that are neither all completely clear nor completely cloudy, then an estimated error of each sensor analysis is used to determine if the most recent analysis also has the lowest estimated error. Only when all these conditions fail is an OI algorithm used to obtain a blended estimate of total cloud fraction from multiple input analyses. Averaging weights for the OI are based on estimated analysis errors computed for each available sensor analysis.

Analysis errors for each sensor analysis are computed assuming an empirically defined initial analysis error plus an additional error growth function that is linear with time. Values for initial analysis error and error growth rate are sensor-dependent and are maintained for both polar orbiting and geostationary platforms. These are tunable parameters, and as such can be used to adjust the merge processing to correct for inconsistencies.

Once integration of total cloud fraction is complete, merging of all other layer parameters is performed. A rules-based procedure similar to that used for total cloud is used to determine if the layer parameters from one analysis is superior to the others. In cases of only one timely analysis, all analyses indicating clear conditions, or when the most timely analysis is also the most accurate, then layer cloud parameters are set in the same way as total cloud amount described above. However, when all timely analyses indicate 100 percent cloud cover or in cases where the OI technique is used to determine total cloud amount the integration of layer parameters requires a more complex algorithm. This is because the vertical distribution of cloudiness and type are determined independently for each analysis and, given the different sensor characteristics, are likely to be different. In these cases one sensor analysis is selected as most reliable and is designated as a master or template profile into which all other timely analyses are blended. For discretely varying quantities such as number of layers and cloud type the integrated analysis profile will simply assume the values of the master analysis. For the continuously varying parameters of layer cloud fraction and cloud top temperature, an OI blending is performed by combining layers that most closely match in cloud top temperature.

The integration algorithm is designed to use additional information provided by multispectral observations from the NOAA/AVHRR and multispectral geostationary sensors. In particular, cloud algorithms developed for these sensors are assumed to better detect the presence of low cloud and transmissive cirrus. Once the integration of all cloud parameters has been performed, the analysis grid box is then checked for the possible addition of these cloud types. This is achieved by imposing separate, less strict timeliness constraints for these special-case clouds. This effectively extends the length of time that these observations will affect subsequent merged analyses. Similarly, conventional, surface-based observations of low cloud are also used to extend the length of time satellite-based low-cloud analyses are used in the merged analysis.

Final output parameters for each 16th mesh grid cell are now computed. Total cloud amount is the total number of cloudy pixels in the grid cell divided by the total number of pixels. Layer fractional cloud amount is computed in the same way as total cloud for the

coldest (top) layer. Cloud top altitude is computed by interpolating temperature/height profile information to the mean cloud top temperature. Cloud type is assigned the most prominent cloud type in the master analysis. A representative time is assigned as the time of the most recent sensor-specific analysis used to produce the merged analysis.

4. SERCAA Phase II

Existing cloud analysis technology does not combine the cloud information measured by diverse sensors. For example, the input satellite data which support the SERCAA Phase I algorithm suite (Gustafson et al., 1994) utilizes only cloud imager data. Furthermore, outputs of the SERCAA Phase I algorithm treat only cloud spatial properties including cloud coverage, cloud layering, and cloud type. The success of overall cloud depiction and forecast improvements for short and extended ranges is dependent on characterization of atmospheric state. The SERCAA Phase I algorithms provide the basis to address requirements for improved specification of cloud initial state for short range forecasts by improving initialization of cloud macrophysics: cloud cover, layers, and heights. For these reasons one objective of the Phase II effort has been to identify approaches to synergistically combine information from both cloud imagers and other sensors such as sounders aboard current platforms to enhance overall cloud analyses.

These algorithms complete the cloud depiction with enhanced parameters such as cloud environment, microphysics, and radiative parameters which are required for cloud forecasting over longer time scales.

4.1 Cloud Detection Using Visible and Near-Infrared Bidirectional Reflectance Distribution Models

The Earth's surface varies widely on a global scale, from deserts to tropical forests to permanent snow and ice cover. Vegetated surfaces and snow cover also vary for a given Earth location as a function of time, both diurnally and seasonally. Surface-based observations of these characteristics are extremely limited both spatially and temporally, and are of limited use in monitoring changes in the Earth's surfaces over longer term, climatic time scales. Satellite sensor observations provide the only truly global measurements of the Earth's surface. Thus observations and monitoring of the Earth's surface are best provided by satellite radiance measurements.

The manner in which a particular surface type reflects incident solar energy (as a function of solar position and the direction from which that surface is viewed) is a fundamental property of the surface. This property is depicted by means of a bidirectional reflectance distribution function (BRDF), which is a mathematical representation of a surface's dependence of reflected energy on the illumination and viewing geometries. BRDFs describe the manner in which surfaces reflect incident solar radiation as a function of the satellite view and solar illumination geometries. Knowledge of BRDFs allows for directional correction (normalization) of satellite radiance data via anisotropic correction factors to a standard view and illumination geometry. Such a capability helps to reduce errors in computed derivatives from visible and near-infrared radiance data such as vegetation indices. BRDFs are of importance in remote sensing for computing location-dependent albedos of the Earth's surface on a global scale.

Modeled BRDFs allow for prediction of visible and near-infrared satellite radiances for a particular location on the Earth's surface prior to the actual measurements of the satellite radiances themselves. Thus, the BRDF-predicted clear-scene anisotropic

correction factors are of particular use in the SERCAA cloud detection model for analyzing visible data from multiple satellite observations of the Earth's surface over varying times and viewing geometries.

In order to estimate an Earth-surface BRDF, a series of reflected radiance measurements from the surface over a range of viewing and solar illumination geometries are required. It is important that these observations not be influenced (contaminated) by clouds or their shadows. Thus corrections are performed to ensure that the cloud-free AVHRR radiance observations used to compute surface BRDFs contain only surface effects. In this study, BRDF models are retrieved to estimate the clear-scene radiance for each 1-km pixel in a series of AVHRR satellite image scenes of New England during a 17-day period in September 1994. Each scene has differing solar illumination and satellite viewing geometries. The observed radiance in each AVHRR pixel is compared to its corresponding BRDF-predicted clear-scene radiance for the appropriate view and illumination geometries and any value that exceeds the predicted clear-scene value is flagged as cloud. Cloud detection results are then compared digitally to manually cloud-cleared AVHRR data taken over New England.

This study has five main steps: (1) collocation of all AVHRR data to a common 1-km Cartesian grid projection using orbital prediction models and visual landmarks (e.g., Cape Cod) observable in the images to map the data; (2) cloud clearing using spectral signature cloud detection tests similar to those of Saunders and Kriebel (1988) and Gustafson et al. (1994); (3) correction of the clear-scene 0.63-μm visible and 0.86-μm near-infrared AVHRR radiances for atmospheric scattering effects using a coupled surface-atmospheric radiative transfer model; (4) fitting six semi-empirical BRDF models to the cloud-cleared and atmospherically corrected clear-scene radiances; and (5) application of the BRDF models to cloud detection.

The NOAA AVHRR dataset used in this study consists of 17 morning-descender orbits of NOAA-10 and NOAA-12 between 3 and 20 September 1996. These data are first mapped to a 400 x 402 Cartesian grid centered over New England, shown in Figure 1. Grid resolution is 1.1 and 0.75 km in the column (north-south) and row (east-west) directions, respectively, corresponding to the nominal along- and cross-track AVHRR HRPT scanner FOV resolutions. Choosing these grid attributes minimizes pixel over- and undersampling during the remapping process. Using orbital prediction models and manual rubber-sheeting software, the two-dimensional remapping residuals for over 500,000 pixels were on average only 0.3 km, or approximately 30 percent of pixel size. This high remapping accuracy minimizes any BRDF retrieval inaccuracy that may be caused by pixel collocation errors.

The visible and NIR data are next atmospherically corrected using surface visibility observations to define the aerosol profile in the MODTRAN atmospheric radiative transfer code. In general, atmospheric scattering effects cause the upwelling satellite-measured reflectance to be less than that of the surface itself. Next are described the cloud-clearing tests used on the New England data.

4.1.1 Spectral Tests for Cloud-Clearing

Seven tests that exploit the spectral attributes of the AVHRR data were used in this study to detect cloud and cloud-contaminated pixels. Each test was run individually on a pixel-by-pixel basis. If any of the tests detected cloud, then that pixel was considered cloudy and not used in subsequent BRDF clear-scene characterizations. In the following

13
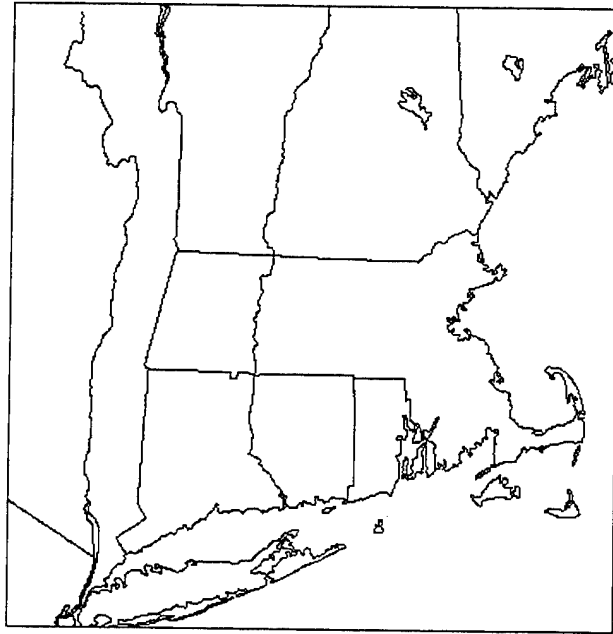
Figure 1. The New England regional area analyzed in the BRDF study.

paragraphs, A_1 denotes the AVHRR Ch1 0.63-μm visible albedo; A_2 denotes the Ch2 0.86-μm near-infrared (NIR) albedo; T_3 denotes the 3.7-μm Ch3 middle-wavelength infrared (MWIR) brightness temperature; and T_4 and T_5 denote the 10.7- and 11.8-μm Ch4/Ch5 long-wavelength infrared (LWIR) brightness temperatures, respectively. The nadir resolution of all five AVHRR channels is 1.1 km.

4.1.1 Spectral Tests for Cloud-Clearing

Seven tests that exploit the spectral attributes of the AVHRR data were used in this study to detect cloud and cloud-contaminated pixels. Each test was run individually on a pixel-by-pixel basis. If any of the tests detected cloud, then that pixel was considered cloudy and not used in subsequent BRDF clear-scene characterizations. In the following paragraphs, A_1 denotes the AVHRR Ch1 0.63-μm visible albedo; A_2 denotes the Ch2 0.86-μm near-infrared (NIR) albedo; T_3 denotes the 3.7-μm Ch3 middle-wavelength infrared (MWIR) brightness temperature; and T_4 and T_5 denote the 10.7- and 11.8-μm Ch4/Ch5 long-wavelength infrared (LWIR) brightness temperatures, respectively. The nadir resolution of all five AVHRR channels is 1.1 km.

4.1.1.1 Bright Clouds Test

The visible brightness, or "obvious bright" cloud detection test is a single-channel threshold test that is used to discriminate relatively high cloud albedos from a uniformly low-albedo New England background. If

$$A_1 > A_{1,Land},$$

(1)

14

then the pixel is cloudy. $A_{1,Land}$ was chosen to be 0.05, which is a liberally high estimate for vegetated surfaces. This test is designed to ensure that clouds with obviously high reflectivities do not go undetected by subsequent spectral tests.

4.1.1.2   Cold Cloud Tests

The "obvious cold" cloud detection test is a single-channel LWIR threshold test that is used to discriminate very cold clouds from a warm background. If

$$T_4 < T_{Land}, \tag{2}$$

then the pixel is cloudy. T_{Land} was chosen to be 273 K, which for September in New England is liberally low. Like the bright test (Eq. 1), this test is designed to ensure that clouds with obviously low temperatures do not go undetected by subsequent spectral tests.

4.1.1.3   NIR-Visible Ratios

This ratio test compares the relative magnitudes of visible and NIR albedos using an interchannel ratio. For clouds, the AVHRR Ch1 and Ch2 albedos are very close to each other, while for vegetated land surfaces the Ch2 NIR albedos are much higher then the corresponding Ch1 visible albedos. Thus if

$$R_{Lo} < A_2 / A_1 < R_{Hi}, \tag{3}$$

then the pixel is cloudy. Clear-land ratios generally have values greater than one, while water ratios have values less than one. In this study $R_{Lo} = 0.80$ and $R_{Hi} = 1.25$ generated very good cloud detection results. The ratio test defined by Eq. (3) also detects coastlines and sub-pixel-sized ponds and lakes quite well, since they are mixed fields of view (i.e., water and land).

4.1.1.4   Low Clouds and Fog

The low cloud and fog test exploits the different radiative characteristics of water droplet clouds in the MWIR and LWIR spectral regions. Low clouds effectively reflect MWIR solar energy as well as emit MWIR thermal energy, while at LWIR wavelengths the clouds essentially only emit thermal energy. Since the upwelling MWIR radiance contains both a solar and terrestrial emission component, the result is that the Ch3 observed brightness temperature for a daytime low cloud is higher than the corresponding Ch4 brightness temperature. Thus if

$$T_3 - T_4 > 5\,K, \tag{4}$$

then the pixel is classified as cloud-filled. All liquid water droplet clouds will reflect enough solar MWIR energy to make T_3 higher than T_4 in the daytime.

4.1.1.5   Thin Cirrus

Split-window LWIR $T_4 - T_5$ brightness temperature differences exhibit small but persistent thin cirrus cloud signatures. There are three radiative effects that combine to

provide this result: (1) ice particle emissivities are slightly lower at 11.8μm than at 10.7μm; (2) atmospheric water vapor attenuation is stronger at 11.8μm; and (3) there is a slightly stronger dependence of Planck radiances on temperature at 10.7μm, so that for thin cirrus pixel radiances that have contributions from warm backgrounds and cold clouds, the 10.7μm T_4 is higher for any given combination of cloud and underlying surface temperatures, all other effects neglected. Thus if

$$T_4 - T_5 > T_{Ci} , \tag{5}$$

then the pixel is classified as cloud-filled. For this study the thin-cirrus LWIR brightness temperature difference T_{Ci} was chosen to be between 2 and 2.5 K, with higher differences for longer atmospheric path lengths and higher water vapor concentrations.

4.1.1.6 Cloud Shadows

Cloud shadows as well as clouds contaminate upwelling surface-reflected energy, so their effects must be removed from the AVHRR data before using them to retrieve surface BRDF models. Cloud shadows have distinctively low NIR albedos in comparison to vegetated land albedos at 0.86μm. Thus if

$$A_2 < A_{2,Land} , \tag{6}$$

the pixel is classified as containing cloud shadow, or a pond or lake. For this study, $A_{2,Land}$ was chosen to be 0.042.

4.1.1.7 Adjacency Effects

To ensure that the scattering effects of cloud edges into adjacent cloud-free pixels do not enter into the Earth-surface BRDF model calculations, any pixel that is adjacent to a cloud edge is flagged as cloud-contaminated and is not used in subsequent BRDF retrievals. Figure 2 illustrates the cloud mask obtained for the NOAA-12 AVHRR image collected at 1221 UTC on 12 September 1994. The mask represents the combined results of each of the cloud tests, and in this case masks out 48 percent of the land pixels in the image.

4.1.2 BRDF Models

Each of the BRDF models tested under this study is semi-empirical in nature; such a model has the general form

$$I = f_{iso} + f_{geo} K_{geo} + f_{vol} K_{vol}, \tag{7}$$

where I is the directionally dependent radiance; the scalars f_x are multivariate regression co-efficients whose values are influenced by the sub-pixel morphologic and spectral reflec-tance attributes of the vegetated surface; and the kernels K_x are deterministic predictors that carry information pertaining to the basic shape of the BRDF, and are analytic functions of
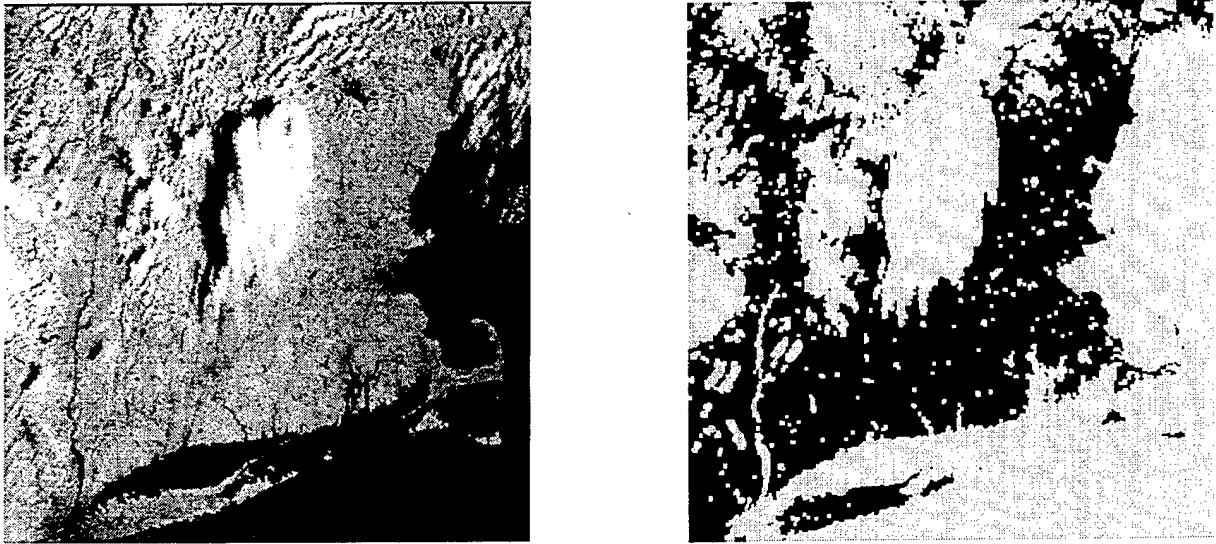
Figure 2.   AVHRR sample image valid 1221 UTC 12 September 1994 (left), and its
            associated manually digitized cloud mask generated using Eqs. 1-6.

the solar illumination and satellite viewing geometries. Kernels are independent of wave-
length and the parameters f_{iso}, f_{geo}, and f_{vol}. If the surface being viewed reflects isotropi-
cally, I is constant for all observations at a given solar zenith angle and Eq. (7) would
reduce to $I = f_{iso}$ (the iso subscript denotes isotropic), independent of view and illumination
geometries. The component of diffuse reflectance by the vegetated surface is represented
by f_{geo}, and includes such effects as shadowing by vegetation canopy elements arranged in
particular geometric fashions. Scattering of radiation (e.g., by leaves or pine needles)
within the canopy volume is represented by f_{vol}. In general, a BRDF that is estimated
using satellite measurements will be a nontrivial linear combination of these isotropic, geo-
metric, and volume-scattering components. Alternatively stated, the f_x parameters in Eq.
(7) will be nonzero. In theory, the relative magnitudes of these parameters designate the
comparative importance of the three reflective effects that define the overall characteristics
of the BRDF of a surface (after Roujean et al., 1992). The kernels K_x are approximations
to deterministic, physical models of radiative transfer in vegetated canopies. Accordingly,
BRDF models of the form given by Eq. (7) are semi-empirical in nature. For a given scene
they describe the association between observed cloud-free radiances and the view and
illumination geometries under which those radiances were measured. Although the
association is (strictly speaking) statistical in nature, the hope is that the deterministic origin
of the kernels argues for the cause of association in a more physically rigorous manner.

Using the cloud-cleared and atmospherically corrected New England AVHRR LAC
data taken during September 1994, six semi-empirical BRDF models were tested on a
pixel-by-pixel basis for their ability to accurately characterize the directional dependences
observed in the satellite radiance measurements. The models are (1) the Ross Radiative
Transfer (RT) model (Ross and Marshak, 1985) for thick canopies; (2) the Ross RT model
for thin canopies; (3) the Roujean geometric optical (GO) model with no mutual shadowing
(Roujean et al., 1992); (4) the Li GO model for dense canopies, which is based on the Li-
Strahler GO model (Li and Strahler, 1992) with mutual shadowing, driven by illuminated
crowns; (5) the Li GO model for sparse canopies, which is based on the Li-Strahler GO

17

model (Li and Strahler, 1992), driven by shadows on the ground; and (6) the modified Walthall model (based on Walthall et al., 1985). Each of these BRDF models has the general form specified by Eq. (7).

4.1.3 BRDF Retrieval Estimates

Cloud-free AVHRR data were then fit to the BRDF models to determine their respective abilities to describe the observed directional dependence of the radiances. Recall that the kernels K_x in Eq. (7) are analytic functions of scene-solar and satellite zenith and azimuth angles. Each cloud-free AVHRR radiance I for a given pixel is first associated with its set of kernels given that pixel's view and illumination geometries. Next the 17-day full set of these radiance-kernel triplets is assembled for each pixel in the New England 402 x 400 Cartesian grid. Finally, the f_x parameters in Eq. (7) are computed in a least-squares sense to provide the best available overall fit to the semi-empirical BRDF models. Comparative goodness-of-fit measures include statistical R^2 hypothesis testing that demonstrates both the strength (via test statistic) and significance of association (via the magnitude of R) between the observed directional AVHRR radiance measurements I_{obs} and the overall BRDF models that predict I_{obs} as a function of the satellite view and solar illumination geometries (Eq. 7).

Figure 3 shows the cloud-clearing results for the 17-day New England dataset. In order to determine the semi-empirical BRDF model that best describes surface anisotropic reflection attributes, a minimum of eight clear- pixel observations must be available for a given pixel. Only 35 percent of the pixels in the New England grid have this minimum number of cloud-free observations. The majority of pixels with enough cloud-free radiance observations occurred in southern and eastern New England. Clouds inhibited BRDF retrievals primarily in the Green and White Mountains.

Figure 4 shows the results of the best-fit BRDF models in the New England grid projection. At this point the best-fit multivariate regression coefficients f_x, the kernels K_x, and the model choices "x" have been determined for each pixel. Thus a mathematical representation of the anisotropic reflectance attributes of each surface in the grid has been obtained. The representation is written in the form given by Eq. (7) as an analytic function of the satellite view and solar illumination geometries, and therefore can be used to predict the clear-scene reflectance of a pixel's surface prior to observation of that surface by satellite. Next, the satellite-observed radiance will be compared to the predicted radiance and any values that exceed the predicted clear-scene value will be flagged as cloud.

4.1.4 Cloud Detection Results

The retrieved BRDFs were next used to cloud-clear an AVHRR test image taken during the same 17-day time period. First, Eq. (7) was used to predict the visible (Ch1) and NIR (Ch2) satellite-observed reflectances for a number of pixels in the test image. Next, the BRDF prediction was directly compared to the radiance observation of each test pixel. Any observed value that exceeds the predicted clear-scene value is flagged as cloud. Cloud detection results are then compared digitally to the manually digitized AVHRR cloud mask obtained during the cloud-clearing process.

Table 1 lists the results of the BRDF cloud clearing. Let "r" denote the BRDF clear-scene reflectance (which is linearly proportional to I_{obs} in Eq. (7)). When r is compared directly to the visible satellite observation, a correct determination of cloud presence is achieved 66 percent of the time. If the threshold r is allowed to vary to within 5 percent of

Figure 3.   17-Day composite cloud mask for AVHRR morning overpasses between 3-20
September 1994.

Figure 4. Map of Ambrals kernel combinations obtained for the 17-day AVHRR Sept 94 dataset.

its actual value, cloud detection accuracy increases dramatically to 89 percent. Table 1 lists a nearly perfect cloud detection accuracy when r is allowed to vary to up to 20 percent of its BRDF-predicted value. Even higher accuracies are listed for AVHRR NIR Ch2, which usually has brighter backgrounds that are more easily and more often confused with cloud than those of AVHRR Ch1.

Table 1.   BRDF cloud detection accuracy (%), measured against the manually digitized 1-km cloud mask.

Threshold	Visible	Near-IR
r	66	83
1.05r	89	90
1.10r	92	97
1.20r	98	99

These test results offer promise for single-channel, threshold-type cloud detection using reflected solar radiance data. BRDF techniques present alternatives to current state-of-the-art single-channel visible cloud detection algorithms that have trouble performing in scenes with high solar zenith angles and surfaces that exhibit strong anisotropic reflectance attributes, since the BRDF cloud/no-cloud thresholds explicitly depend on the solar illumination and satellite viewing geometries. Current operational cloud detection models such as the RTNEPH (Hamill et al., 1992) attempt to define clear-scene background reflectances for polar-orbiting satellite data using a nearly constant value that does not account for variations in solar zenith angle and view geometries over the course of several days.

The test results also hold promise for significantly increasing the amount of early-morning and late-afternoon visible and NIR satellite data that are used operationally by cloud models such as the RTNEPH. This is because clear-scene reflectances at these times of day vary significantly for the smallest of changes in sun-satellite positions, so much so that constant-threshold background reflectivities simply cannot provide accurate cloud detection results.

4.2   Cirrus Radiative and Spatial Properties

The transmissive nature of cirrus clouds turns out to be its most important (in a climate sense) and elusive (in a retrieval sense) attribute to specify. If the semi-transparent nature of cirrus clouds is not accounted for, its altitude is consistently underestimated when using passive infrared brightness temperature data. Although it is generally agreed that cirrus has a net warming effect on climate, determination of the magnitude of this effect depends critically on the accurate specification of cirrus radiative and spatial attributes. For example, in the case of very thin (sub-visual) cirrus, ice particles have a more significant interaction effect with incident solar and upwelling thermal radiation than does upper tropospheric water vapor (Smith et al., 1990).

4.2.1   Observation of Cirrus from Satellite

There are many sources of passive satellite data that can be used to detect and analyze cirrus attributes. Among the earliest are visible and infrared data of the 1960s from the TIROS series of polar orbiting satellites, augmented in the early 1970s by geostationary GOES data. Current GOES-Next Imager and Sounder channels useful for detection of

cirrus include 3.9, 6.7, 11.2, 12.7, and CO_2 13.3 - 14.5μm spectral bands. The 3.9, 6.7, and 11.2 and 12.7μm channels will be discussed in detail shortly; the 6.7μm water vapor band has proven useful for detection of very thin cirrus over warm backgrounds such as deserts and tropical oceans, and has use in discriminating water-droplet clouds from ice clouds in daytime 3.7/6.7-μm imagery.

More recent TIROS sensors include the Advanced Very High Resolution Radiometer (AVHRR), a five-channel passive radiometer with detectors that measure upwelling visible (0.63μm), near-infrared (NIR, 0.86μm), middle wavelength IR (MWIR, 3.7μm), and split longwave IR (LWIR, 10.7 and 11.8μm) energy both day and night. The sounder instruments collectively known as TOVS (TIROS Operational Vertical Sounder) also collect data in the wings of the 15μm CO_2 absorption band that are useful for detection of thin cirrus and specification of their height. There are also very high spatial resolution (500 m) Defense Meteorological Satellite Program data available in visible/NIR (0.4 - 1.1μm) and LWIR (10 - 12μm) bands that are helpful in ascertaining the small-scale spatial attributes of cirrus.

4.2.2 Passive Infrared Physics of Cirrus Cloud Signatures

The upwelling spectral thermal radiance I_{obs} measured by a downward pointing radiometer for a field of view completely filled by a non-reflective, thin cirrus cloud is

$$I_{obs} = (1 - \varepsilon) I_{sfc} + \varepsilon I_{cld} , \qquad (8)$$

where ε is the bulk cirrus emissivity, I_{sfc} is the upwelling radiance emitted by the underlying surface and clear atmosphere, and I_{cld} includes the cirrus blackbody radiance plus the radiance emitted by the atmosphere above the cloud. In practice, reflection from cirrus clouds at thermal infrared wavelengths is ignored. This is reasonable not only because the cirrus bulk reflectivity is low, but also because there is only minor downwelling thermal emission incident on the top of cirrus clouds to be reflected back to space. In theory the specification of I_{sfc} in equation (8) requires information on many of the physical properties of the atmosphere and surface that underlies the cirrus cloud: the temperature T_{sfc} and atmospheric transmittance τ (for water vapor attenuation) are two of the more important attributes. As discussed later, I_{sfc} is specified using nearby measurements of cirrus-free pixels.

The two unknowns of interest in Eq. (8) are the cirrus bulk emissivity ε and the cirrus Planck blackbody emission I_{cld}, which is a known function of the cirrus effective temperature T_{cld}. In contrast there is only one known in Eq. (8), namely the radiance measurement I_{obs}. In order to specify these two unknowns, additional measurement information is needed. This is achieved first by considering Eq. (8) for simultaneous radiance measurements at two different infrared wavelengths.

For purposes of discussion, assume that the radiance data are being measured by the AVHRR MWIR Channel 3 and LWIR Channel 4 sensors. The two cirrus radiance equations are then

$$I_{obs,3} = (1 - \varepsilon_3) I_{sfc,3} + \varepsilon_3 I_{cld,3} \qquad (9a)$$

and

$$I_{obs,4} = (1 - \varepsilon_4) I_{sfc,4} + \varepsilon_4 I_{cld,4}, \qquad (9b)$$

where the 3 and 4 subscripts denote the 3.7 and 10.7μm AVHRR Channels 3 and 4 radiances, respectively. Eqs. (9a) and (9b) are two equations, but with the second equation a third unknown ε_4 has been introduced. A third equation is needed that contains no new variables and that relates at least two of the three unknowns already established. This is

done by assuming a relationship between the cirrus bulk optical depths δ_3 and δ_4 as follows. First, radiative transfer calculations are available that compute bulk cirrus optical depth as a function of wavelength and hexagonal ice particle size for varying cirrus cloud thicknesses (Takano and Liou, 1989; Hunt, 1973). Once computed, a simple linear regression between corresponding pairs of the two optical depths is performed to obtain a relationship of the form

$$\delta_3 = m \, \delta_4 + b \, , \tag{10}$$

where m and b are the regression slope and intercept, respectively. The slope m is nonzero; the intercept b, however, turns out to be very close to zero since the two optical depths are close to each other for optically very thin cirrus. Thus Eq. (10) is generally of the form

$$\delta_3 = m \, \delta_4. \tag{11}$$

The value of the regression slope (m) is dependent on the effective ice crystal size which in turn is dependent on cirrus temperature (after Ou et al, 1993). Values range from m=2.603 for T_{cld}= 210 K to m=1.088 for T_{cld}=253 K.

Considering the radiative properties of cirrus within a satellite field of view in a bulk sense, the cirrus cloud optical depth δ is related to the cirrus transmissivity t by the relation

$$\delta = -\ln t \, , \tag{12a}$$

so that Eq. (11) can be rewritten

$$\ln t_3 = m \ln t_4 \, . \tag{12b}$$

Since it is assumed that the cirrus cloud is non-reflective, $\varepsilon + t = 1$ so that

$$\ln (1 - \varepsilon_3) = m \ln (1 - \varepsilon_4) \, . \tag{12c}$$

Finally, solving for ε_3 in terms of ε_4 yields

$$\varepsilon_3 = 1 - (1 - \varepsilon_4)^m \, . \tag{13}$$

This is the third of the three-set equation, so that there are now three equations (9a), (9b), and (13) in three unknowns ε_3, ε_4, and T_{cld}. The three measurements consist of the linear regression slope m, and the satellite-measured radiances $I_{obs,3}$ and $I_{obs,4}$. This three-equation system forms the basis for the SERCAA cirrus retrieval techniques that analyze multispectral infrared satellite radiances.

In practice, nearby cirrus-free pixels are used to obtain accurate estimates of $I_{sfc,3}$ and $I_{sfc,4}$. Atmospheric emission above the cirrus is neglected. Cirrus reflectivity is neglected as well. As previously mentioned, this does not introduce into the retrieval process a major source of error at night, but during the daytime incident solar radiances at the shorter 3.7-μm wavelengths noticeably affect cirrus radiance measurements. The daytime problem is a challenging one. Although cirrus reflectivities are relatively small, incoming 3.7-μm solar radiation is strong enough so that measured radiances are solar-contaminated. Subsequently, Eq. (9a) is no longer accurate and the retrieval process becomes considerably more complex because of it. Thus,the use of Eqs. (9a), (9b), and (13) are presently restricted to nighttime scenes when there is no incident solar energy being reflected back to space by either the cirrus cloud itself or the underlying background. Research is ongoing to separate out the solar component in the 3.7μm daytime data (Ou et al., 1993). Another major constraint is that in assigning a single cloud temperature T_{cld} to the cirrus, it is assumed that

23

the cloud is a thin sheet that lies precisely at one atmospheric level. Clearly this is not the case. Lidar backscatter returns from cirrus clouds consistently show their complex structure on both horizontal and vertical scales. In midlatitudes their altitudes range from 6 to 13 km, and their thicknesses anywhere from 1 to 5 km and, on occasion, even higher. Thus the assignment of a single cirrus temperature is a gross one which in the case of multispectral infrared radiance retrievals results in the assignment of one effective cirrus cloud altitude. However, the severity of this constraint affects only the cirrus altitude determination. Its effects on the bulk optical properties of the cloud are far less detrimental. Nonetheless, it is important to remember that current satellite-retrieved cirrus altitudes are not an accurate assessment of the true levels at which the cirrus lie, but rather are only correct in a radiatively bulk, energy-average sense. For this reason the cirrus temperature T_{cld} and corresponding altitude z_{cld} are labeled as effective properties, since they afford little inference on the detailed vertical structure of the cloud.

In practice Eqs. (9) and (13) can also be used with AVHRR channels 3 and 5. Thus for every triplet of AVHRR infrared satellite radiance measurements $I_{obs,3}$, $I_{obs,4}$, and $I_{obs,5}$ it is possible to retrieve at sensor resolution the 3.7, 10.7, and 11.8µm cirrus bulk emissivities ε_3, ε_4, ε_5 and optical depths δ_3, δ_4, and δ_5 along with cirrus effective temperature (altitude) T_{cld} (z_{cld}).

4.2.3 Cirrus Retrievals Using 6.7-µm Water Vapor Imager Data

In light of the 3.7-µm daytime solar contamination issue, ongoing SERCAA studies are revealing that 6.7-µm water-vapor channel data can be used in place of those taken at 3.7µm. This finding is significant in that (a) the complexity of retrieving cirrus properties during daytime (due to mixed solar/thermal energy at 3.7-µm) is eliminated, and (b) there are 6.7-µm water vapor channels on all currently operational meteorological satellites, both geostationary and polar, save DMSP. Thus with the development of a 6.7-µm cirrus optical depth and effective altitude algorithm comes a capability for cirrus spatial and optical property analyses that are truly global in nature and that span the full diurnal cycle. The water-vapor cirrus retrieval physics is identical to the MWIR retrieval physics in that Eq. (9a) is written for 6.7-µm (vice 3.7-µm) satellite radiance observations. Initial retrieval results over a 10-case data set compare quite well with ground- and aircraft-based observations of cirrus clouds.

4.2.4 Cirrus Retrieval Validation Results

The figures that follow compare directly the SERCAA satellite-based cirrus retrievals with coincident ground-based 35-GHz active radar observations of cirrus base, top, and optical thickness. The ground-based data were collected by the PL Atmospheric Sciences Division TPQ-11 radar as a part of the Space-Based Infrared Systems (SBIRS) field experiment conducted over Hanscom AFB, MA and Madison, WI during mid-September 1995. Three examples are shown of cirrus altitude retrievals plotted against radar altitude observations for 2330 UTC at Hanscom AFB on 16 September 1995. Figure 5 has a predominantly blue background, is labeled G08_ORH_259_2315 across the top, and has the label 3.7-µm - 10.7-µm Emissivity in the vertical on the right-hand side. The colors on the slide are representative of the reflected power received as a function of altitude by the active 35-GHz radar, with warm colors (reds, oranges, yellows) corresponding to strong returns (optically thick clouds) and cool colors (green, cyan) corresponding to weaker returns (optically thin clouds). Dark blue denotes cloud-free radar observations. Yellow diamonds denote the SERCAA 3.7-10.7-µm satellite-retrieved cirrus altitudes that correspond with their respective coincident radar observations. As can be seen, the

Figure 5.   SERCAA cirrus altitude retrievals using MWIR/LWIR-channel data compared to coincidence TPQ-11 35 GHz radar returns over Hanscom AFB, 2315 UTC 15 Sept 95.

retrievals match well with observation. Corresponding cirrus effective emissivities are plotted in red squares against the right-hand vertical (emissivity) axis. It is seen that the retrieved emissivities are higher where the radar returns are stronger and vice versa.

Figure 6 is similar to the first, except it has the label 6.7-μm - 10.7-μm Emissivity next to the vertical axis on the right-hand side. Yellow diamonds denote the SERCAA 6.7-10.7-μm satellite-retrieved cirrus altitudes that correspond with their respective coincident radar observations. (The 3.7-μm data and the 6.7-μm data from these two examples are both from the GOES-8 Imager.) The water-vapor retrievals also match well with observation. However, there is a bias of sorts in the water-vapor altitude retrievals that weights them much more closely to the true tops of the transmissive cirrus, in comparison to the respective 3.7-μm MWIR retrievals. This bias is due primarily to the fact that in the cirrus environment there is more atmospheric water vapor than in the clear-column (i.e., cirrus-free) regions. The net result is that the 6.7-μm cirrus brightness temperature observations are more strongly influenced by this excess water vapor than are the corresponding 3.7-μm MWIR measurements (since 3.7-μm is an atmospheric window region wherein water-vapor absorption effects are minimal). However, there are two useful attributes to this bias. The first is that for the SBIRS program, cirrus cloud top altitudes are of more value than the radiative center-of-mass altitudes that the 3.7-μm data provide. The second is that in differencing the MWIR and water-vapor altitude retrievals, information on cirrus physical thickness can be inferred that has to now been unobtainable using passive infrared retrieval techniques.

Figure 7 is a simple plot of AVHRR-retrieved 3.7-μm cirrus effective altitudes with the corresponding 35-GHz radar observations. The radar-observed cirrus tops and bases are plotted as brown and cyan lines, respectively. The blue diamonds are the AVHRR altitude retrievals; they compare well with observation, as did their GOES Imager counter-parts. The green squares correspond to blackbody altitude retrievals obtained using 10.7-μm brightness temperatures that have been uncorrected for cirrus transmissive effects (i.e., assuming the cirrus is a blackbody cloud). This is the technique typically used by most cloud analysis models to compute cloud altitude for both opaque and transmissive clouds. Altitudes retrieved in this manner agree reasonably well with true cirrus altitudes wherever cirrus transmissivities are low (optically thick cirrus), as is seen on the left side of the plot. However, where cirrus is optically thin, the comparison differences are dramatic: on the right half of the plot are cirrus blackbody retrievals that differ by as much as 6 km from the true, SERCAA-retrieved cirrus altitudes. It is important to note that the green squares denote state of the art in the current Air Force operational global cloud analysis model, the RTNEPH (Hamill et al., 1992), as well as in the Phase-I SERCAA algorithms being implemented as a part of CDFS-II.

4.2.5 Summary

As a part of SERCAA cloud analysis development efforts, new and innovative multi-spectral infrared cirrus analysis techniques are being developed and successfully applied and validated to real-time cirrus detection and analysis scenarios. Integration of these and other retrieval techniques into the overall SERCAA cloud analysis allows the strongest and most reliable attributes of each technique to be combined into one comprehensive cloud analysis product that is more realistically representative of cirrus spatial and optical proper-ties than the current RTNEPH. With increasing amounts of multispectral infrared satellite data becoming available, the goal is to continue to retrieve from these data high quality augmented radiative, spatial, and microphysical properties of cirrus clouds in real-time and for climatological purposes at finer spatial and temporal resolution.

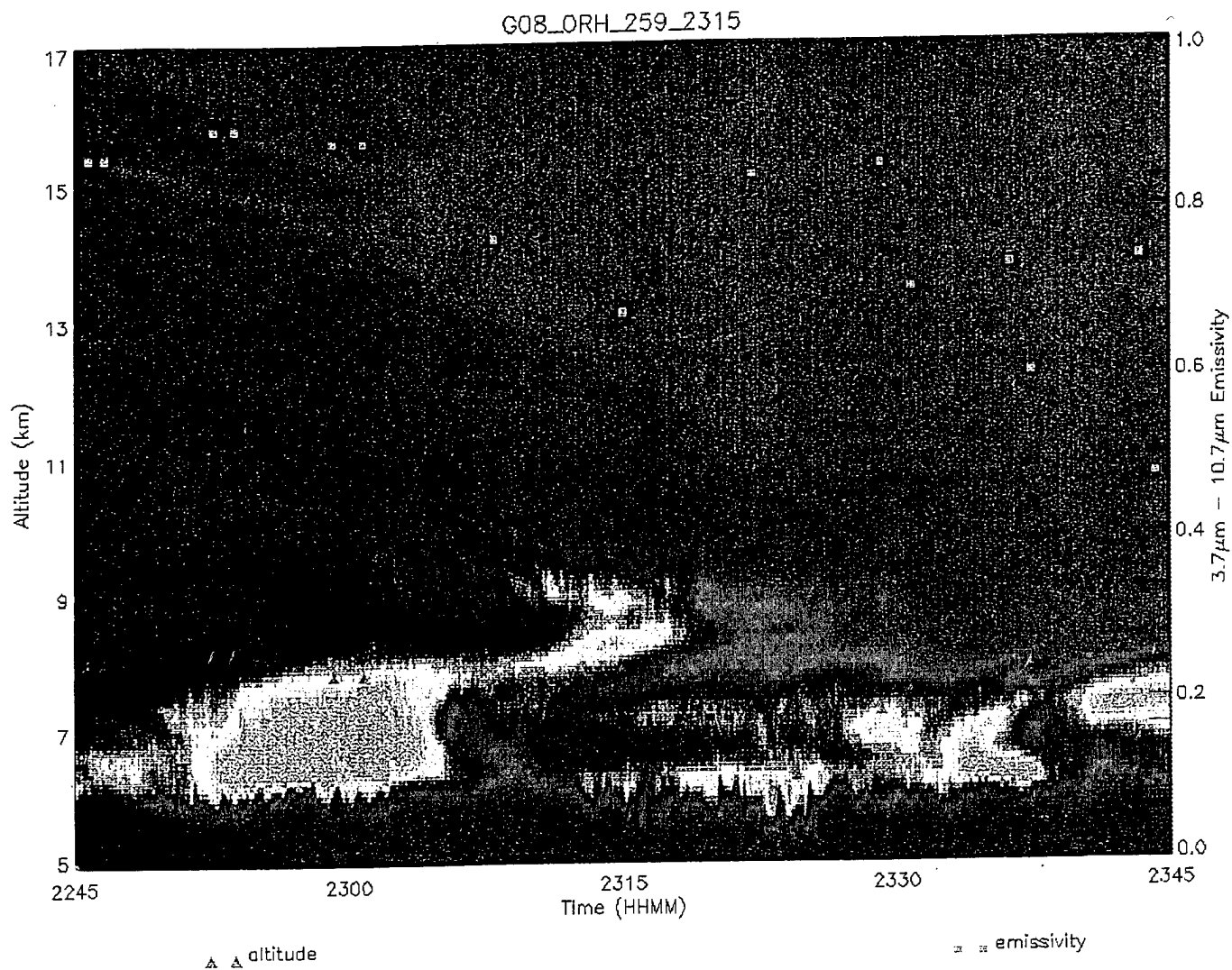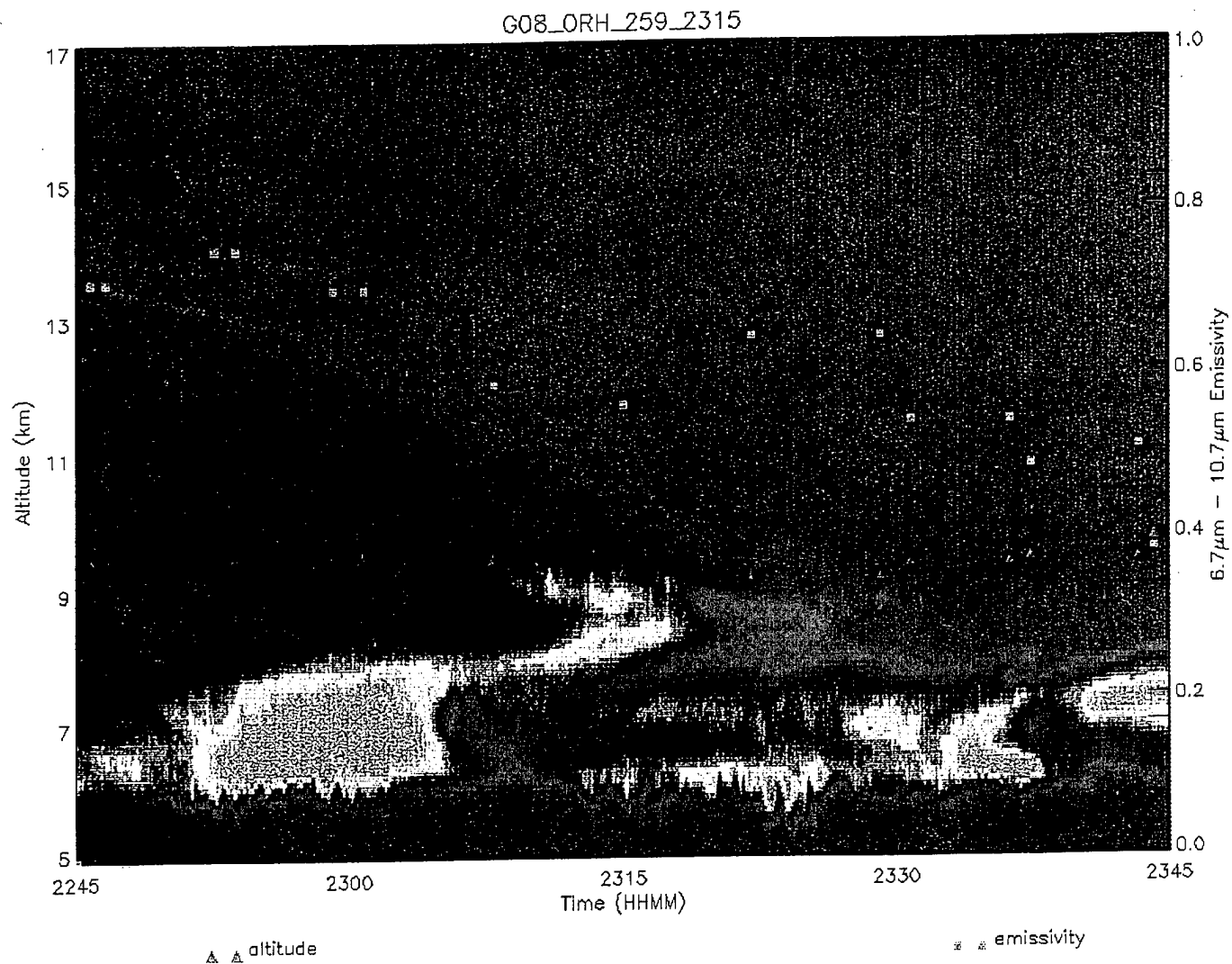Figure 6.   SERCAA cirrus altitude retrievals using Water-Vapor/LWIR-channel data
compared to coincidence TPQ-11 35 GHz radar returns over Hanscom AFB,
2315 UTC 15 Sept 95. Contrast to Figure 5 whose MWIR-channel data were
used in place of Water-Vapor-channel data.

27
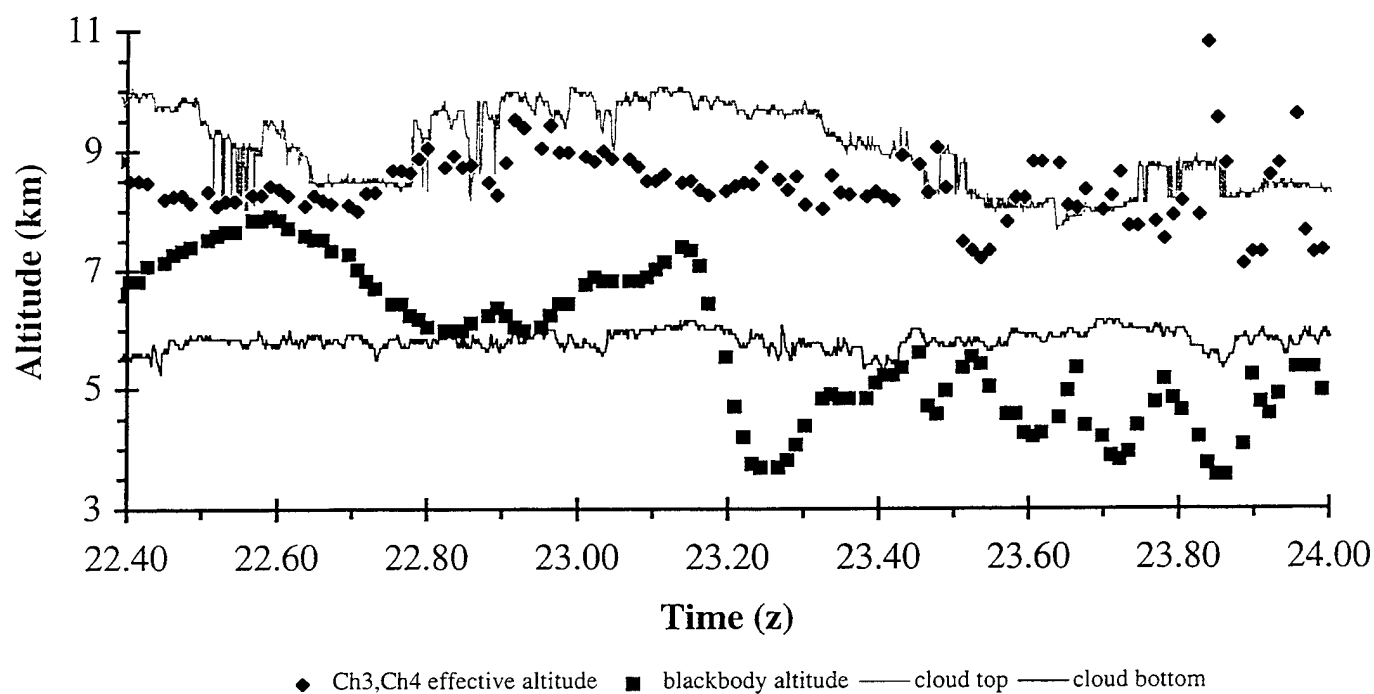
Figure 7. Plots of SERCAA and RTNEPH-derived cirrus altitudes for the cirrus samples shown in Figures 5 and 6.

4.3 Optical and Microphysical Parameters for Water Droplet Clouds

A comprehensive radiative transfer scattering theory was applied to model the response of NOAA AVHRR and GOES-Next satellite imager data to realistic variations in cloud microphysical, optical, and radiative processes. In this manner the sensitivity of multispectral MWIR-LWIR measurements to variations in the microphysical properties of liquid water-droplet clouds was assessed. Results of these theoretical computations can be applied in the development of retrieval concepts to infer cloud drop size distributions, MWIR emissivity, and normalized cloud liquid water content (LWC).

Calculations were made for the nighttime MWIR and LWIR channels of NOAA AVHRR. Atmospheric properties including relevant gas absorption profiles and aerosol scattering extinction profiles (parameterized by surface visibility) are evaluated using the multiple scattering version (Isaacs et al., 1987) of the Phillips Laboratory LOWTRAN-7 radiative transfer model (Kneizys et al., 1983). LOWTRAN standard atmospheres (tropical, mid-latitude summer/winter, subarctic, and U.S. Standard) drive the calculation of gas absorption as a function of altitude within the atmosphere. Aerosol properties (optical thickness, single-scattering albedo, phase functions) are also specified within LOWTRAN-7 by selecting an aerosol model (e.g., rural, maritime). Analogous cloud properties are based on Mie scattering calculations (Longtin and Shettle, 1988) using specified cloud-type-dependent modified gamma droplet size distributions for the cloud particles. Complex index of refraction data of Hale and Querry (1973) are used. These input data are processed by an interface routine that generates an input file for a discrete ordinate method (DOM) multiple scattering radiative transfer model that computes scattering, absorption, and thermal emission in a vertically inhomogeneous, non-isothermal atmosphere (Stamnes et al., 1988). This interface merges the gaseous, aerosol, and cloud (if present) optical properties profiles and produces the required input profiles for use by the radiative transfer model. The DOM model also accounts for bidirectional reflection and thermal emission from the Earth's surface. Reflectance functions for ocean, soil, ice, and vegetation are used to provide the required surface properties. AVHRR upwelling radiances have been calculated as a function of viewing angle, solar zenith angle, and atmospheric state (e.g., clouds, water vapor). These results were then mapped to the input cloud microphysical properties in order to determine whether a measurable multispectral MWIR/LWIR signature could be expected to uniquely specify cloud water droplet size distributions.

The DOM adding-doubling radiative transfer model was used to simulate the dependence of AVHRR radiances on cloud droplet size and cloud LWC. The effects of upwelling bandpass-weighted MWIR-LWIR radiances were determined using the modified gamma distribution of Deirmendjian (1969). This distribution characterizes cloud microphysical attributes in terms of two parameters: cloud LWC and droplet mode radius r_m. This droplet distribution is then used by the Mie scattering code to generate the angular distribution of monochromatic optical depth for the desired cloud layer attributes. Mie calculations are subsequently used by the adding-doubling model to generate theoretically-expected AVHRR upwelling radiances.

For low- and mid-level clouds, the particle density distributions of Stephens (1979) for stratocumulus (Sc) and Diem (1948) for altostratus (As) were used to specify the cloud microphysical parameters r_m and LWC. Each distribution is plotted in Figure 8.

Radiative transfer model results indicated little if any LWIR sensitivity to cloud liquid water content (i.e., cloud thickness) for a given cloud type and particle size distribution. In other words, water-droplet-cloud thermal emission at MWIR and LWIR wavelengths is independent of LWC starting at values of total liquid water as low as 17 g m^{-2}. Thus for clouds with integrated LWC of 17 g m^{-2} or higher, the modeled MWIR-LWIR brightness
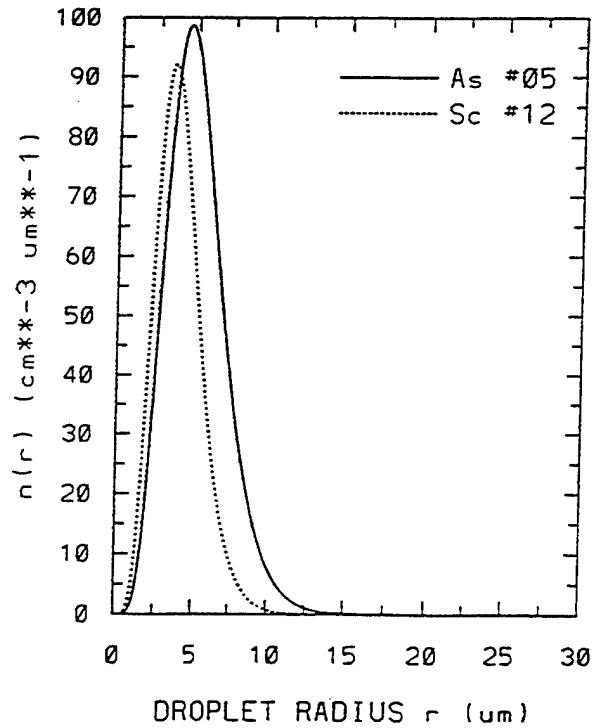
Figure 8.   Modified gamma droplet size distributions for stratocumulus (dot,dot) and altostratus (solid). Distributions are from Stephens (1979) and Diem (1948), respectively.

temperature differences are not strongly dependent on water content. The dependence of particle size distribution was investigated by parametrically varying the mode radius r_m from 2 to 10 μm. For a given view angle, there is considerable sensitivity of brightness temperature to droplet mode radius. Figure 9 shows this sensitivity for a mid-latitude summer atmosphere and a cloud of 1-km thickness whose top is at 1, 2, 3, 4, 5, and 6 km. Note that in general, larger drop sizes result in lower absolute-magnitude brightness temperature differences.

Figure 10 shows the angular dependence of brightness temperature to cloud droplet mode radius in a tropical atmosphere, for As clouds. Note in general that the absolute magnitude of the MWIR-LWIR brightness temperature difference is larger for higher satellite viewing angles, i.e., for longer atmospheric paths. This is primarily due to the increased and proportionally higher atmospheric water vapor attenuation effects at the LWIR wavelengths in comparison to the MWIR wavelengths.

Results of the radiative transfer computations were next summarized in multivariate linear regression form to obtain a closed-form relation between droplet mode radius r_m and the MWIR-LWIR brightness temperature difference T_3-T_4 and satellite view angle θ as a function of atmospheric type: tropical, mid-latitude summer, mid-latitude winter, subarctic summer, and subarctic winter. The best associations were obtained using a regression equation of the form

$$r_m = a_0 + a_1 (T_3 - T_4)^2 \cos\theta + a_2\cos\theta + a_3 (T_3 - T_4) + a_4 (T_3 - T_4)^2 . \quad (14)$$

The coefficients a_i are listed in Table 2 as a function of atmosphere (e.g., tropical, mid-latitude winter) and cloud top altitude z_{cld}, which is obtainable from the water-vapor-attenuation corrected LWIR brightness temperature. The regression errors are smaller than 10 percent. It is then possible to use Eq. (14) for a given satellite scene to determine the drop size distribution and cloud-thickness-normalized LWC given the measured MWIR-LWIR brightness temperature difference from AVHRR.

30
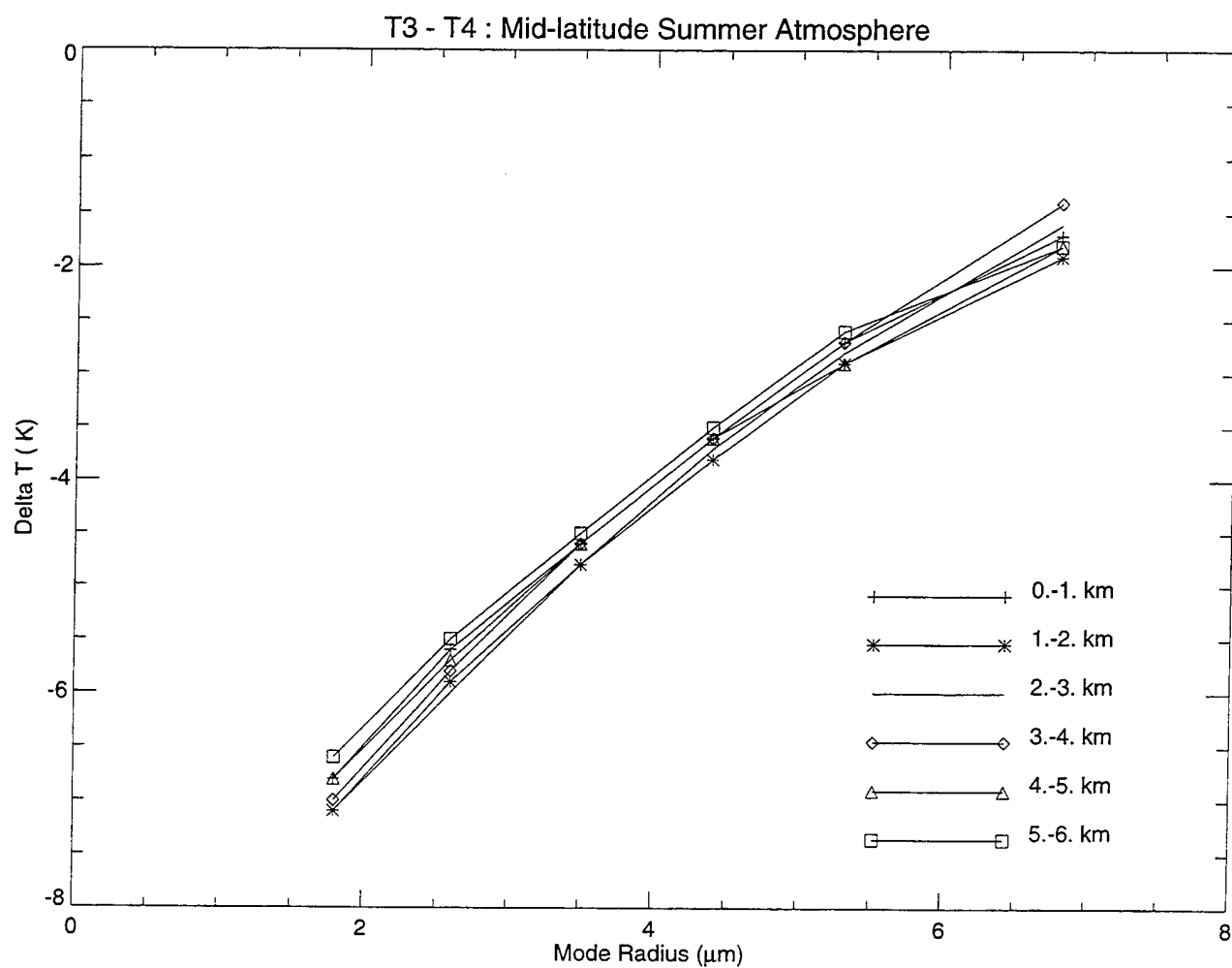
Figure 9.   Plots of nighttime MWIR/LWIR brightness temperature differences as a function of cloud top altitude for the mid-latitude summer atmosphere.
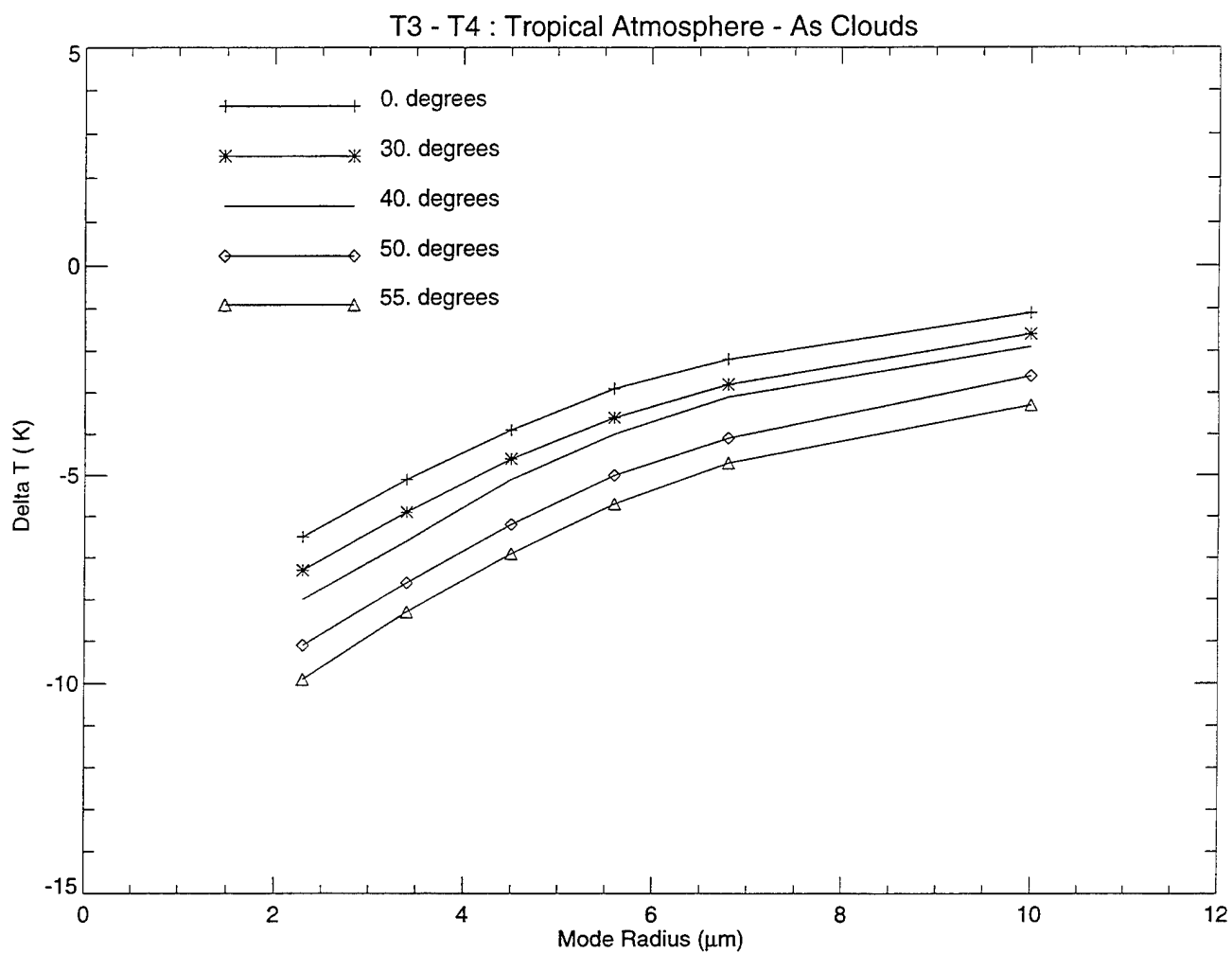
Figure 10. Plots of nighttime MWIR/LWIR brightness temperature differences as a function of satellite view angle for altostratus in a tropical atmosphere.

Table 2. Regression coefficients for Eq. (14) that yield droplet mode radius as a function of the MWIR-LWIR brightness temperature pair and the satellite look angle, for each model atmosphere.

Mid-Latitude Summer

Cld Hgt (km)	a_0	a_1	a_2	a_3	a_4
0-1km	13.8768654	0.0309042	-4.8211699	1.5821823	0.0426597
1-2km	14.2211437	0.0234482	-4.9754000	1.5184215	0.0401019
2-3km	13.8027706	0.0231690	-4.9726338	1.4157032	0.0346063
3-4km	13.2925663	0.0199931	-4.7398143	1.3609697	0.0342111
4-5km	14.4715405	0.0254101	-5.0803456	1.6378285	0.0490300
5-6km	14.3149967	0.0244705	-5.0080938	1.6739343	0.0532231

Subarctic Summer Atmosphere

Cld Hgt (km)	a_0	a_1	a_2	a_3	a_4
0-1km	13.7166748	0.0312264	-4.7909217	1.5540760	0.0404421
1-2km	13.9235210	0.0243387	-4.8280582	1.5504421	0.0433875
2-3km	13.5413494	0.0217502	-4.8088727	1.4445802	0.0377909
3-4km	13.2689419	0.0212684	-4.7162375	1.4258769	0.0381388
4-4km	14.5154686	0.0256623	-5.1110134	1.7134761	0.0546654
5-6km	13.7188549	0.0208300	-4.6964335	1.6611785	0.0558874

Tropical Atmosphere

Cld Hgt (km)	a_0	a_1	a_2	a_3	a_4
0-1km	11.9033222	0.0329830	-3.9397399	1.4436375	0.0387454
1-2km	13.6360912	0.0269514	-4.9876447	1.4249316	0.0330761
2-3km	14.2441406	0.0236156	-5.0845866	1.4694586	0.0373121
3-4km	13.0778732	0.0172403	-4.6029153	1.3105589	0.0330673
4-5km	14.2904015	0.0229082	-5.0103798	1.5672971	0.0453061
5-6km	14.1846523	0.0251303	-4.9360580	1.6399782	0.0507642

4.4 Cloud Environment

Current operational, automated cloud analysis approaches underutilize available meteorological satellite remote sensing data resources. For example, onboard the two U.S. polar orbiting satellite platforms, DMSP and NOAA, there are two different multispectral imagers, four different microwave sounders, and a multi-channel infrared sounder. Table 3 provides a compilation of the multispectral, multisensor data sources currently available from the DMSP, NOAA, and geostationary platforms. Current approaches also lack the potential to fully exploit the next generation of satellite sensors. The planned National Polar-orbiting Operational Environmental Satellite System (NPOESS) and Earth Orbiting System (EOS) will add an even greater number of sensor suites. The amount and accuracy of cloud information potentially obtainable by passive remote sensing is dependent upon the number of quasi-independent radiance measurements used in the analysis. The spectral diversity of satellite sensors is great, providing the potential to infer significant high quality cloud information.

This section provides a discussion of algorithmic approaches to utilize combined data sets of DMSP cloud imager and microwave imager (SSM/I) and microwave sounder (SSM/T-1 and SSM/T-2) data to support the inference of cloud environment parameters including vertical temperature and moisture profiles and cloud liquid water. We also address approaches to deal with some current deficiencies in nephanalysis which can be treated by combining cloud imager and other sensor data sets. These include the "black" stratus problem over land, inference of land surface temperatures in the presence of cloud, and the identification of precipitation (including thunderstorms). All of the above approaches might be considered for eventual operational implementation as extensions to the existing SERCAA Phase 1 algorithm suite. Here we focus on DMSP based approaches. Much of this work is based on applications of the unified retrieval approach for DMSP developed under separate funding.

The cloud spatial properties (coverage, layering, and type) resulting from the objective analysis of cloud imager data by the SERCAA Phase I algorithm suite result from threshold, contrast, multispectral, and temporal tests. For example, the determination of cloud presence in an individual pixel might be determined by whether satellite-measured radiance at visible wavelengths is greater than a predetermined background value or whether the radiance in neighboring channels is similar indicating a reflective (white) cloud. The analysis does not consider meteorological factors in determining the presence of cloud although it is understood that cloud environment, i.e. temperature, moisture, and attendant circulations will determine the thermodynamic characteristics for cloud presence. This problem, i.e., that of diagnosing cloud presence and properties from the properties of the generating cloud environment, is a very active area of research for general circulation modelers including those specifically interested in cloud forecasting (see Zivkovic and Louis, 1992; Nehrkorn and Zivkovic, 1996). The availability of simultaneous measures of cloud spatial properties afforded by the SERCAA Phase I algorithms and cloud environment data such as the vertical profiles of temperature and moisture alone would be extremely useful to this community.

There are other reasons for supplementing the information available from cloud imaging sensors with that from collocated sounding sensors. The specification of simultaneous vertical temperature and moisture profiles provides important information in the determination of other desired cloud parameters such as cloud top height and more complete information of cloud layering and type. Additionally, cloud liquid water content available from microwave sensors can also be used to help in cloud typing.

34

Table 3. Sensor data suite

Satellite	Sensor	Channel Wavelength/Frequency
DMSP	OLS	0.4-1.1 and 10.5-12.6 μm
	SSM/I	19.35 V&H, 22.235 V, 37.00 V&H, 85.5 V&H GHz
	SSM/T	50.5, 53.2, 54.35, 57.9, 58.4, 58.825, 59.4 GHz (O_2 absorption band)
	SSM/T2	91.5, 150, 183±1, 183±3, and 183±7 (H_2O absorption band)
NOAA	AVHRR	0.58-0.68, 0.725-1.10, 1.58-1.64[1], 3.55-3.93, 10.3-11.3, 11.5-12.5 μm
	HIRS	0.69, 3.76, 4.00, 4.13, 4.40, 4.46, 4.52, 4.57, 6.72, 7.33, 9.71, 11.11, 12.55, 13.35, 13.64, 13.97, 14.22, 14.49, 14.71, 14.95 μm (CO_2, N_2O, O_3, and H_2O absorption bands)
	MSU	50.30, 53.74, 54.96, and 57.95 GHz (O_2 absorption band)
GOES	imager	0.55-0.75, 3.8-4.0, 6.5-7.0, 10.2-11.2, 11.5-12.5 μm
GMS	imager	0.5-0.75, 10.5-12.5 μm
METEOSAT	imager	0.5-0.9, 5.7-7.1, 10.5-12.6 μm

[1] 1.6 μm channel will first fly on NOAA K ~1997

Temperature profile data can be used to determine cloud top heights (or equivalently, pressures). When cloud is determined to be present in a pixel, the cloud imager equivalent black body brightness temperatures (EBBT) for that cloudy pixel is available. In order to transform this EBBT into a cloud top height, two procedures are required. First, estimation of water vapor continuum effects on the infrared window measurements can be made based on the relevant column integrated water vapor amount obtained from the moisture profile (see below). Second, the temperature profile can be used to assign a cloud top height (or pressure) to the corrected EBBT.

The SERCAA Phase I cloud layering approach clusters cloud imager equivalent black body brightness temperatures (EBBT) into defined layers. Layers are characterized by their presence and the resultant cloud top EBBT. In analog to the pixel-by-pixel discussion of cloud top height in the preceding paragraph, temperature profile information can be used to make layer height (pressure) assignments as required.

Vertical moisture profiles provide both the vertical distribution of water vapor and the total integrated water vapor. In conjunction with the retrieved temperature profiles, the vertical moisture profiles provide simultaneous relative humidity information. Integrated water vapor from the cloud top to space is necessary to estimate water-vapor-continuum

effects on infrared window measurements. The impact of water vapor absorption is to decrease the EBBT seen by the sensor. This effectively raises the cloud top height determined if water vapor absorption were not considered. In tropical atmospheres where the burden of water vapor is large, this effect may be important in the determination of cloud top heights, especially for low clouds (since most of the water vapor is near the surface).

Microwave imager (SSM/I) and millimeter wave moisture sounder (SSM/T-2) data can be used to infer integrated cloud liquid water content. Integrated cloud liquid water content available from microwave sensors can also be used to help in cloud typing. In general integrated cloud liquid water content is largest for bright, low clouds and smallest for darker, higher clouds.

In our previous work, we have described a unified retrieval (UR) algorithm applicable to the Defense Meteorological Satellite Program SSM/T-1, SSM/T-2, SSM/I microwave sensors which employs physical retrieval concepts and utilizes the full multispectral information content of the available data (Isaacs, 1987; Moncet and Isaacs, 1992, 1994; Moncet et al., 1996). The UR algorithm is a general non-linear physical retrieval algorithm for the simultaneous retrieval of temperature profiles, water vapor profiles, cloud liquid water content, surface temperature and surface emissivity from the DMSP multi-sensor platforms. The UR concept offers the distinct advantage of simultaneously characterizing the atmospheric and surface state vector from the available multifrequency sensor observations by combining the traditionally separate functions of atmospheric sounding and surface property imaging. Through the physical retrieval process, it intrinsically recognizes the dependence of atmospheric properties on the observed background and surface properties on atmospheric transmission effects.

The potential usefulness of cloud environment information available from DMSP microwave sounding sensors to enhance IR based automated cloud detection is illustrated by examining the problem of detecting so-called "black stratus" clouds (Moncet et al., 1996). Black stratus, which is problematic to most IR cloud detection schemes including the SERCAA Phase 1 algorithms, refers to low level clouds that form within an inversion layer at night as the surface cools. Common at high latitudes, particularly during winter, these clouds are difficult to detect using satellite data because their radiative signature is greater than of the underlying surface. IR threshold satellite cloud detection schemes generally require surface-to-cloud contrast in either an infrared-channel brightness temperature or visible-channel brightness in order to detect a cloud. However, since the black stratus are warmer than the surface any infrared signature that can be detected by the satellite will be in the wrong direction (i.e., clouds are assumed to be colder than the surface). Similarly, since black stratus tend to occur under limited or no sunlight conditions (e.g., high latitude winter) or over reflective snow or ice backgrounds, reliance on visible cloud signatures is severely restricted.

Working collaboratively with the SERCAA Phase II team, Moncet et al. (1994) formulated an algorithm to treat "black stratus" detection. The algorithm illustrated in Figure 11 uses both IR imager brightness temperatures applied to a simple threshold algorithm similar to the one currently used in SERCAA Phase I for the processing of the

OLS IR Brightness Temperature

Microwave Derived Temperature Profile and Surface Skin Temperature (T_{skin})

NO INVERSION		INVERSION		
$IR < T_{skin} - \Delta T_0$	$IR \geq T_{skin} + \Delta T_0$	$IR < T_{skin} - \Delta T_1$	$T_{skin} - \Delta T_1 \leq IR \leq T_{skin} + \Delta T_2$	$IR > T_{skin} + \Delta T_2$
Cloud (Type 4)	Clear (Type 1)	Cold Cloud (Type 3)	Clear (Type 2)	Warm Cloud (Type 0)
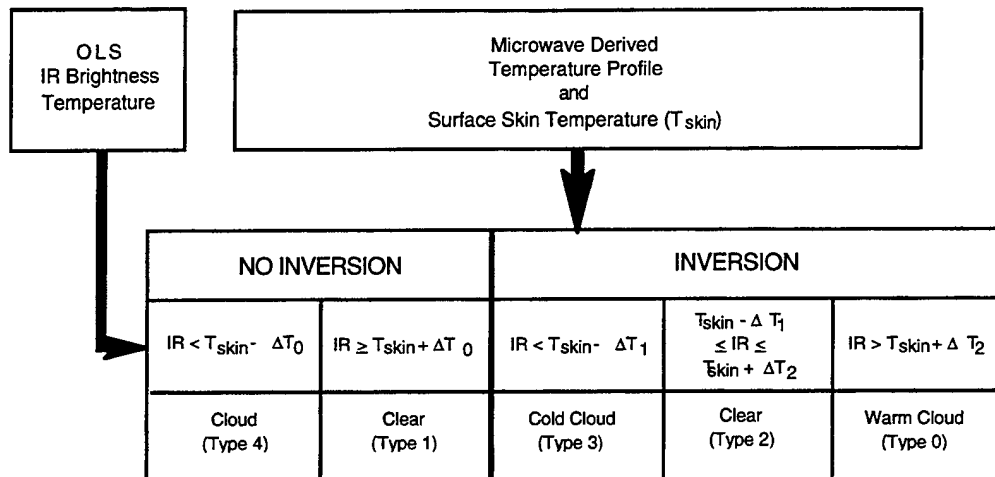
Figure 11. Schematic of a prototype infrared cloud detection scheme that integrates microwave derived information.

OLS infrared data. Additionally, however, it uses microwave sensor retrieved temperature profiles and surface skin temperatures to identify and classify inversion conditions. Like the SERCAA Phase 1 OLS algorithm, a cloud is detected if the IR measured brightness temperature is colder than the estimated surface skin temperature by some pre-set margin under so-called "normal" conditions. However, when an inversion is present, the algorithm also detects a low cloud if the IR brightness temperature is warmer than the surface temperature (i.e. the black stratus condition).

Moncet et al. (1994) illustrate an example applying this algorithm over snow/ice fields based on data from the DMSP SSM/T-2 Calibration/validation effort (Falcone et al., 1992) using DMSP 5D-2 data. While additional validation of the algorithm is required, the approach integrates well into the overall SERCAA algorithm suite framework.

The existing imager based cloud analysis approaches for the infrared LWIR channels are based on discriminating cloud (usually cold; except in the case of black stratus described above) from the warmer, cloud-free background. The determination of cloud free background temperatures is supported by the cloud imager LWIR data itself (using adjacent cloud free pixels). This becomes problematic in overcast situations. One approach is to rely on model predicted surface temperatures (as in the use of the SCFTMP model by AFGWC). Practice indicates that these may be inaccurate resulting in over or underanalysis of cloud. Kopp et al. (1994b) discussed the use of SSM/I derived surface temperatures in improving results of the RTNEPH model at AFGWC. In their application, SSM/T surface temperatures are used along with those of SFCTMP based on a weighting determined within SCFTMP.

As a result of the UR approach described above, surface temperatures may be retrieved over ocean and land in fully overcast situations using the combined DMSP micro-wave sensor suite. Over the ocean standard deviations of between 2 and 3 K are obtained between the retrieved sea surface temperatures (SSTs) and Navy SST fields. Over land, there is little sensitivity of retrieved surface skin temperatures to cloud. This provides the basis for retrieval of surface skin temperature in completely overcast conditions. Results indicate that it would be worth investigating whether coupling OLS information with the microwave skin temperature retrievals would be helpful in enhancing IR based low cloud

37

detection capabilities over land (Moncet et al., 1996). An advantage of the UR approach over that of using SSM/I derived temperatures alone is the retrieval of surface emissivity which decouples the surface temperature results from those of surface type.

Convective storms represent a significant weather aviation hazard and are given special treatment in operational cloud typing. At AFGWC, the approach adopted to identify thunderstorms is the convective-stratiform technique (CST) of Adler and Negri (1988). The CST technique is based on the use of satellite imagery alone. In particular it uses the spatial properties of LWIR EBBT's to differentiate between convective and stratiform situations. A description of the approach applied can be found in Kopp et al. (1996). One immediate suggestion based on our experience with the DMSP microwave sounder and imager data is the use of these data to help characterize the presence and vertical extent and hence intensity of thunderstorms and convective precipitation.

A number of studies have indicated that multifrequency microwave observations of convective systems can be used to identify both liquid and glaciated hydrometeors (see Wilheit et al., 1982; and Hakkarinen and Adler, 1988; Adler et al., 1990; Kummerow et al., 1991, Petty, 1994; Petty, 1995; Petty and Miller, 1995). These studies have generally tended to focus on window channel observations (i.e. 91 GHz and channels away from the center of the 183.31 GHz water vapor line). Microwave brightness temperatures (T_bs) tend to be dominated by emission from rain below the freezing level, while higher frequency millimeter brightness temperatures are affected by scattering from frozen hydrometeors. These signatures thus provide gross information on the vertical structure of storms (Spencer et al., 1989).

The key to using window channel data is associating these signatures with consistent vertical temperature structure information and exploiting sounding channel sensitivity to the same phenomenon. Notably, precipitation estimates from SSM/I are obtained using microwave window channels and thus assume a model of the vertical distribution and phase of precipitation. Recent aircraft observations of precipitating convective systems at microwave and millimeter wave frequencies indicate the potential for inferring the vertical distribution of precipitation properties (Wilheit et al., 1982; Hakkarinen and Adler, 1988). The channel set of the DMSP microwave sensor suite (Falcone and Isaacs, 1987) provides information content from 19.35 to 183 GHz which can be exploited to provide such information. Since the multifrequency response of liquid precipitation differs from that of glaciated precipitation, an indication of the freezing level is also possible. Examining the effect of clouds and precipitation on SSM/T-2 channels, non-precipitating clouds over water generally displayed warmer 91 GHz T_bs compared to clear FOVs (Figure 12). There was no difference between T_b signatures in the SSM/T-2 channels for cloud-filled FOVs over land. Griffin et al. (1994) showed a distinct SSM/T-2 T_b signature for precipitation (data set used was that from a developing typhoon in the western Pacific Ocean) (Figure 13). The presence of light rain over water caused the warmest T_b to shift to 150 GHz. As the rain rate and scattering in the FOV increased, the 183±1 GHz T_b became the warmest of the three atmospheric channels. This work and that of Pickle et al. (1996) suggest that DMSP microwave imager and sounder data would be useful in delineating precipitating cloud types, particularly thunderstorms.
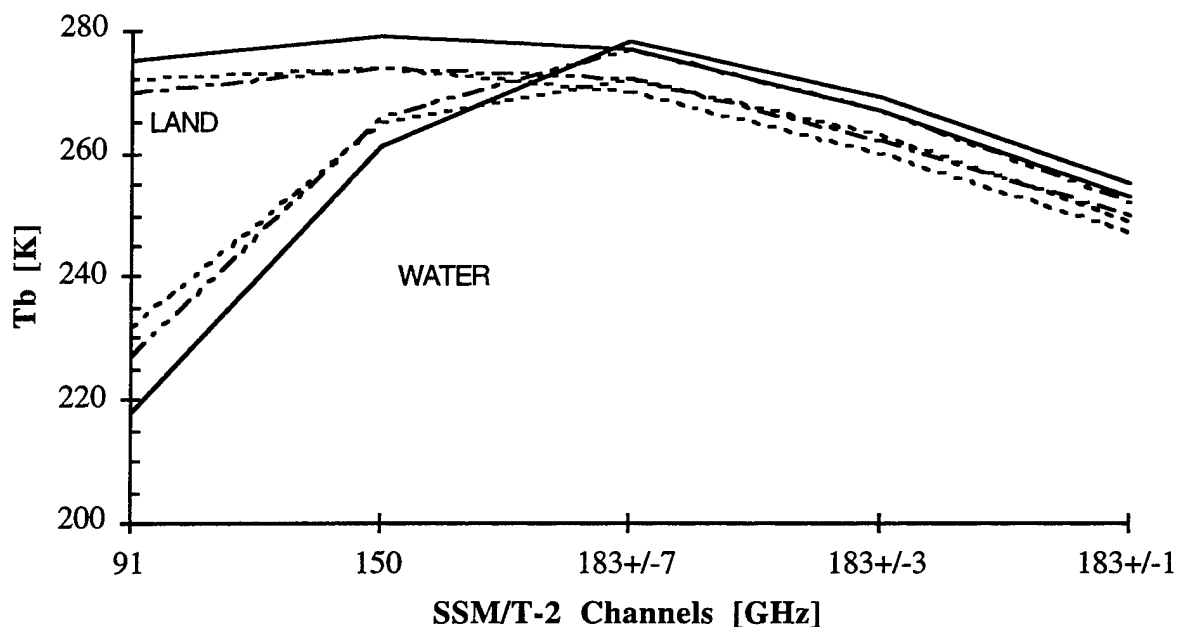
Figure 12. Typical T_b signatures for clear over ocean (solid), partly cloudy over ocean (dash-dot), cloudy over ocean (dash), clear over land (solid), partly cloudy over land (dash-dot), and cloudy over land (dash) for data collected during May and July, 1992 for the east and west coast of the United States.
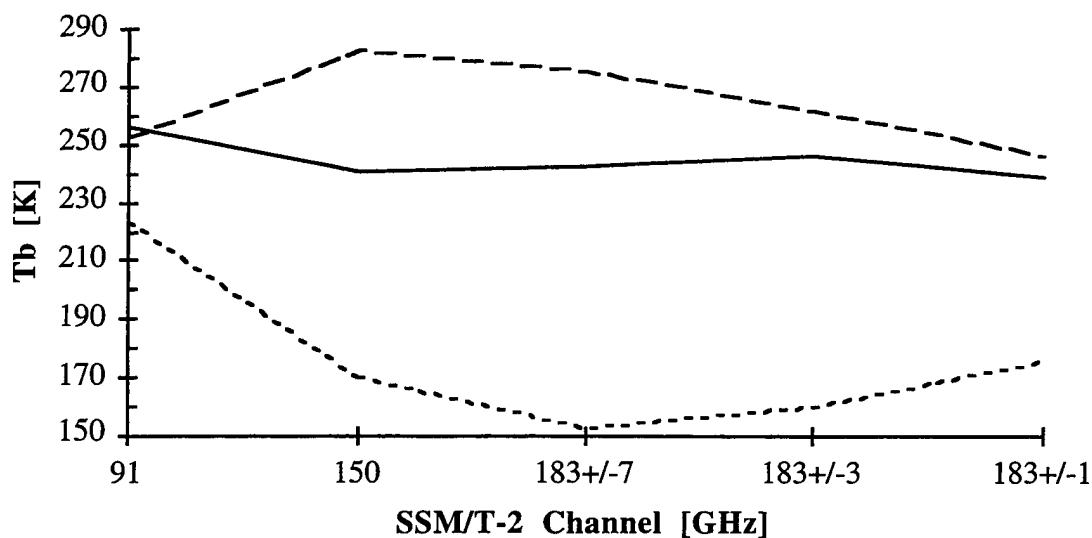

Figure 13. Typical T_b signatures for clear (dash), light precipitation (solid) and heavy precipitation (dot) observed in Typhoon Oliver, February 4, 1993 in the western Pacific Ocean.

4.5 Implementation Changes for Cloud Typing and Layering

The SERCAA I cloud typing algorithm provided a broad classification of pixels into one of two types of clouds, cumuliform or stratiform, based on their spectral and spatial properties (Gustafson et al., 1994). Cloud-filled longwave IR pixels were segregated into cloud classes using an unsupervised classification approach. The classes were then processed in a top-down fashion by applying a multi-pass, region growing segmentation routine in concert with variance-based texture information. The segmentation routine resulted in the formation of regions, or groups of connected pixels, whose size was the basis of the cloud type determination. The underlying assumption governing the process is that cumuliform clouds are represented by small, connected and compact regions of pixels while stratiform clouds extend over larger regions of connected pixels within a given temperature class. Therefore, a size threshold was applied to each new region and regions were then sorted into cumuliform or stratiform types.

While this implementation provided an accurate reflection as to the nature of cloud formations in a scene, the calculation of the texture derivative and the region-growing feature of the segmentation routine proved to be computationally intensive. An improved technique has been developed and implemented in which composite temperature classes are segmented using a fast, single-pass algorithm based solely on pixel contiguity. Pixels in each composite mask are analyzed in turn with respect to their immediate neighbors and are assigned either a new region identification (ID) number or that belonging to their top or left neighbor. Ultimately, all pixels that are connected in one of the four adjoining spatial directions (left, right, top, bottom) will belong to the same region. As in the original implementation, the number of pixels in a region determines the cloud type label it will receive. Regions less than a given threshold size are assigned a cumuliform label; all others receive a stratiform label. By omitting both the multi-pass segmentation technique and the derivation of a texture layer, the new routine successfully operates several orders of magnitude faster than its predecessor despite the continued iterative, top-down processing.

In addition to the improved speed and performance of the SERCAA Phase I cloud typing algorithm, a new technique for discriminating among cloud layers was also developed and tested. The SERCAA Phase-1 cloud layering algorithm was achieved by performing a second, local-scale unsupervised classification (clustering) layering process that operates on the cloudy pixels within a 3x3 floating window of 1/16th-mesh grid cells centered on the grid cell currently being analyzed (Gustafson et al., 1994). This process is conceptually similar to the large-scale layering procedure just described; unsupervised clustering and maximum likelihood classification are performed on the cloudy pixels that lie within the floating window. Under Phase 1, these pixel values were linearly proportional to the cloudy pixel's LWIR brightness temperature. This technique worked well for opaque clouds whose brightness temperatures are very close to the true physical temperature of the cloud. However, for thin cirrus the LWIR brightness temperature, being a mix of cold cloud and warm background, is not representative of the physical temperature of the cloud. Thus cirrus that has varying optical thicknesses in the horizontal but whose tops are essentially at the same vertical level was being separated into too many layers because of the large variation in cirrus brightness temperatures. In this case the relatively large spread of LWIR brightness temperatures misleads the clustering algorithm into separating the cirrus into too many layers when the spread in cloud top altitudes is not nearly as large.

To alleviate this problem, tests were conducted using the SERCAA Phase 2 retrieved cloud top altitudes instead of the raw brightness temperatures as input to the layer unsupervised clustering and maximum likelihood classification (MLC) routines. Recall that SERCAA Phase 2 cloud top altitudes include water-vapor-attenuation corrected altitudes for

opaque clouds, and transmissive cirrus corrections for thin ice-particle clouds. These altitudes were passed to the clustering and MLC routines in tandem with the original LWIR brightness temperatures, and the results were subjectively compared.

Figure 14 contains an LWIR NOAA-14 image over New England in November 1994. Note that the image contains a large cirrus shield of varying brightness temperatures. The corresponding LWIR brightness-temperature layer analysis is shown in Figure 15. In Figure 15, gray 16th-mesh boxes have one cloud layer in them while white 16th-mesh boxes have two. Note that in the left side of the image the SERCAA Phase 1 algorithm has found two layers where there is a large variation in cirrus LWIR brightness temperatures. However, the Phase 2 height analysis indicates that the cirrus tops are all within 1-2 km of each other over this region. When the Phase-2 altitudes were fed into the clustering procedure, far fewer 16th-mesh boxes were analyzed as containing two layers, as is shown in Figure 16. Note that in the heart of the thin cirrus shield, the Phase 2 altitude-generated layer algorithm assigns only one layer to the cirrus. In Figure 15, the corresponding brightness-temperature layer analysis seems overdone, again being confused by the large variations in brightness temperature that are caused by variation in cirrus optical properties across the scene. Overall the results that were obtained for two dozen cases using the altitude-generated layers were noticeably improved in areas of thin cirrus. However, it is recommended that the technique be tested over many more samples and that some sort of objective measure of goodness be established to judge whether layers should be generated from altitudes or brightness temperatures.

4.6 Analysis Consistency

The existing RTNEPH cloud analysis process (Kiess and Cox, 1988; Hamill et al., 1992) was designed to produce quarter orbit based cloud analysis products based on individual polar orbiting passes from two-channel (VIS and IR) data, primarily supplied from the DMSP/OLS. To address known deficiencies in the RTNEPH's polar platform a primary objective of the SERCAA effort was to incorporate both polar multispectral data from the NOAA TIROS Advanced Very High Resolution Radiometer (AVHRR) and hourly geostationary data from GOES, Meteosat, and GMS (Neu et al., 1994). The availability of the multispectral data significantly improves the ability to detect low stratus and thin cirrus, while geostationary data complements that of the polar platforms by providing higher temporal sampling of diurnal cloud development and dissipation, particularly in the tropics. A key element of SERCAA is the integration algorithm to optimally combine the most recently available cloud product analyses from all platforms into a single optimal analysis.

As discussed in Section 3 above, the design philosophy for the SERCAA analysis integration algorithm was to provide an optimal 16th mesh merged cloud analysis valid at a specific instant in time based on the analyzed cloud products derived from the most recent observations available from the three independent classes of environmental satellites. The key attribute of the integration scheme is that the RMS error at each grid cell will be minimized independent of the cells around it. Thus, the algorithm design does not include logic to enforce meteorological consistency between temporally or spatially adjacent grid cells. This was neither the requirement nor the design philosophy during SERCAA. However, evaluation of SERCAA-derived integrated cloud products using real satellite data has revealed that meteorological consistency between hourly-generated products can be degraded by numerous factors including: changes in the mix and relative age of input satellite data, variations in solar illumination and satellite viewing geometry, and the type of cloud present.

41

Figure 14. NOAA-14 10.7-μm brightness temperature image over New England for November 1994. High tones denote low brightness temperatures.

Figure 15. SERCAA Phase-1 cloud layer analysis for the image in Figure 14. This
analysis was generated using LWIR brightness temperatures as input to the
clustering and unsupervised classification routines. Each square represents a
16th-mesh box. White boxes contain two cloud layers, and gray boxes contain
only one.
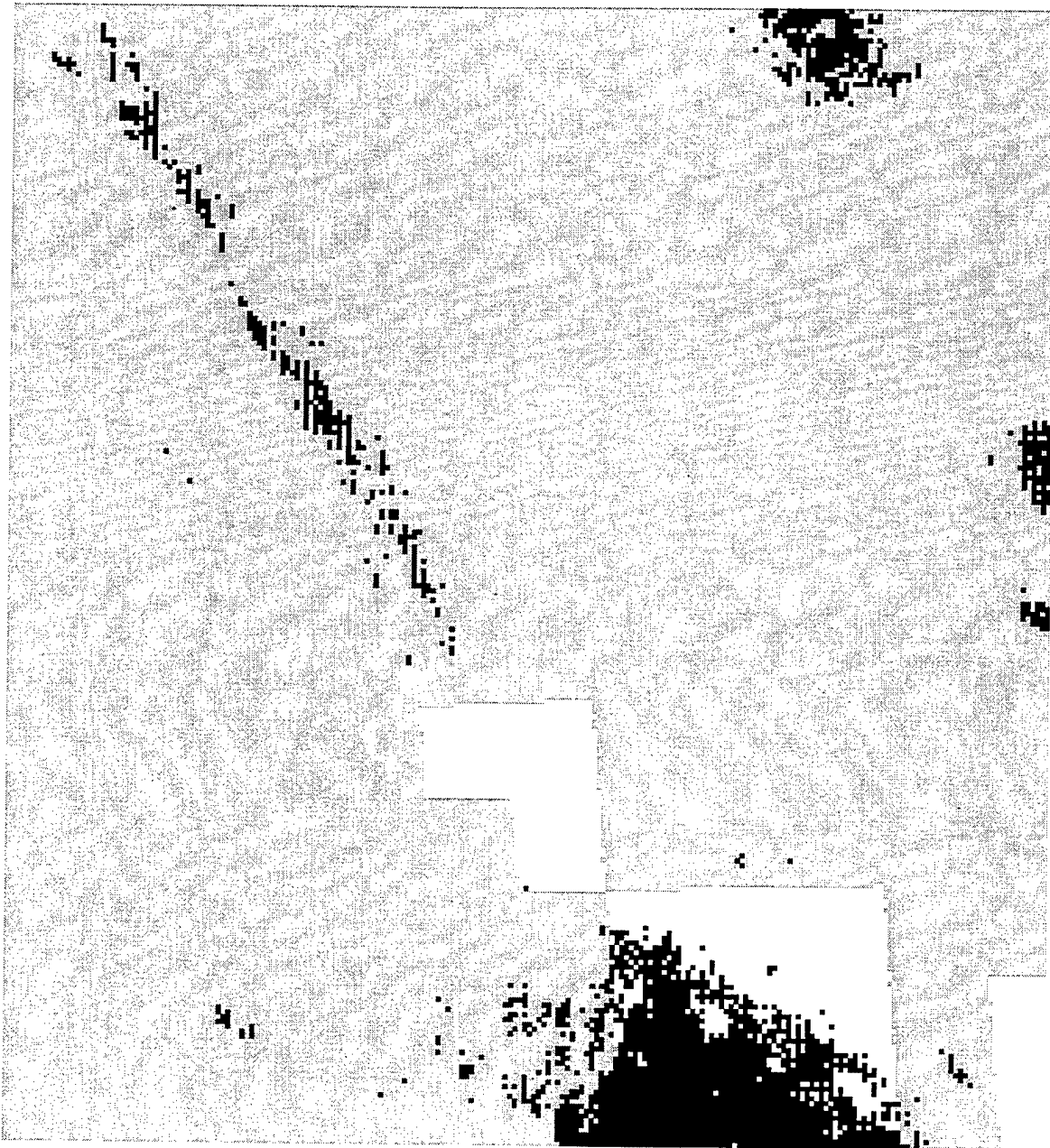
Figure 16. SERCAA Phase-2 cloud layer analysis for the image in Figure 14. This analysis was generated using SERCAA Phase-2 pixel-resolution corrected altitudes as input to the clustering and unsupervised classification routines. Each square represents a 16th-mesh box. White boxes contain two cloud layers, and gray boxes contain only one.

The SERCAA analysis and integration algorithms were evaluated using a series of ten-day satellite data sets obtained from NOAA 11 and 12, DMSP F10 and F11, GOES-7, GMS-4, and METEOSAT 3, 4, and 5 for the months of March and July from 1993 and 1994. The algorithms were applied over three regions of interest including eastern Asia and tropical Indonesia, central and northern South America, and north-central Africa and the Mediterranean that were selected for geographic and climatic diversity (Figure 17). Results from this real-data study were analyzed to establish baseline characteristics of both the analysis and integration algorithms.

Generally, results of the source-specific analysis algorithms showed good agreement with manual interpretation of satellite imagery generated from the input sensor data (Heideman et al., 1994; 1995). Examination of the final integrated results showed the complementary nature and relative strengths of the different data sources. However, under some conditions, inconsistencies were found to exist between contemporaneous polar- and geostationary-based cloud analyses. These are manifested as either spatially and/or temporally inconsistent cloud fields in the integrated products. Gustafson et al. (1995) investigated the source of these inconsistencies and concluded that they were due, at least in part, to differences in the inherent information content provided by each of the satellite systems used as data sources. Table 4 summarizes some of the relevant satellite sensor characteristics. The unique information content of each source with respect to cloud detection capability is a well understood (see Isaacs and Barnes, 1988) function of number of channels, channel band passes, sensor resolution, and solar illumination geometry.
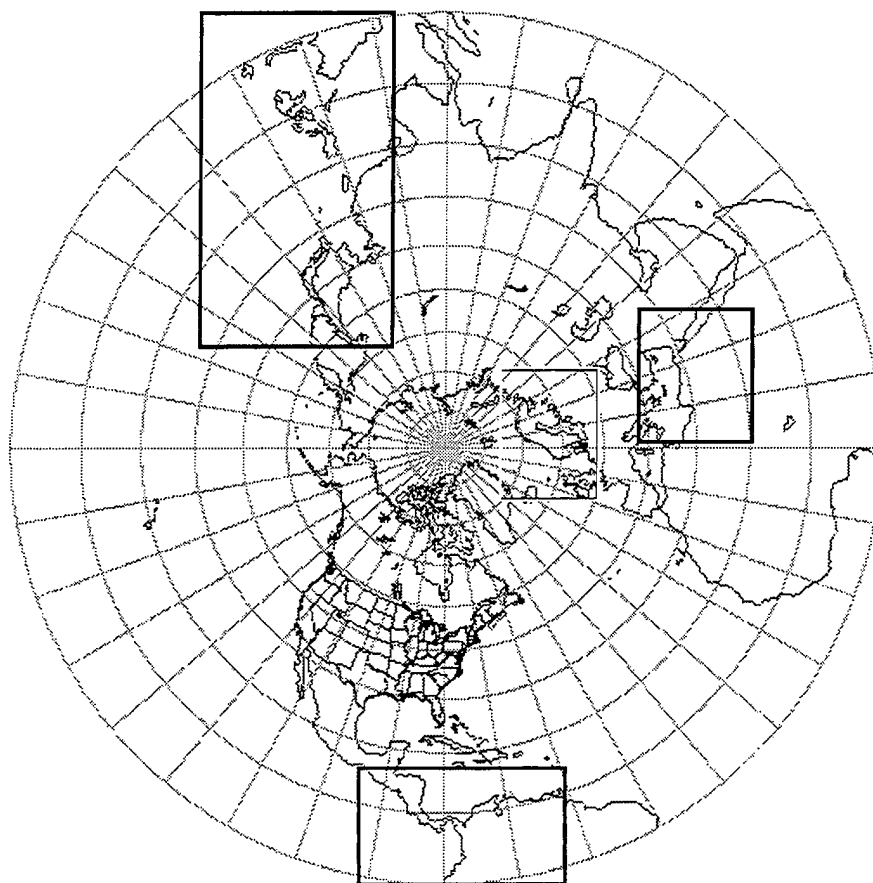
Figure 17. SERCAA evaluation regions of interest.

45

Table 4. Summary of operational environmental satellite imaging sensor characteristics

Satellite	Sensor	Channel Number	Channel (μm)	IFOV Resolution (km)[1]	Bits per Pixel	Minimum Repeat Cycle (h)[2]	Maximum Repeat Cycle (h)[2]
DMSP	OLS	1	0.40-1.10	2.7-4.8	6	3.5	8.5
		2	10.5-12.6	2.7-4.8	8		
NOAA	AVHRR-2	1	0.58-0.68	4.0-18.0	10	5.5	6.5
		2	0.72-1.10	4.0-18.0	10		
		3	3.71-4.18	4.0-18.0	10		
		4	10.3-11.3	4.0-18.0	10		
		5	11.5-12.5	4.0-18.0	10		
GOES I/M	imager	1	0.55-0.75	1.0-3.5	10	0.25	3.0
		2	3.80-4.00	4.0-14.0	10		
		3	6.50-7.00	8.0-28.0	10		
		4	10.2-11.2	4.0-14.0	10		
		5	11.5-12.5	4.0-14.0	10		
METEOSAT-5	VISSR	1	0.55-0.75	2.5-9.0	8	0.5	0.5
		2	5.7-7.1	5.0-17.0	8		
		3	10.5-12.6	5.0-17.0	8		
GMS-5	VISSR	1	0.5-0.75	1.25-4.5	6	1.0	1.0
		2	6.50-7.00	5.0-17.0	8		
		3	10.5-11.5	5.0-17.0	8		
		4	11.5-12.5	5.0-17.0	8		

[1]Field of View on the ground varies from satellite subpoint (highest resolution) out to edge of scan (lowest resolution).

[2]Assumes a two satellite constellation for each polar system; DMSP in early and mid morning orbits and NOAA in early morning and afternoon orbits. Geostationary minimum repeat cycles are for selected subregions, maximum cycles are for full disk.

Also given the current constellation of gaps of polar satellites, up to four hour gaps can occur between the crossing times of consecutive orbits. While it is these differences that the SERCAA analysis integration algorithm exploits in producing a combined analysis, the different sensor characteristics can lead to different analyses of the same scene from multiple platforms.

Figure 18 illustrates the essential nature of the temporal consistency issue using SERCAA analyses produced under contract with the DNA. The analyses shown cover a large region over the western Pacific Ocean and eastern Asia and are valid for the period 1600 to 2200 UTC on 26 March 1993. The top row of panels show a 4-h sequence of integrated SERCAA analyses (gray shade is proportional to total cloud fraction with white representing completely overcast) beginning 1700 and ending at 2200 UTC. The bottom row contains a simple persistence forecast based on the SERCAA analysis valid at 1600 UTC. The 1 and 2-h persistence forecasts correspond fairly well with the verifying SERCAA analyses because the available input satellite analyses during these time period were limited to GMS only. However at 1900 and 2000 UTC the SERCAA analysis

abruptly changes in appearance, and this is directly attributable to the addition of low cloud detected by the available AVHRR analyses valid at 1820 and 1958 UTC, respectively.

While it is true that the later analyses in the above example provide a more complete picture of the actual clouds, the sudden appearance of analyzed low cloud fields over areas covered by the AVHRR sensor are not consistent with the analyses from other sensors. Note that this is strictly a consequence of the increase sensitivity to those types of clouds in the multispectral AVHRR data relative to the other data sources. However, since the overall time series is not meteorologically consistent, even though the analysis is compatible with the SERCAA goal of providing the best analysis based on the most recently available data, it may negatively impact user assessment of the accuracy and usefulness of the cloud analyses. This problem, however, is not unique to SERCAA: even in the current RTNEPH with its much more restricted input data, cloud fields are updated abruptly over areas covered by more recent satellite passes, and the cloud analyses also exhibit spatial artifacts of the data coverage. A potentially more serious concern is the effect of temporal inconsistencies on the initialization and verification of cloud forecast models.

In adopting the SERCAA algorithm suite as the basis of the CDFS II-NEPH, an often stated assumption was that the most accurate cloud depiction would support the best cloud forecast. In the current suite of forecast models in use at GWC, which are all advective in nature, there are no technical difficulties in using cloud analyses with temporal or spatial discontinuities in the cloud fields for initialization. The difficulty arises when one tries to verify the resulting forecasts against subsequent cloud analyses. As an illustration of this problem, a simple persistence forecast from the hour preceding the cloud analyses is shown in Figure 18 alongside the verifying analyses. It is clear that for hours 1 and 2 of the forecast, neither the analysis nor the forecast show the low cloud fields because of the lack of multispectral AVHRR data. As a result, the verification provides an unrealistically optimistic assessment of the forecast accuracy. Only at hours 3 and 4 would the detection of the low cloud in the verifying analyses result in an apparent sudden reduction in forecast skill to its more realistic value. In this case the apparent reduction in forecast skill is an artifact of the verification procedure, caused by an unrealistically high apparent forecast skill at hours 1 and 2. Other scenarios are possible in which the apparent forecast skill is reduced because of temporal inconsistency in the analysis. For example, in a situation where an analysis at the initial time contains multispectrally-detected low cloud, but later analyses do not as the multispectral data age out of the analysis. In this scenario, forecasts generated from the initial analysis will be penalized for (correctly) predicting low clouds not present in the (later) verification analyses. Here the apparent forecast skill reduction is caused by an unrealistically pessimistic assessment of the forecast skill by the verification procedure. Similar problems would occur with advective forecasts since analysis inconsistencies at the start and end point of the cloud trajectories would result in artificially low verification score.

As noted, the potential for a high level of temporal inconsistency in CDFS II has potentially significant implications for the apparent accuracy of cloud forecasts initialized from these fields. It is important to point out that, given the above example, the issue of cloud forecast accuracy is as much an issue of validation data set characteristics as it is one of forecast quality itself. A possible mitigation strategy would be development of a new integration algorithm with modified design criteria that emphasized consistency over fidelity to the input data. Validation methodology should also be reviewed to determine if requirements are better served by validation criteria that consider temporal consistency of both the input and verification data. This is addressed in Section 6.2.5 below.
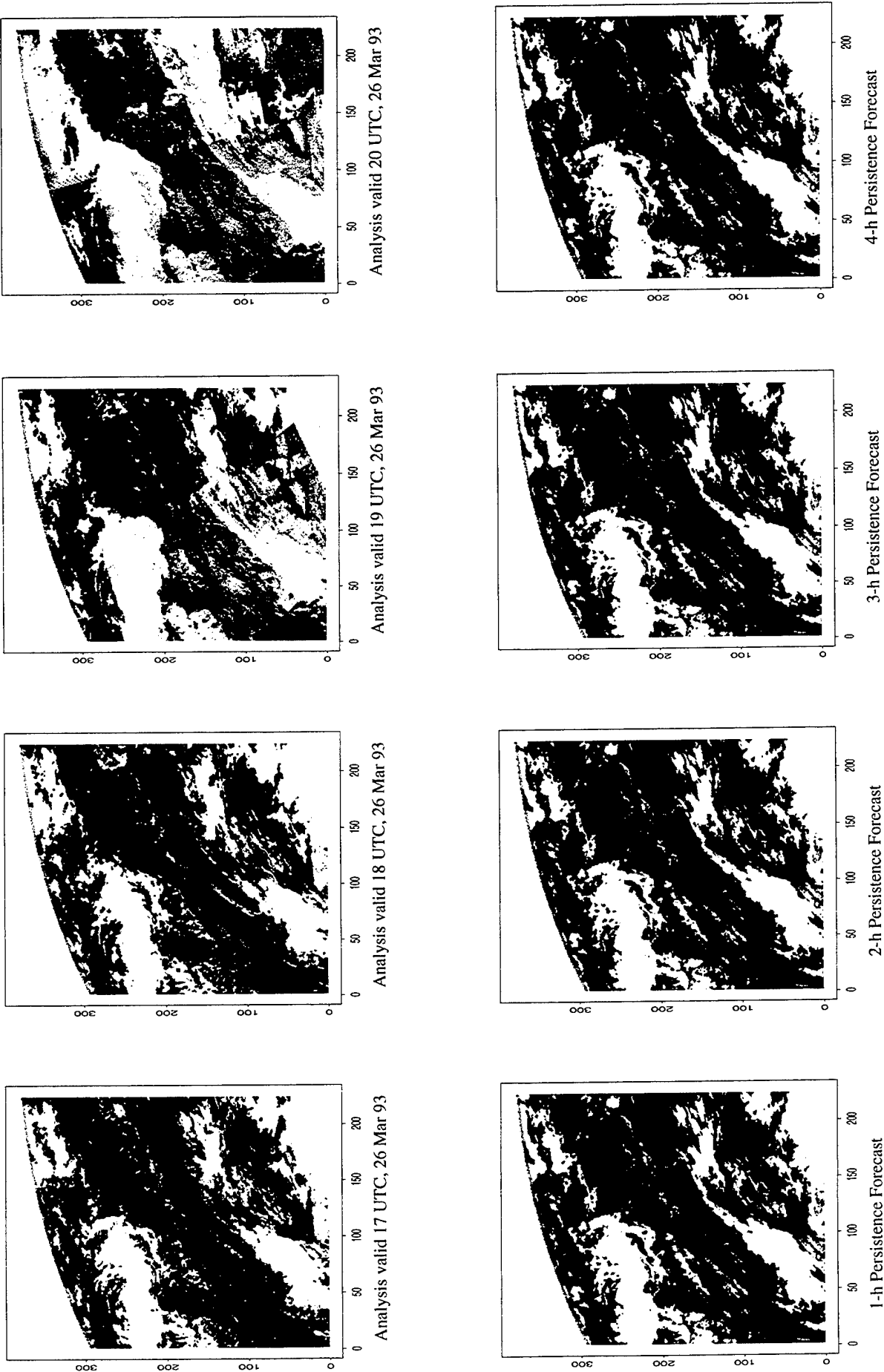
Figure 18. SERCAA analyses of total cloud fraction over the western Pacific Ocean and eastern Asia on 26 March 1993. Top row contains hourly analyses starting at 1700 UTC and ending at 2000 UTC. Bottom row shows a simple persistence forecast based on the analysis at 1600 UTC. Greyshade is proportional to analyzed cloud amount.

4.7 Daytime Cirrus/Low-Cloud Discrimination Using MWIR Data

Nighttime cirrus cloud detection tests compare the 3.7-µm and 10.7-µm brightness temperatures; generally, MWIR temperatures are higher then corresponding LWIR temperatures, with the magnitude of the difference dependent on cirrus cloud altitude and optical depth. At night, thin cirrus MWIR-LWIR spectral signatures are unambiguous.

There are three main reasons why cirrus detection using multispectral infrared measurements is successful at night. The most dominant effect has to do with the nature of the dependence of the Planck function on temperature at the MWIR and LWIR wavelengths. Proportionally less energy comes from the warmer part of the scene as wavelength increases; this effect is due solely to the exponential dependence of the Planck function on temperature at 3.7 and 10.7µm. The second effect is that of the varying emissivities of ice particle clouds themselves among the three wavelengths. In general, cirrus emissivities increase with increasing wavelength from 3.7 to 12µm. This means that, on the basis of emissivity alone, increasingly more of the upwelling radiant energy in a cirrus-filled pixel comes from the colder cloud. This is an analogous but weaker effect to that of the Planck function in that it amplifies the brightness temperature differences that comprise the thin cirrus signature. Finally, a third effect that causes brightness temperatures for cirrus pixels to decrease with increasing wavelength is that of varying atmospheric water vapor attenuation. In general, atmospheric water vapor attenuation is stronger at longer wavelengths. This operates in the same sense as do the previous two, increasing the difference between 3.7 and 10.7-µm-channel brightness temperatures, although typically it is the weakest effect of the three.

In the daytime, solar energy adds complexity to the cirrus MWIR-LWIR signature. At 3.7µm there is a noticeable solar component to incident MWIR energy; this component can be either reflected or transmitted by thin cirrus. Any transmitted energy continues downward to the underlying surface where it is reflected upward and re-transmitted by the cirrus. These effects cause the 3.7µm brightness temperature to be even higher for thin cirrus during the day, so that the MWIR-LWIR difference remains positive. However, during daytime the magnitude of this positive 3.7-10.7µm difference is ambiguous. Low water droplet clouds such as cumulus, stratus, and fog also have very high brightness temperatures at 3.7µm because they are relatively efficient reflectors of solar energy at MWIR wavelengths. Thus low clouds have a combination of thermal emission and solar reflection of MWIR radiation that causes their brightness temperatures to be high as well. In turn, the MWIR-LWIR brightness temperature difference is often as high for low, opaque clouds as it is for high, transparent cirrus.

For meteorological satellites with 6.7-µm water vapor sensors, this problem is surmountable. Such channels sense predominantly upwelling thermal energy that has been absorbed and re-emitted by atmospheric water vapor, with little or no contribution to the upwelling radiance coming from low clouds or the Earth's surface. The only type of clouds that influence strongly the 6.7-µm thermal energy are cirrus clouds. The weighting function of a 6.7-µm sensor peaks relatively high in the atmosphere, not often any lower than cirrus altitudes. Thus water-vapor brightness temperatures for thin cirrus are similar to the true physical temperature of the cirrus itself, while for low clouds they are very different. It is very conceivable therefore that a 6.7-10.7-µm brightness temperature difference will be routinely small for cirrus, but large for low clouds and fog.

It is be possible to quantify this relationship through manual cloud-clearing of daytime multispectral GOES-Next imagery and comparing the observed cirrus water-

49

vapor/LWIR differences with those that correspond to water-droplet clouds. Thus a potential daytime ice/water-cloud discrimination test is to first check for large MWIR-LWIR differences; this detects thin cirrus and stratus and fog. The second check is then to determine how large the water-vapor/LWIR difference is: if small, then cirrus; if large, then low cloud. Such a suite of daytime tests will allow for confident daytime cloud phase discriminations.

5. Future Research Topics

The scope of the SERCAA program was large and multifaceted. However, as with any large research program, issues came up during the period of the project that are of interest to Air Force mission requirements but that were outside the scope of the current program. Many of these issues are not being adequately addressed by existing or currently planned capabilities. There were also lessons learned that could potentially improve future operational capabilities. This section provides an overview of these topics and a discussion of possible approaches and how they might be used to address Air Force requirements.

5.1 New Sensors

Over the coming decade a number of new environmental satellite and sensor systems are scheduled for launch. Table 5 provides a list of proposed satellites and respective characteristics of the primary sensors that are potentially useful for cloud applications. Extant satellites, depending on the suite of onboard sensors, provide varying levels of information that can be exploited for cloud property retrieval. The SERCAA cloud analysis model currently being implemented for operational Air Force use as part of CDFS II is unique in that it analyzes data from multiple satellites and accommodates differences in information content through the use of multiple cloud analysis algorithms, each tailored to a specific satellite sensor system (Gustafson et al., 1994). Thus as new satellites are launched, the SERCAA model is intended to be easily expandable to include the new data sources simply through the addition of another source-specific analysis algorithm. However, for this or any other plan to improve cloud analysis accuracy using new sensor data to succeed it is necessary that the appropriate algorithms be developed prior to introduction of the data into the analysis system.

High spectral resolution data from new satellites offer the potential for significantly advancing the state of the art for analysis of cloud from space. Numerous studies have addressed the advantages of adding specific channels or higher resolution sensors to the existing constellation of environmental satellites (e.g., Di Girolamo and Davies, 1995; King et al., 1992; Eyre and Menzel, 1989; Arking and Childs, 1985). These new data sources are applicable for addressing specific weaknesses in current cloud analysis algorithms. For example, discrimination and accurate altitude assignments for optically thin cirrus is extremely difficult during daytime conditions. However, 8.55 μm channel data, has been demonstrated to provide sufficient information, when combined with data from split long wave IR channels, to develop a robust, daytime thin cirrus detection algorithm (Strabala et al., 1994; Ackerman et al., 1990). An 8.55 μm channel is planned for instruments on the ADEOS I and EOS/AM platforms, and data in case-study quantities are available now from the MODIS Airborne Simulator (MAS). Similarly, improved cloud altitude assignments of high cloud can be made from temperature sounding instruments (Wylie et al., 1994; Menzel et al., 1992) and multispectral IR instruments (d'Entremont et al., 1995; d'Entremont et al., 1992) such as HIRS-3, MODIS, OCTS, AVHRR-3, and NPOES/Imager.

50

Table 5. Planned environmental satellite systems with primary sensor characteristics

Satellite	Proposed Initial Launch Date	Sensors	Characteristics
GOES I-M	1994	Imager	moderate-resolution 5 channel radiometer in visible to thermal IR
		Sounder	12-channel infrared sounding radiometer
GMS-5	1995	Imager	moderate-resolution 4 channel radiometer in visible to thermal IR
NOAA K-N	1996	AVHRR-3	high-resolution 6-channel radiometer in visible-thermal IR
		AMSU	15-channel microwave temperature sounding radiometer with 12 channels in the 50-60 GHz oxygen absorption band
		HIRS-3	20-channel infrared temperature and moisture sounder with channels along CO_2 and water vapor absorption lines
		MHS	5-channel microwave moisture sounder with 3 channels along the 183 GHz water vapor absorption line
ADEOS I	1996	NSCAT	Ku band active scatterometer for measurement of ocean-surface wind velocity (speed and direction)
		OCTS	high-resolution 12-channel radiometer in visible-thermal infrared
		AVNIR	very-high-resolution 5-channel radiometer in visible to near infrared with daytime cross-track pointing, stereo capability
TRMM	1997	CERES	moderate resolution radiometer with 3 channels covering broad band visible to long wave IR, visible to short wave IR and long wave IR
		LIS	staring telescope/filter imager at 0.777 μm for lightning detection
EOS/AM	1998	CERES(2)	moderate resolution dual radiometer, each with 3 channels, covering broad band visible to long wave IR, visible to short wave IR and long wave IR
		MISR	moderate resolution, multiple-angle imaging radiometer with 4 channels in visible to near-IR
		MODIS	moderate resolution scanning radiometer with 36 channels covering visible to long wave IR
		ASTER	very-high-resolution, 3-instrument radiometer with 3 visible to near IR channels, 6 short wave IR channels, and 5 thermal IR channels
		MOPITT	low resolution scanning spectrometer with 4 channels in gaseous absorption bands
METEOR	1998	SAGE III	limb scanning and solar and lunar occultation spectroradiometer with 9 channels covering visible to long wave IR
ADEOS II	1999	SeaWinds	Ku band active scatterometer for measurement of ocean-surface wind velocity (speed and direction)
		AMSR	scanning microwave radiometer with 6 frequencies in 6-90 GHz for humidity profiling and precipitation/surface temperature retrieval
		GLI	scanning radiometer with 35 channels covering ultraviolet to thermal IR
EOS/PM	2000	AIRS	high spectral resolution infrared sounder using a 2300 channels spectrometer between 0.4 and 15.4 μm for retrieval of temperature and humidity profiles and surface temperature
		AMSU	see NOAA K-N above
		MHS	5-channel microwave humidity sounding radiometer with 3 channels along the 183 GHz water vapor absorption line
		CERES(2)	see EOS/AM above
		MODIS	see EOS/AM above
METOP	2001	AVHRR-3	see NOAA K-N above
		AMSU	see NOAA K-N above
		HIRS-3	see NOAA K-N above
		MHS	see NOAA K-N above
NPOESS	2006	imager	TBD
		sounder(s)	TBD

Changes and advances in satellite sensor design, and how they affect the cloud algorithm performance, is an ongoing issue. The recent launches of GOES 8 and 9, the first two satellites in the GOES I-M series of next generation of the U.S. operational geostationary program, provide the opportunity to evaluate the impact of new sensor channels using data available now. These satellites have a sensor design that is a significant departure from the previous series (Menzel and Purdom, 1994). The principal instrument package consists of completely separate and autonomous imaging and sounding sensors with additional channels and enhanced resolution. Existing geostationary cloud analysis algorithms will require modifications to exploit the additional channels. The potential benefits from making these modifications are both large and relatively easily identified since the new sensor configuration is similar to the current AVHRR sensor which has been studied extensively. Advantages of a multispectral sensor over the previously-available two-channel system include improved low cloud detection, cloud phase determination, transmissive cirrus identification and characterization of cloud radiative and microphysical properties.

The Japanese Meteorological Agency has also recently launched a new geostationary satellite, GMS-5. The imaging sensor is modified over the previous version with the addition of a pair of split long wave infrared window channels in place of a single broad band channel. This offers the potential for improved thin cirrus detection, one of the recognized weaknesses of current geostationary-data analysis algorithms.

5.2 Advanced Retrieval Techniques

Existing and planned objective cloud analysis capabilities at the Air Force Global Weather Central (AFGWC) make use of multispectral data from multiple satellite systems. However in a number of important areas, gaps or weakness exist in the analysis methodology that affect the ability to adequately address Air Force requirements: 1) quantitative interpretation of daytime sensor channel data in the visible to midwave-infrared (MWIR) spectrum; 2) discrimination of transmissive cirrus over hot and bright backgrounds; 3) accurate cloud typing as a first-order determinant of cloud microphysical and radiative properties; 4) use of remotely sensed cloud radiative and environment characteristics to improve retrieval accuracy for cloud altitude; and 5) use of inferred cloud physical characteristics to provide temporal consistency within time series of analyzed cloud parameters derived from multiple satellites.

5.2.1 Interpretation of Visible to Midwave-Infrared Data

All satellite-based cloud analysis techniques require some knowledge of the terrestrial background radiative characteristics at the various sensor wavelengths in order to accurately discriminate cloud. Reliance on this knowledge varies by technique and information content of the satellite data. However, quantitative background information is difficult to obtain globally since Earth surface radiative characteristics vary widely with geography and surface cover (e.g., deserts, tropical forests, permanent snow and ice cover). Vegetated surfaces and snow cover also vary for a given Earth location as a function of time, both diurnally and seasonally.

The problem of background surface characterization is particularly acute for data channels sensitive to reflected solar radiation. Changes in solar illumination with time of day, anisotropic reflection, and similarities between reflective terrestrial backgrounds and cloud all contribute to make objective cloud detection using these channels complex and

often problematic. However, visible to midwave infrared sensor data are extremely useful for objective cloud detection since they generally exhibit a strong liquid-water cloud signature (i.e., the clouds are good reflectors). For two-channel sensors like the OLS and METEOSAT satellites, the visible channel adds significantly to low cloud detection accuracy during daytime. Also for the new AVHRR-3 sensor scheduled for launch in 1996 (Table 5), loss of the 3.7 μm channel during sunlight hours will place increased reliance on the visible and near-IR (NIR) channels for daytime low cloud detection.

Proposed research topics related to improved use of visible to MWIR data fall generally in the area of better cloud-free background characterization. The ratio of two-channel visible/near IR data has been used successfully to detect reflective clouds (Gustafson et al., 1994; Stowe et al., 1991; Saunders and Kriebel, 1988). The principle advantage of using a ratio, instead of the absolute magnitude of a single visible data channel compared to some threshold, is that as long as the channels are spectrally close, some uncertainties in the measurements (e.g., solar illumination, geometry) tend to cancel out. However, problems persist with reflective backgrounds exhibiting ratio signatures similar to cloud (e.g., deserts, snow and ice). Development of databases of clear-scene ratio values to characterize the problematic backgrounds offer the potential to improve cloud discrimination. This approach retains the advantages of using channel ratios while relying on locally adaptive thresholds to account for changes in background characteristics. Single-channel algorithms have traditionally used this type of approach to characterize the background reflectance (e.g., Hamill et al., 1992; Rossow and Schiffer, 1991).

The AVHRR is the only extant sensor system that contains narrow-band channels in both the visible and near IR. All other environmental satellite systems are limited to a single, broad band "visible" channel covering that spectral range. Reflectance of most terrestrial surfaces at these wavelengths is anisotropic resulting in potentially large changes in measured cloud-free radiance as a result of relatively small changes in the solar and/or viewing geometry. This uncertainty in the cloud-free radiance has constrained the accuracy of single-channel techniques. Bi-directional Reflectance Distribution Functions (BRDF) are potentially useful for describing changes in surface reflectivity as a function of geometric considerations. Earlier work investigating the application of deterministic BRDF models to real-world conditions (d'Entremont et al., 1995; d'Entremont et al., 1996) has demonstrated their feasibility of using BRDF models for predicting the bandpass weighted clear-scene visible and near IR reflectance of known surfaces. BRDF-derived clear-scene reflectance information can be applied to visible and NIR cloud detection algorithms to improve cloud-retrieval accuracy. Improved characterization of clear-scene reflectance conditions is also expected to increase the amount of visible to MWIR data that can be used for quantitative evaluation by objective cloud analysis algorithms.

Knowledge of MWIR surface reflectance characteristics provides the potential for significantly improving the accuracy of operational cloud analysis models that use daytime 3.7-3.9 μm data. During daylight hours surfaces both reflect solar energy and emit thermal energy at these wavelengths. If surface-reflectance effects can be successfully separated from thermal effects, improved detection and characterization of cloud (particularly thin transmissive cirrus) and more accurate skin temperature retrievals can be expected. MWIR reflectivity (r) can be expressed as a function of emissivity (ε) only (i.e., $r = 1-\varepsilon$), since the transmissivity of terrestrial surfaces at these wavelengths can be assumed to be zero. Thus, if the directional dependence of the surface emissivity can be calculated, then the directional dependence of the surface reflectivity is also known. LWIR emissivity is assumed to be 1.0 for most terrestrial surfaces, therefore the physical surface skin temperature can be retrieved by applying an atmospheric correction to the observed LWIR brightness temperature. This can then be used to compute the coincident MWIR emissivity from the corresponding atmospherically corrected MWIR brightness temperature. Directional dependence

could be determined from a series of observations of the same geographic location over multiple orbits (i.e., varying view angles). GOES-8 and GOES-9 data along with NOAA AVHRR data are all useful sources of coincident LWIR and MWIR observations.

5.2.2 Transmissive Cirrus over Warm and Reflective Backgrounds

When cirrus optical depth is sufficiently small, transmission of background radiation through the cloud can reduce the cloud-background contrast to a level that cannot be detected by automated cloud algorithms. This can occur in visible, MWIR, and LWIR image bands, and is particularly severe over reflective and warm backgrounds such as desert. Under such conditions it may be possible to determine the presence of these transmissive cirrus using wavelengths where the atmosphere is opaque such as the 6.7-µm water-vapor band.

Water vapor imaging channels centered near 6.7 µm are available on most geostationary satellites and on IR sounders on the NOAA polar platforms. At these wavelengths the sensors measure upwelling thermal radiation emitted primarily by water vapor in the atmosphere, with little or no contribution from the underlying terrestrial surface. Under cloud-free conditions, the absolute magnitude of a 6.7-µm brightness temperature is dependent on the amount of water vapor that is present along the atmospheric path. If an estimate of the water vapor profile is available (e.g., from IR and microwave satellite sounders), a predicted clear-scene 6.7 µm brightness temperature can be calculated using radiative transfer code. Any cloud in a satellite-observed 6.7 µm field of view would produce a negative departure from the corresponding predicted brightness temperature. While this approach is identical in form to standard single-channel threshold cloud tests, it effectively eliminates any problematic surface contributions that can act to mask weak cloud signatures. Sensitivity of this test can be evaluated using nighttime cases where conventional multispectral tests perform well for detecting thin cirrus. This will provide an experience base that can be used to determine the usefulness of the water vapor channels for upper-level cloud detection. It is possible to employ this technique not only with 6.7-µm data but with any water-vapor imagery in the 6.5-7.5-µm spectral regions such as are typically available on infrared moisture sounders. Using additional water vapor sounding channels also offers the potential for discriminating multiple cloud layers at different levels in the atmosphere.

Water vapor imagery is also potentially useful for improving cloud forecasts. Cross-correlation short-term cloud forecasting techniques have been demonstrated to produce useful 0 to 6-hour forecast products (Hamill and Nehrkorn, 1993). These techniques generate short-term trajectory forecasts for a particular region using cloud-track wind vectors that have been computed by correlating cloudy areas in time series of geostationary data. Regions in later images that correlate most strongly with a cloudy region in an earlier image are used to define a displacement vector that is used to generate a trajectory cloud forecast. One of the problems in relying on cloud-track winds from satellite imagery is that no displacement vector data can be retrieved in cloud-free areas. No vectors can be obtained since there are no wind tracers in the clear regions from which to infer horizontal atmospheric motion. This in turn poses a problem when trying to advect clouds into previously cloud-free regions. One possibility for inferring motions in cloud-free regions is to study the correlation of water-vapor imagery patterns from one time to the next in cloud-free regions. This would provide a truly satellite-only short-term cloud forecast capability and could potentially be extended to derive wind profiles using water vapor channels that peak at differing levels in the atmosphere. With wind profile information it could then be feasible to advect low, middle, and high clouds separately with multiple wind fields that vary with altitude.

5.2.3 Cloud Typing

Cloud type information is often used as a surrogate to infer cloud physical and optical properties (e.g., physical and optical depth, drop or ice crystal size distribution, transmission) due to the difficulty of retrieving these parameters directly from environmental satellite data. However, the cloud type retrievals themselves may be suspect. For example, the RTNEPH model currently identifies eight cloud types from only one visible and one IR channel (Hamill et al., 1992). Numerous approaches to cloud typing have been tried with varying degrees of success. A common technique discriminates type through a measure of the surface spatial texture generally evaluated through the local variance of infrared brightness temperature or visible reflectance (e.g., Lamaei, 1994; Hawkins and d'Entremont, 1990; Ebert 1989). Recently, neural networks have been used to assimilate multispectral satellite sensor data to retrieve a number of parameters including cloud type (e.g., Bankert, 1994, Lee et al., 1990). Garand (1988) stratified multispectral satellite data into a taxonomy of classes and used a knowledge-base system to identify different cloud types. In SERCAA a hybrid technique is used that first vertically stratified LWIR data and then applies standard image processing segmentation and classification techniques to discriminate cumuliform from stratiform cloud. Current Air Force requirements call for nine cloud types: cirrus, cirrostratus, altocumulus, altostratus, stratocumulus, stratus, cumulus, cumulonimbus, and nimbostratus. Robustness is a major issue in that any typing algorithm must be applicable to data from all available sensor systems over globally varying conditions. While most cloud typing techniques use some form of nephanalysis algorithm to provide cloud spatial information (e.g., location, extent, altitude), typically no use is made of cloud physical or optical properties available from advanced analysis algorithms. However, numerous approaches exist to retrieve this type of information from existing sensor systems (e.g., Ou et al., 1993; d'Entremont et al., 1993; Nakajima and King, 1989).

Processing time and efficiency are primary factors in operational implementations of cloud typing algorithms. If neural nets were to be shown feasible for cloud type retrieval this could significantly reduce the system resources required to perform that function. Also, depending on the quality of the training set and the information content in the satellite data, neural nets may be able to discriminate more cloud types than traditional retrieval techniques. It is important to note that the accuracy and robustness of neural networks are strongly tied to the amount and accuracy of the available training data; they are positively correlated.

5.2.4 Cloud Altitude

Cloud altitude is typically derived from LWIR brightness temperature data that are assumed to be representative of the cloud-top temperature (usually either an average or median brightness temperature computed from all cloudy pixels). Some temperature/height profile is then used to establish the cloud top altitude or pressure. Inherent assumptions are that derived LWIR brightness temperatures are representative of the cloud top temperature, that atmospheric transmission between the cloud and satellite can be ignored, and that the available temperature/height profile information is sufficiently accurate for the desired retrieval accuracy.

More accurate and timely temperature and moisture profiles would improve not only fixing the height of the retrieved cloud-top temperature but also the accuracy of that temperature through modeling of the LWIR attenuation caused by the atmosphere above the cloud. Use of satellite-derived soundings provide much improved coverage in comparison to conventional radiosonde measurements, both in terms of geographic density and temporal frequency. Also, since they are coincident with the satellite imaging sensor

measurements used for the cloud analyses, satellite-derived soundings are the optimal information source for quantifying the environment in which clouds are embedded. The sounder and imager data are best analyzed together since 1) the accuracy of the retrieved soundings is dependent on the presence of cloud (microwave-based soundings are less affected than IR based, particularly for non precipitating clouds) and 2) both cloud detection and altitude calculations are potentially improved with better understanding of the vertical structure of the atmosphere.

Cloud top altitude is typically determined by comparing a measured cloud-top LWIR brightness temperature with its coincident atmospheric temperature profile and choosing the profile altitude that corresponds with the brightness temperature observation. Not accounted for are the possible transmissive nature of the clouds and the effects of atmospheric water vapor attenuation on upwelling LWIR brightness temperatures. In-situ or NWP-derived profiles of atmospheric temperature and water vapor are not always available in real-time. However, retrievals of atmospheric temperature and water vapor from collocated satellite LWIR and microwave sounder data eliminate the need for external data sources.

The first step in correcting LWIR brightness temperature measurements for water vapor attenuation is to compute the atmospheric transmittance profile. Such computations can be quickly made using band-model transmittance codes such as those of Weinreb and Hill (1980) and Weinreb and Neuendorffer (1973). These models are well suited for this purpose since they can be customized for a satellite band-pass and response function, and they are fast, computationally efficient, and accurate. Input for these models includes atmospheric temperature and water vapor profiles that can be obtained from coincident satellite sounder data and/or NWP upper-air analysis fields.

Once a transmittance profile is obtained, predicted infrared brightness temperature can be computed as a function of altitude for a cloud at that altitude. If a blackbody cloud is placed at some level in the atmosphere, the measured brightness temperature for that cloud will in general be lower than the actual cloud top temperature due to attenuation by the atmosphere above the cloud. This attenuation is computable by evaluating the radiative transfer equation in the forward direction using the band-model transmittance profile corresponding to cloud-satellite atmospheric path. Thus for black clouds, true cloud top altitude as a function of satellite-measured brightness temperature can be computed a priori and used in lookup-table form to adjust satellite-measured cloud top temperature, and subsequently the cloud top height, for water vapor attenuation.

For transmissive cirrus clouds, the non-blackbody effects on upwelling LWIR radiances must also be accounted for. This has been accomplished using physical techniques such as those employed by d'Entremont et al. (1993), Ou et al. (1993) d'Entremont et al. (1990) and Rao et al. (1995). These models all use a deterministic approach to account for the low bias in retrieved cirrus altitudes caused by an incorrect blackbody assumption. However, the topic of cirrus radiative and spatial property retrieval using daytime MWIR and LWIR data remains problematic. During nighttime, the physical retrieval of cirrus emissivity and effective altitude (two unknowns) is accomplished using a coincident pair of MWIR and LWIR thermal-only radiance measurements (two knowns). The retrieval process capitalizes on the thermal properties of cirrus clouds at the 3.7-μm and 10.7-μm wavelengths. During daytime this retrieval is complicated by the addition of a reflected solar component to the measured MWIR radiances, essentially adding a third unknown to the system without the addition of a third measurement. Thus for daylight observations there are three unknowns (emissivity, altitude, and 3.7-μm solar reflection) and only two measurements (a combined solar-plus-thermal MWIR radiance and a thermal-only LWIR radiance). Before the cirrus optical and radiative properties can be retrieved, the solar component of the MWIR radiance observation must be removed. Rao et al.

56

(1995) have presented and successfully implemented a deterministic technique for removal of the MWIR solar component. Their technique requires a priori computations of very complex processes that model the MWIR bidirectional scattering properties of ice crystals.

An alternative solution to the daytime MWIR-LWIR cirrus retrieval problem requires separation of the solar and thermal MWIR components from the overall MWIR measurement. Recall that the fundamental cirrus retrieval model requires as input the upwelling MWIR and LWIR thermal-only radiances. Cirrus effective altitude can be independently retrieved both day and night using data along the wing of an LWIR absorption band using a technique such as CO_2 Slicing (Wylie and Menzel, 1989; Menzel et al., 1992, 1993). CO_2 slicing generates cirrus effective altitude analyses using 15-μm sounder data that are available with GOES and NOAA sounder data. Using this approach, the effective altitude can be eliminated from the list of unknowns and the imager MWIR-LWIR retrievals of the cloud effective emissivity can proceed.

A cirrus BRDF for 3.7-μm reflected solar energy using coincident measures of CO_2 effective altitude and MWIR-LWIR radiances could be used to specify the reflected-solar MWIR radiance component in situations where CO_2 Slicing analyses are not available. As discussed above, daytime retrieval of cirrus attributes is initially posed as a problem with three unknowns and two measurements, which in general has no mathematically unique solution. Using CO_2 Slicing to eliminate effective cirrus altitude from the unknowns, the reflected-solar portion of the MWIR cirrus radiance can then be retrieved whenever coincident CO_2 Slicing analyses are available. Tabulated retrievals over a range of view and illumination angles will be used to construct a cirrus MWIR BRDF that will be used where CO_2 Slicing analyses are not available. The resultant two-channel cirrus retrievals can be compared to results using the technique of Rao et al. (1995). Also, to check for consistency, the cirrus BRDFs can be directly and quantitatively compared with the full-blown radiative transfer (scattering by ice crystals) calculations of Rao et al. (1995). Other issues that will require investigation are the potential dependencies of measured cirrus BRDFs on effective ice crystal size (effective temperature) and optical depth (effective emissivity).

5.2.5 Temporal Consistency

As discussed in Section 4.6 above, integrated analyses produced by combining data from multiple satellite platforms to produce a single unified or integrated cloud analysis can exhibit inconsistencies between collocated results obtained from different satellite platforms at approximately the same time. The problem consists of combining data from high spatial and spectral resolution polar-orbiting satellites with high temporal resolution geostationary data. Under some conditions geostationary-based analyses tend to identify less cloud than corresponding polar-based analyses. Investigation of a limited number of cases has revealed no apparent problems with the accuracy of any of the individual, source-specific analyses. However, when combined the temporal consistency of the resultant integrated analysis can be degraded. This in turn may negatively impact subsequent applications that use the cloud analysis data as input, such as cloud forecast models. Depending on the source, age and mix of satellite data available over a given time period, certain clouds can appear in an integrated analysis only to later disappear and then reappear as different data sources are used and subsequently aged out of the analysis.

Inconsistencies between polar- and geostationary-based analyses are most likely due to inherent differences in their respective scan methodologies and major sensor characteristics (i.e., the available information content varies with platform). Table 4 summarizes the imaging sensor characteristics of the currently operational environmental

satellites. From the table it can be seen that each data source exhibits characteristic strengths that contribute to the relative accuracy of derived cloud products. OLS data have high spatial resolution but are relatively low in spectral information content and temporal resolution. AVHRR has the greatest spectral information content and its repeat cycle is consistent with synoptic scale events, but the spatial resolution is relatively coarse. Geostationary data exhibit the greatest temporal resolution, but the spatial resolution is significantly degraded for a large fraction of the coverage area, and spectral information content varies widely with satellite.

An investigation of the magnitude and frequency of inconsistencies between cloud analyses derived from different satellite systems and of their root causes is needed to characterize the problem more completely. To date only a few cases have been documented where differences between the polar- and geostationary-based analyses exist. It is not known how often this situation occurs or whether it is limited only to specific types of cloud (e.g., low cloud, transmissive cirrus). The cases that have been identified are consistent with conditions described above where the accuracy of the individual source-specific analyses have been confirmed through visual inspection yet discrepancies between coincident geo- and polar-based analyses exist. One possible explanation is the relatively coarse resolution, both spatially and spectrally, of geostationary compared to the polar-orbiter data. Geostationary sensors used in the earlier studies have a spatial resolution of 5 km at the subpoint that degrades to approximately 17 km at the edge of scan. Also they were only two-channel instruments with a radiometric resolution of no better than 8 bits. This is in contrast to the five-channel AVHRR data with a 10 bit radiance quantization range and 4 km footprint degrading only near the edges of scan, and the OLS with an 8 bit quantization and a roughly fixed 2.7 km footprint throughout the scan. The data quality hypothesis can be tested using the new GOES-8 data now available in real-time at PL. The imaging sensor on GOES-8 has additional channels plus improved spatial and spectral resolution that should increase cloud detection sensitivity and possibly reduce differences in the derived cloud analyses as compared to polar-based analyses. However, even if the improved data quality from the new GOES satellites does resolve the geostationary vs. polar consistency issue for those platforms, the problem will remain for the other international geostationary satellites (i.e., Meteosat and GMS).

To the extent inconsistencies exist between cloud data analyzed from different satellites, and the inconsistencies are detrimental to subsequent applications, mitigation is probably best achieved through modifications to the integration algorithm used to combine the separate analyses. This could be made more effective if inconsistency problems are linked to a particular range of conditions or cloud types that can be identified algorithmi-cally. An approach capable of quantifying system related impacts on analysis charac-teristics derived from geostationary satellites is to selectively degrade GOES 8 capabilities and observe the impact on cloud analysis accuracy and consistency. GOES 8 has improved radiometric and spatial resolution plus additional spectral capabilities (i.e., additional channels) relative to other geostationary systems. Sensitivity to system capabilities can be derived by parametrically varying GOES 8 system parameters (e.g., sensor or spectral resolution, channel configuration) and tabulating the change in retrieved cloud properties.

The principal objective of such sensitivity studies would be to identify cloud types or characteristics for which retrieval accuracy are most heavily impacted by the degraded system capabilities of geostationary satellites. Using this information, a mitigation strategy could be developed to best exploit the relative strengths of the individual satellites. For example, if it is demonstrated that geostationary analyses poorly resolve, say, low stratus cloud, then the integration algorithm could be modified to selectively persist low cloud identified from earlier polar passes, even in cases where more recent geostationary analyses indicate clear. Another strategy is to use a short-term cloud forecast algorithm such as

58

cross correlation (Hamill and Nehrkorn, 1993) to extend the influence of the polar-based analyses for longer time periods. A similar approach can be applied to analyzed data from nearly-coincident NOAA and DMSP scans (e.g., at high latitudes) to identify any cloud types that are sensitive to sensor-specific system characteristics.

5.3 Validation

A recurring criticism of objective satellite-based cloud analysis algorithms is the general lack of formal validation. There are several reasons for the paucity of quantitative validation work, however, most derive from a single cause: the absence of independently derived or measured cloud parameter databases with an established accuracy sufficient to be classified as ground truth.

A need exists for an established procedure and accepted objective measures of algorithm accuracy over a range of conditions. The initial step in development of an algorithm validation methodology is to first identify certain fundamental study attributes:

- goal: what information is required from the validation study, what is the end user's application and what information is needed to determine if the subject algorithm can provide that information with sufficient accuracy, does the accuracy metric need to be absolute or relative to some known standard (e.g., an existing legacy technique);

- scope: does the subject cloud algorithm need to be applied globally or regionally, only over certain background conditions (e.g., ocean, land, desert, snow), day and night, to specific satellite or sensor types (e.g., polar, geostationary, infrared, microwave);

- supporting data: what supporting data are available for use as part of the validation study, is there a truth data set that is accepted by the end user, what is the scale, resolution, projection of the supporting data relative to the satellite data, are the supporting or truth data parameters directly relatable to the algorithm output parameters; and

- results: is there specific quantitative information required by the end user, what statistical measures or form of results are required, are these results sufficient to meet the goals.

Comparisons with truth sets, if they are available, provide an absolute metric that is potentially useful for Air Force programs such as SERCAA and CDFS II that need to gauge algorithm performance in terms of absolute accuracy. Given the requirements placed on cloud algorithms for near real time global analyses, any ground truth data set would need to be representative of globally varying surface and atmospheric conditions for a full range of seasonal and diurnal conditions. The only practical data source capable of providing the required level of coverage is environmental satellites. Thus to date, most validation studies that require an absolute accuracy metric have involved some form of subjective comparison between satellite-derived algorithmic results and the corresponding satellite imagery; and even those studies tend to be limited to validation of cloud spatial properties (e.g., coverage, amount, height).

Other Air Force programs have requirements for cloud climatologies, rather than real-time analyses. This drives a need to establish a measure of relative accuracy between available climatological data and to quantify any differences. Intercomparisons over

extended time periods between results from real-time cloud analysis algorithms and coincident data being ingested into candidate climatological data sets are potentially useful for establishing any characteristic biases or artifacts in the climatologies, particularly if the absolute accuracy of the cloud algorithms is previously established. Radiative and microphysical retrieval algorithms can realistically only be validated against in-situ and/or active remotely sensed data. Well calibrated lidars and radars can provide necessary information on cloud altitude and optical properties but are typically only available from intensive field study programs for a limited range of meteorological conditions and a single geographic region for perhaps one season. These data need to be collected from as many locations and time periods as possible to provide a more complete validation of the retrieval algorithms.

An acceptable validation methodology must identify factors or techniques that can minimize problems associated with the limited availability of truth data and that can provide the required accuracy information. There is evidence that using a man-computer technique to analyze satellite imagery is an acceptable approach for developing ground truth information for some applications. Gustafson et al. (1993) produced a quantitative measure of the absolute accuracy of total cloud amount retrievals produced by a set of tactical cloud analysis algorithms. Their approach used direct comparison with ground truth images produced through manual analysis of satellite imagery following a formalized technique developed by Gustafson and Felde (1988). This technique has also been successfully applied to previous studies of the RTNEPH (d'Entremont et al., 1989) and an SSM/I cloud algorithm (Gustafson and Felde, 1989).

Comparison of results from multiple cloud models to determine the optimal approach for a particular application is another common validation requirement (e.g., Rossow et al., 1985). During the recent cloud algorithm development program conducted at the Phillips Laboratory, a validation study was designed and executed to establish a relative accuracy metric for comparison of cloud algorithm results against a known standard (Phillips Laboratory, 1994). The focus of this study was to identify the impact on analysis accuracy of the differing analysis approaches used by the respective algorithms. Two validation criteria were established: 1) did differences between the two techniques exceed a specified level of statistical significance and 2) where they were different, which was more accurate. To minimize the impact on comparison statistics of minor algorithmic differences such as output resolution and precise positioning of cloud edges, the output data were first gridded and stratified into three categories: clear, partly cloudy, and completely cloudy. Direct comparison statistics were then computed using collocated output pairs taken from the two algorithms at matching analysis times. A χ^2 test was used to demonstrate that the computed differences were not attributable to random chance. A dichotomous test using a single-blind manual evaluation was then applied to establish if one analysis was superior for those cases where the results differed. A similar approach was used by Welch et al. (1992) to intercompare results from three independent cloud classification schemes and establish a relative accuracy metric for each algorithm.

The above-cited studies provide useful insight into possible validation approaches to determine the accuracy or applicability of candidate cloud algorithms to a given application. Note that in each case, available supporting data were used in the way best suited to meet the goals of the individual studies. This insured that the information required to establish the usefulness of the analysis approach to the desired application would be provided. In some cases the amount of available data was too small to allow for comprehensive conclusions, however in each case the study met the stated goals.

6. Summary

Development of improved automated nephanalysis capabilities from multiplatform sensor data is an important goal of the Strategic Environmental Research and Development Program (SERDP). One such SERDP initiative is the Support of Environmental Requirements for Cloud Analysis and Archive (SERCAA) project. SERCAA as a two-phase research and development program has provided both the next generation nephanalysis model for CDFS II and a new global cloud algorithm for use in determining the radiative and hydrological effects of clouds on climate and global change. SERCAA cloud analysis products will be available to a wide community of users both within and outside of the Department of Defense. The principal accomplishments of SERCAA are: 1) incorporation of high-resolution sensor data from multiple military and civilian satellites, polar and geostationary, into an integrated real-time cloud analysis model, 2) demonstration of multi-spectral cloud analysis techniques that improve the detection and specification of clouds, especially cirrus and low clouds, and 3) development of cloud microphysical and radiative property retrieval algorithms and support database specifications for an improved cloud model.

7. References

Adler, R.F. and A. J. Negri, 1988: A satellite Infrared technique to estimate tropical convective and stratiform rainfall. *J. Appl. Meteor,* 27, 30-51.

Adler, R.F., R.A. Mack, N. Prasad, H.-Y.M. Yeh and I.M. Hakkarinen, 1990: Aircraft microwave observations and simulations of deep convection from 18 to 183 GHz. Part I: Observations, *J. Atmos. Ocean. Technol.,* 7, 377-391.

Ackerman, S.A., W.L. Smith and H.E. Revercomb, 1990: The 27-28 October 1986 FIRE IFO cirrus case study: spectral properties of cirrus clouds in the 8-12 micron window. *Mon. Wea. Rev.,* 118, 2377-2388.

AMS Council, 1992. Needs and Opportunities in Mesoscale Research - A Call for Action. *Bull. Amer. Meteor. Soc.,* 73, 63-65.

Arking, A. and J. Childs, 1985: Retrieval of cloud cover parameters from multispectral satellite images. *J. Clim. and Appl. Met.,* 24:322-333.

Bankert, R.L., 1994: Cloud classification of AVHRR imagery in maritime regions using a probabilistic neural network. *J. Appl. Meteor.,* 33, 909-918.

Bunting, J.T. and R.P. d'Entremont, 1982: Improved cloud detection utilizing Defense Meteorological Satellite Program near Infrared measurements. AFGL-TR-82-0027, Air force Geophysics Laboratory, ADA118751.

Chahine, M.T., 1992: GEWEX: The Global Energy and Water Cycle Experiment. *EOS, Trans. of the Amer. Geophys. Union,* 73, 9-14, 1992.

Corell, R.W., 1990: The United States Global Change Research Program (US/GCRP): An Overview and Perspectives on the FY 1991 Program. *Bull. Amer. Meteor. Soc.,* 71, 507-511.

d'Entremont, R.P., 1986: Low and mid-level cloud analysis using nighttime multispectral imagery. *J. Clim. and Appl. Met.*, 25:1853-1869.

d'Entremont, R. P., and L. W. Thomason, 1987: Interpreting Meteorological Satellite Images Using a Color-Composite Technique. *Bull. Amer. Meteor. Soc.*, **68**, 762-768.

d'Entremont, R. P., L. W. Thomason, and J. T. Bunting, 1987: Color-composite Image Processing for Multispectral Meteorological Satellite Data. Proceedings of Digital Image Processing and Visual Communications Technologies in Meteorology, Cambridge, MA. *SPIE, the International Society for Optical Engineering*, **846**, 96-106.

d'Entremont, R. P., G.B. Gustafson, J.T. Bunting, M.K. Griffin, C. Barker Schaff, P.L. Nowak and J.M. Ward, 1989: Comparisons between the RTNEPH and AFGL cloud layer analysis algorithms. AFGL-TR-89-0175, ADA216637.

d'Entremont, R. P., M. K. Griffin, and J. T. Bunting, 1990: Retrieval of Cirrus Radiative Properties and Altitudes Using Multichannel Infrared Data. Proceedings, Fifth Conference on Satellite Meteorology and Oceanography, Amer. Meteor. Soc., 3-7 September 1990, London, England, 4 - 9.

d'Entremont, R. P., D. P. Wylie, J. W. Snow, M. K. Griffin, and J. T. Bunting, 1992: Retrieval of Cirrus Radiative and Spatial Properties Using Independent Satellite Data Analysis Techniques. In Preprints, Sixth Conference on Satellite Meteorology and Oceanography, Jan. 5-10, Atlanta, GA, AMS, Boston, pp. 17-20.

d'Entremont, R.P., D. P. Wylie, D. C. Peduzzi, and J. Doherty, 1993: Retrieval of Cirrus Radiative and Spatial Properties Using Coincident AVHRR and HIRS Satellite Data. Proceedings, Passive Infrared Remote Sensing of Clouds and the Atmosphere. SPIE 1934, 13-15 April 1993, Orlando, 180-196.

d'Entremont, R. P., D. P. Wylie, S-C. Ou and K-N. Liou, 1995: Retrieval of cirrus radiative and spatial properties using coincident multispectral imager and sounder satellite data. Preprints, Cloud Impacts on DoD Operations and Systems, Oct. 24-26, Hanscom AFB, MA, pp. 155-156.

d'Entremont, R. P., D. P. Wylie, S-C. Ou and K-N. Liou, 1996: Retrieval of cirrus radiative and spatial properties using coincident multispectral imager and sounder satellite data. Preprints, Eighth Converence on Satellite Meteorology and Oceanography, Jan 28 - Feb 2, 1996, AMS, Boston, MA.

Deirmendjian, D., 1969: Electromagnetic scattering on spherical polydispersions. Elseveier, New York.

Diem, M., 1948: Messungem der Frosse Von Walkendementen II. Meteor. Rundschau, 9, 261-273.

Di Girolamo, L. and R. Davies, 1995: The image navigation cloud mask for the Multi-angle Imaging SpectroRadiometer (MISR). *J. Atmos. and Oceanic Tech.*, 12.

Ebert, E.E., 1989: Analysis of polar clouds from satellite imagery using pattern recognition and a statistical cloud analysis scheme. *J. Appl. Meteor.*, 28, 282-299.

Eyre, J.R. and W.P. Menzel, 1989: Retrieval of cloud parameters from satellite sounder data: A simulation study. *J. Appl. Meteor.*, 28, 267-275.

Falcone, V.J. and R.G. Isaacs, 1987: The DMSP microwave suite. In *Proceedings, NOAA Conference on Passive Microwave Observing from Environmental Satellites*, Tech. Rpt. NESDIS 35, pg. 174-185. U.S. Dept. of Commerce, Washington, DC.

Falcone, V.J., M.K. Griffin, R.G. Isaacs, J.D. Pickle, J.F. Morrissey, A.J. Jackson, A. Bussey, R. Kakar, J. Wang, P. Racette, D.J. Boucher, B.H. Thomas, A.M. Kishi, 1992: SSM/T-2 Calibration and Validation Data Analysis, PL-TR-92-2293, Phillips Laboratory, Hanscom AFB, MA 01731-5000, ADA265817.

Garand, L., 1988: Automated recognition of oceanic cloud patterns. Part I: Methodology and application to cloud climatology. *J. Climate*, 1, 20-39.

Griffin, M.K., V.J. Falcone, J.D. Pickle, and R.G. Isaacs, 1994: SSM/T-2 Brightness Temperature Signatures, AMS 7th Conference on Satellite Meteorology and Oceanography Proceedings, Monterey, CA, 110-113.

Gustafson, G.B. and G.W. Felde, 1988: Interactive satellite image processing applied to cloud detection. Preprints: *4th Conference on Interactive Information Processing Systems*, American Meteorological Society, Boston, MA.

Gustafson, G.B. and G.W. Felde, 1989: Validation of automated cloud detection from microwave imagery. Preprints: *5th Conference on Interactive Information Processing Systems*, American Meteorological Society, Boston, MA.

Gustafson, G.B. and R.P. d'Entremont, 1992: Single channel and multispectral cloud algorithm development for TACNEPH. In: *Preprints, Sixth Conference on Satellite Meteorology and Oceanography*, American Meteorological Society, pp. 13-16.

Gustafson, G. B., R. G. Isaacs, J. M. Sparrow, J. T. Bunting, and R. P. d'Entremont, 1993: Validation of infrared cloud detection algorithms developed for TACNEPH. Proceedings Passive Infrared Remote Sensing of Cloud and the Atmosphere. Orlando, 13-15 April 1993, SPIE, the International Society for Optical Engineering, 1934, 62 - 71.

Gustafson, G.B., R.G. Isaacs, R.P. d'Entremont, J.M. Sparrow, T.M. Hamill, C. Grassotti, D.W. Johnson, C.P. Sarkisian, D.C. Peduzzi, B.T. Pearson, V.D. Jakabhazy, J.S. Belfiore, and A.S. Lisa, 1994: Support of Environmental Requirements for Cloud Analysis and Archive (SERCAA): Algorithm Descriptions. PL-TR-94-2114, Phillips Laboratory, Hanscom AFB, MA, ADA   283240, 100 pp.

Gustafson, G.B., R.P. d'Entremont and D.C. Peduzzi, 1995: Cloud data sets derived from combined geostationary and polar-orbiting environmental satellite sensors using the SERCAA cloud model. Preprints, Cloud Impacts on DoD Operations and Systems, Oct. 24-26, Hanscom AFB, MA, pp. 79-90.

Hakkarinen, I.M. and R. F. Adler, 1988: Observations of precipitating convective systems at 92 and 183 GHz: aircraft results. *Meteorol. Atmos. Phys.*, 38, 164-182.

Hale, G. M., and M. R. Querry, 1973: Optical constants of water in the 200 nm to 200μm wavelength region, Apl. Optics, 12, 555-563.

Hamill. T. M., and R. Hoffman, 1993: SERCAA Cloud Analysis Integration: Design Concepts and Interaction with Cloud Forecast Models. Phillips Laboratory Tech. Report PL-TR-93-2100, Phillips Laboratory Geophysics Directorate, Hanscom AFB, MA, 54 pp., ADA 269104.

Hamill, T. M., and T. Nehrkorn, 1993: A Short-Term Cloud Forecast Scheme Using Cross Correlations. *Wea. and Forecasting*, 8, 401-411.

Hamill, T.M., R.P. d'Entremont, and J.T. Bunting, 1992: A Description of the Air Force Real-Time Nephanalysis Model, *Wea. and Forecasting*, 7, 288-306.

Hawkins, R. S., and R. P. d'Entremont, 1990: Automated Cloud Typing Using Satellite Imagery. GL-TR-90-0326, Hanscom AFB, MA, 6 pp, ADA230492.

Heideman, K. F., J. M. Sparrow, and T. S. Lisa, 1994: Validation of the SERCAA Cloud Analysis Algorithm. Proceedings, Seventh Conference on Satellite Meteorology and Oceanography, Amer. Meteor. Soc., 6-10 June 1994, Monterey CA, 326 - 329.

Heideman, K. F., R. P. d'Entremont, J. M. Sparrow, T. S. Lisa, and G. B. Gustafson, 1995: SERCAA Integrated Cloud Analysis Validation. Preprint of the Cloud Impacts on DoD Operations and Systems 1995 Conference (CIDOS-95), D. Grantham, ed., Phillips Laboratory Tech. Paper PL-TR-95-2129, Hanscom AFB, MA, 1 Oct 95, ADA300914.

Hunt, G. E., 1973: Radiative Properties of Terrestrial Clouds at Visible and Infrared Thermal Window Wavelengths. Quart. Journ. Royal Meteor. Soc., 99, 346-369.

Inoue, T., 1987: A Cloud Type Classification with NOAA-7 Split-Window Measurements. Journ. Geophys. Res., 92, No. D4, 3991-4000.

Isaacs, R. G., W. C. Wang, R. D. Worsham, and S. D. Goldenberg, 1987: Multiple scattering treatment for use in the LOWTRAN and FASCODE models. Appl. Optics, 26, 1272-1281.

Isaacs, R.G., E. Kalnay, G. Ohring, R. McClatchey, 1993: Summary of the NMC/NESDIS/DoD Conference on DMSP Retrieval Products. Bull. AMS, 74:1, 87-91.

Kiess, R.B. and W.M. Cox, 1988: The AFGWC automated real-time cloud analysis model. Tech. Note 88/001, AFGWC.

King, M.D., Y.J. Kaufman, W.P. Menzel, and D. Tanre, 1992: Remote sensing of cloud, aerosol, and water vapor properties from the Moderate Resolution Imaging Spectrometer (MODIS). *IEEE Trans. Geosci. Rem. Sens.*, 30, 2-27.

Kneizys, F. X., E. P. Shettle, W. O. Gallery, J. H. Chetwynd Jr., L. W. Abreu, E. A. Selby, S. A. Clough, and R. W. Fenn, 1983: Atmospheric transmittance/radiance: Computer Code LOWTRAN6. AFGL-TR-83-0187, Air Force Geophysics Laboratory. ADA137786.

Kopp, T.J., T. J. Neu, and J.M. Lanicci, 1994a: A Description of the Air Force Global Weather Central's Surface Temperature Model. Preprints, 10th Conf. Num. Wea. Pred., Portland, Amer. Meteor. Soc., 435-437.

Kopp, T. J., T. J. Neu, and P. J. Broll, 1994b: Application of SSM/I to a real time automated satellite nephanalysis model. 7th Conference of Satellite Meteorology and Oceanography. American Meteorological Society, Boston MA, pp 247-250.

Kopp, T. J., S. G. Zahn, and R. B. Kiess, 1996: Application of a convective stratiform technique in an operational global nephanalysis. 8th Conference of Satellite Meteorology and Oceanography. American Meteorological Society, Boston MA, pp 395-398.

Kummerow, C., I.M. Hakkarinen, H.F. Pierce, and J.A. Weinman, 1991: Determination of precipitation profiles from airborne passive microwave radiometric measurements. *J. Atmos. Oceanic Tech.*, 8, 148-158.

Lamaei, N., 1994: Cloud-type discrimination via multispectral textural analysis. *Opt. Engineer.*, 34, 1303-1313.

Lee, J., R. Weger, S.K. Sengupta, and R.M. Welch, 1990: A neural network approach to cloud classification. *IEEE Trans. Geosci. Rem. Sens.*, 28, 846-855.

Li, X., and A. H. Strahler, 1992: Geometric-Optical Bidirectional Reflectance Modeling of the Discrete Crown Vegetation Canopy: Effect of Crown Shape and Mutual Shadowing. IEEE Trans. Geosci. and Remote Sens., 30, 276-292.

Lorenc, A., 1981: A global three-dimensional multivariate statistical interpolation scheme. *Mon. Wea. Rev.*, 109: 701-721.

Menzel, W.P. and J.F.W. Purdom, 1994: Introducing GOES-I: The first of a new generation of geostationary operational Environmental satellites. *Bull. Amer. Meteor. Soc.*, 75, 757-781.

Menzel, W.P., D.P. Wylie, and K.I Strabala, 1992: Seasonal and diurnal changes in cirrus clouds as seen in four years of observations with the VAS. *J. Appl. Meteor.*, 31, 370-385.

Menzel, W.P., D.P. Wylie, and K.I. Strabala, 1993: Trends in global cirrus inferred from three years of HIRS data. Proceedings, Seventh Int'l TOVS Conference, Igls, Austria, 10-16 February 1993.

Menzel, W. P., and J.F. W. Purdom, 1994: Introducing GOES-I: The First of a New Generation of Geostationary Operational Environmental Satellites. Bull. Amer. Meteor. Soc., 75, 757-781.

Moncet, J.L. and R.G. Isaacs, 1994: Unified retrieval of atmospheric temperature, water substance, and surface properties from the combined DMSP sensor suite. Preprints, 7th Conference on Satellite Meteorology and Oceanography, American Meteorological Society, June 6-10, Monterey, CA, 489-492.

Nakajima, T. and M.D. King, 1989: Cloud optical parameters as derived from the multispectral cloud radiometer. In Lenoble and Gelyn, eds, *IRS '88*, pgs. 18-21. A. Deepak Pub.

Nehrkorn, T. and M. Zivkovic, 1996: A comparison of cloud cover schemes. *Mon. Weather Rev.* (in press).

Neu, T.J., R.G. Isaacs, G.B. Gustafson and J.W. Snow, 1994: Improved cloud analysis for CDFS II through the SERCAA research and development program. *Preprints, 7th Conference on Satellite Meteorology and Oceanography,* June 6-10, Monterey, CA, 239-242.

Ou, S. C., K. N. Liou, W. M. Gooch, and Y. Takano, 1993: Remote Sensing of Cirrus Cloud Parameters Using Advanced Very High Resolution Radiometer 3.7- and 10.9-mm Channels. *Appl. Opt.,* 32, 2171-2180.

Petty, G. W., 1994: Physical retrievals over-ocean rain rate from multichannel microwave imagery. Part II: Algorithm Implementation. *Meteorol. Atmos. Phys.,* 54, p. 101-121.

Petty, G. W., 1995: The status of satellite-based rainfall estimation over land, *Remote Sensing Environment,* 51, p 125-137.

Petty, G. W., and D. K. Miller, 1995: Satellite microwave observations of precipitation correlated with intensification rate in extratropical oceanic cyclones, *Mon. Weather Rev.,* 123, No. 6, p. 1904-1911.

Pickle, J. R. G. Isaacs, V. Jakabhazy, M. Griffin, and V. J. Falcone, 1996: Detection of precipitation using SSM/T-2 Measurements. 8th Conference of Satellite Meteorology and Oceanography. American Meteorological Society, Boston MA, pp 238-242.

Phillips Laboratory, 1994: SERCAA integrated cloud analysis validation using satellite data from May 1993. Phillips Laboratory Technical Memorandum, 3 June 1994.

Prabhakara, C. J.-M. Yoo, G. Dalu, and R. S. Fraser, 1990: Deep Optically Thin Cirrus Clouds in the Polar Regions. I - Infrared Extinction Characteristics. Journ. Appl. Meteor., 29, 1313 - 1329.

Rao, N. X., S. C. Ou, and K. N. Liou, 1995: Removal of the Solar Component in AVHRR 3.7-mm Radiances for the Retrieval of Cirrus Cloud Parameters. Journ. Appl. Meteor., 34, 482-499.

Ross, J.K., and A. Marshak, 1985: A Monte Carlo Procedure for Calculating the Scattering of Solar Radiation by Plant Canopies. Sov. Journ. Remote Sens., 4, 783-801.

Rossow, W.B. and R.A. Schiffer, 1991: ISCCP Cloud Data Products. *Bull. Amer. Meteor. Soc.,* 72, 1, 2-20.

Rossow, W., F. Mosher, E. Kinsella, A. Arking, M. Debois, E. Harrison, P. Minnis, E. Ruprecht, G. Seze, C. Simmer and E. Smith, 1985: ISCCP Cloud Algorithm Intercomparison. *J. Clim. Appl. Met*, 24, 877-903.

Roujean, J-L., M. Leroy, and P-Y. Deschamps, 1992: A Bidirectional Reflectance Model of the Earth's Surface for the Correction of Remote Sensing Data. Journ. Geophys. Res., 97 D18, 20455-20468.

Saunders, R.W. and K.T. Kriebel, 1988: An improved method for detecting clear sky and cloudy radiances from AVHRR data. *Int. J. Remote Sensing*, 9:1, 123-150.

Schiffer, R.A. and W.B. Rossow, 1983: The International Satellite Cloud Climatology Project (ISCCP): The First Project of the World Climate Research Program. *Bull. Amer. Meteor. Soc.*, 64, 779-784.

Schiffer, R.A. and W.B. Rossow, 1985: ISCCP Global Radiance Data: A New Resource for Climate Research. *Bull. Amer. Meteor. Soc.*, 66, 1498-1505.

Smith, W.L., H. E. Revercomb, H. B. Howell, and M.-X. Lin, 1990: Multi-spectral Window Radiance Observations of Cirrus From Satellite and Aircraft, November 2, 1986 Project FIRE. FIRE Science Results 1988, NASA Langley Res. Ctr., 89 - 93.

Spencer, R.W., H.M. Goodman, R.E. Hood, 1989: Precipitation retrieval over land and ocean with the SSM/I: identification and characterization of the scattering signal. J. Atmos. and Ocean. Tech., 6, 254-274.

Stamnes, K., S. C. Tsay, W. Wiscombe, and K. Jayaweera, 1988: Numerically stable algorithm for discrete ordinate method radiative transfer in multiple scattering and emitting layered media. Appl. Optics, 18, 994-1008.

Stephens, G. L., 1979: Optical properties of eight water cloud types. Commonwealth Scientific and Industrial Research Organization, Division of Atmospheric Physics, Tech. Paper #36, Australia.

Stowe, L.L., E.P. McClain, R. Carey, P. Pellegrino, G.G. Gutman, P. Davis, C. Long and S. Hart, 1991: Global distribution of cloud cover derived from NOAA/AVHRR operational satellite data. *Adv. Space Res.*, 3, 51-54.

Strabala, K.I., S.A. Ackerman and W.P. Menzel, 1994: Cloud Properties inferred from 8-12 micron data. *J. Appl. Meteor.*, 33, 212-229.

Takano, Y., and K. N. Liou, 1989: Solar Radiative Transfer in Cirrus Clouds. Part I: Single Scattering and Optical Properties of Hexagonal Ice Crystals. Journ. Atmos. Sci., 46, 3 - 19.

Walthall, C. L., J. M. Norman, J. M. Welles, G. Campbell, and B. L. Blad, 1985: Simple Equation to Approximate the Bidirectional Reflectance for Vegetative Canopies and Bare Soil Surfaces. Appl. Optics, 24, 383-387.

Weinreb, M. P., and A.C. Neuendorffer, 1973: Method to Apply Homogeneous-Path Transmittance Models to Inhomogeneous Atmospheres. *Journ. Atmos. Sci., Amer. Meteor. Soc.*, 30, 662-666.

Weinreb, M.P., and M. L. Hill, 1980: Calculation of Atmospheric Radiances and Brightness Temperatures in Infrared Window Channels of Satellite Radiometers. NOAA Tech. Rep. NESS 80, U.S. Dept. of Commerce, Washington, D.C., 40 pp.

Welch, R.M., S.K. Sengupta, A.K. Goroch, P. Rabindra, N. Rangaraj, and M.S. Navar, 1992: Polar cloud and surface classification using AVHRR imagery: an intercomparison of methods. *J. Appl. Meteor.*, 31, 405-420.

Wilheit, T.T., A.T.C. Chang, J.L. King, E.B. Rodgers, R. A. Nieman, B.M. Krupp, A. S. Milman, J. S. Stratigos, H. Siddalingaiah, 1982: Microwave radiometric observations near 19.35, 92 and 183 GHz of precipitation in tropical storm Cora. *J. Appl. Meteor.*, 21, 1137-1145.

World Meteorological Organization (WMO), 1989: Report of the Tenth Session of the Joint Scientific Committee. *IRD-No. 314*, World Meteorological Organization, 57 pp., Geneva Willefranche-sur-mer, France.

Wylie, Donald P., and W. P. Menzel, 1989: Two Years of Cloud Cover Statistics Using VAS. *J. Clim.*, 2, 380 - 392.

Wylie, D.P., W.P. Menzel, H.M. Woolf, and K.I. Strabala, 1994: Four years of global cirrus cloud statistics using HIRS. *J. Clim.*, 7, 1927-1986.

Zivkovic M. and J.-F. Louis, 1992: A new method for developing cloud specification schemes in general circulation models. *Mon. Weather Rev.*, 120, pp 2928-2941.

Appendix A

AER SERCAA-Related Papers and Technical Presentations for 1993 - 1996:

AMS 8th Conference on Satellite Meteorology and Oceanography - 28 January - 2 February 1996, Atlanta, GA

Evaluation of SERCAA integration algorithm for analysis of multiplatform/multisensor satellite-derived cloud parameters. Gary Gustafson, Christopher Grassotti, Robert d'Entremont (AER).

Cloud detection and land-surface albedos using visible and near-infrared bi-directional reflectance distribution models. Robert d'Entremont (AER), Crystal Schaaf (PL), and Alan Strahler (BU).

Retrieval of cirrus radiative and spatial properties using coincident multispectral imager and sounder satellite data. Robert d'Entremont (AER), Donald Wylie (UW), Szu-Cheng Ou, Kuo-Nan Liou (UU).

Retrieval of cloud spatial, microphysical, radiative and environment parameters from multisource satellite data using SERCAA. Ronald Isaacs, Gary Gustafson, Robert d'Entremont (AER).

Cloud Impacts on DoD Operations and Systems (CIDOS 95) - 24-26 October 1995, Hanscom AFB, MA

Cloud data sets derived from combined geostationary and polar-orbiting environmental satellite sensors using the SERCAA cloud model. Gary Gustafson, Robert d'Entremont, Daniel Peduzzi (AER)

Enhanced satellite cloud analysis by the development of a higher resolution (6-km) global geography data set. Lt. Rad Robb (PL), Daniel Peduzzi (AER), Joan Ward (SRC)

Cloud detection using visible and near-infrared bidirectional reflectance distribution models. Robert d'Entremont (AER), Crystal Schaaf (PL), Alan Strahler (BU)

SERCAA Phase II: cloud radiative, microphysical, and environmental properties. Ronald Isaacs, Gary Gustafson, Robert d'Entremont, David Hogan (AER), Maj. Michael Remeika, James Bunting (PL)

Retrieval of cirrus radiative and spatial properties using coincident multispectral imager and sounder satellite data. Robert d'Entremont (AER), Donald Wylie (UW), Szu-Cheng Ou, Kuo-Nan Liou (UU).

Support of environmental requirements for cloud analysis and archive (SERCAA) integrated cloud analysis validation. Kenneth Heideman (PL), Robert d'Entremont, Jeanne Sparrow, Anthony Lisa, Gary Gustafson (AER).

69

European Symposium on Satellite Remote Sensing II, Conference on Passive Infrared Remote Sensing of Clouds and the Atmosphere III, 25-29 September 1995, Paris, France.

Multi-spectral multi-platform satellite cloud and cloud environment retrievals for SERCAA. Ronald G. Isaacs, Gary B. Gustafson, and Robert P. d'Entremont

Strategic Environmental Research and Development Program Symposium - 12-14 April 1994, Washington, D.C.

Multi-spectral multi-platform satellite cloud and cloud environment retrievals from SERCAA. Ronald G. Isaacs, Gary B. Gustafson, and Robert P. d'Entremont (AER), James T. Bunting and Maj. Michael F. Remeika (PL)

European Symposium on Satellite Remote Sensing - 26-30 September 1994, Rome, Italy

Integration of multiplatform/multisensor satellite global cloud analyses within SERCAA. C. Grassotti, R. Isaacs, G. Gustafson (AER).

Improved cloud analysis for CDFS II through the SERCAA research and development program. R.G. Isaacs, G.B. Gustafson, R.P. d'Entremont (AER), T.J. Neu (AFGWC), J.W. Snow (PL).

AMS 7th Conference on Satellite Meteorology and Oceanography, 6-10 June 1994, Monterey, CA

Cloud Cover Determination Using the DMSP OLS. Gary B. Gustafson, Daniel C. Peduzzi, and Jean-Luc Moncet (AER).

Validation of the SERCAA Cloud Analysis Algorithm. Kenneth F. Heideman (PL) and Jeanne M. Sparrow (AER).

Analysis of Geostationary Satellite Imagery Using a Temporal Differencing Approach. Robert P. d'Entremont, Gary B. Gustafson, and Brian T. Pearson (AER).

Analysis Integration Within SERCAA: Optimizing the Analysis of Multiplatform/Multisensor Satellite-Derived Cloud Parameters. C. Grassotti, T. Hamill, R. Isaacs, G. Gustafson, D. Johnson (AER).

Improved Cloud Analysis for CDFS II Through the SERCAA Research and Development Program. Thomas J. Neu (AFGWC), Ronald G. Isaacs and Gary B. Gustafson (AER), and J. William Snow (PL).

70

Cloud Impacts on DoD Operations and Systems (CIDOS 93) - 16-19 November 1993, Ft. Belvoir, VA

Satellite Cloud Analysis Programs at the Air Force Phillips Laboratory: An Overview: Part 1 Tactical Nephanalysis (TACNEPH). Gary B. Gustafson, Ronald G. Isaacs (AER), Robert P. d'Entremont and James T. Bunting (PL).

Satellite Cloud Analysis Programs at the Air Force Phillips Laboratory: An Overview: Part 2 Support of Environmental Requirements for Cloud Analysis and Archives (SERCAA). R. G. Isaacs and G. B. Gustafson (AER) and J. W. Snow and R. P. d'Entremont (PL).

Validation of TACNEPH Cloud Detection Algorithms. Jeanne M. Sparrow, Gary B. Gustafson, Anthony S. Lisa and Robert P. d'Entremont (AER).

Remote Sensing of Cloud Thickness and Base from Multispectral Cloud Imager Data. Ronald G. Isaacs, Alberto Bianco, Gary Gustafson, and Charles Sarkisian (AER).

A Short-Term Cloud Forecast Scheme Using Cross Correlations. Thomas M. Hamill and Thomas Nehrkorn (AER).

Robust Database Management for Virtual-Application Environments. James S. Belfiore (AER).

SPIE Conference on Passive Infrared Remote Sensing of Clouds and the Atmosphere - 13-15 April 1993, Orlando, FL

Remote sensing of cloud for defense and climate studies: an overview (invited paper). R.G. Isaacs (AER).

Validation of infrared cloud detection algorithms developed for TACNEPH. G.B. Gustafson, R.G. Isaacs, J.M Sparrow (AER), J.T. Bunting, and R.P. d'Entremont (PL).